MASTER OF SCIENCE IN ELECTRICAL AND ELECTRONIC ENGINEERING

Analysis of Subsynchronous Resonance (SSR) in Single Machine Infinite Bus (SMIB) with Pulse Width Modulated Series Compensator (PWMSC)

B. M. Ruhul Amin

Department of Electrical and Electronic Engineering

Islamic University of Technology

October 2015

Certificate of Approval

The thesis entitled **"Analysis of Subsynchronous Resonance (SSR) in Single Machine Infinite Bus (SMIB) with Pulse Width Modulated Series Compensator (PWMSC)"** submitted by **B. M. Ruhul Amin**, Student No. **102603** of Academic Year 2010- 2011 has been found as satisfactory and accepted as partial fulfillment of the requirement for the Degree of MASTER OF SCIENCE IN ELECTRICAL AND ELECTRONIC ENGINEERING on 30 October, 2015.

Board of Examiners:

1. _____ Chairman
   Dr. Md. Shahid Ullah (Supervisor)
   Professor
   Dept. of EEE, IUT, Board Bazar, Gazipur-1704

2. _____ Member (Ex-Officio)
   Dr. Md. Shahid Ullah
   Professor and Head
   Dept. of EEE, IUT, Board Bazar, Gazipur-1704

3. _____ Member
   Dr. Kazi Khairul Islam
   Professor
   Dept. of EEE, IUT, Board Bazar, Gazipur-1704

4. _____ Member
   Dr. Md. Ashraful Hoque
   Professor
   Dept. of EEE, IUT, Board Bazar, Gazipur-1704

5. _____ Member (External)
   Dr. Md. Sekendar Ali
   Professor and Head
   Dept. of EEE, University of Asia Pacific (UAP), Dhaka.

Declaration of Candidate

It is hereby declared that this thesis/report or any part of it has not been submitted elsewhere for the award of any degree or diploma.

_____

(Signature of the Supervisor)

Prof. Dr. Md. Shahid Ullah
Designation: Professor
Address: Dept. of EEE, IUT,
Board Bazar, Gazipur-1704

_____

(Signature of Candidate)

B. M. Ruhul Amin
Student ID.: 102603
Academic Year:2010-2011

Dedication

My Beloved Parents, Inspiring Elder Sister, Loving Younger Brother

&

My Sincere Wife

List of Contents

Chapter 3

Small-signal Analysis of Subsynchronous Resonance (SSR) Phenomenon

Chapter 4
Dynamic Modeling of PWMSC and Performance Evaluation for SSR Damping

Chapter 5
Summary and Conclusions

List of Figures

List of Tables

List of Abbreviations and Symbols

Abbreviations

EHV	Extra High Voltage
SSR	Subsynchronous Resonance
FBM	First Benchmark Model
PSS	Power System Stabilizer
FACTS	Flexible AC Transmission System
PWMSC	Pulse Width Modulated Series Compensator
GTO	Gate Turn-Off
IGBT	Insulated Gate Bipolar Transistor
VSC	Voltage Source Converter
STATCOM	Static Compensator
SSSC	Static Synchronous Series Compensator
UPFC	Unified Power Flow Controller
HVDC	High Voltage Direct Current
TCSC	Thyristor Controlled Series Capacitor
GCSC	Gated Control Series Capacitor
SVC	Static VAR compensator
GA	Genetic Algorithm
AIA	Artificial Immune Algorithm
PSO	Particle Swarm Optimization
DE	Differential Evolution
ABC	Artificial Bee Colony
BBO	Biogeography Based Optimization
pf	power factor
p.u.	per unit

Symbols

A	State matrix
B	Control or input matrix
C	Capacitor in the compensated transmission line
C_v	Steam valve position
C_{VOPEN}, C_{VCLOSE}	Maximum permitted rate of opening and closing the steam valve respectively
D_E, D_g, D_B, D_A, D_I, D_H	Damping co-efficient of the corresponding inertia
D_i	Damping coefficient of the i^{th} rotating mass
E_{fd}	exciter output voltage
E_R	Output voltage of the voltage regulator amplifier
E_{ref}	Reference voltage of the excitation system
E_{SB}	Feedback stabilizing signal of the excitation system
e_a, e_b, e_c	Stator three-phase voltage respectively
e_d, e_q	Stator voltage in the d-q reference frame
e_{fd}	Field voltage
F_B, F_A, F_I, F_H	Power fraction of the stages of the turbine
i_a, i_b, i_c	Stator currents in phase a,b,c
i_d, i_q,	Stator currents in the d-q reference frame
i_{dc}	Current through the dc capacitor
i_{fd}, i_{1d}, i_{1q}, i_{2q},	Field and damping winding currents in the d-q reference frame respectively
K_A	Gain of the voltage regulator amplifier
K_E	Exciter constant
K_{Eg}, K_{gB}, K_{BA}, K_{AI}, K_{IH}	Stiffness of the connecting shafts
K_F	feedback stabilizing loop gain of the exciter system
K_C	Gain of the supplementary controller

K_g	Speed regulation in governor system
$K_{i,i+1}$	Stiffness between i^{th} and $(i+1)^{th}$ mass-spring
L_T	Total inductance of the electric system
L_{ad}, L_{aq}	Mutual inductance
L_d, L_q	d and q synchronous inductances
$L_{ffd}, L_{lld}, L_{llq}, L_{22q}$	Rotor and damping windings self-inductances respectively
$M_E, M_g, M_B, M_A, M_I, M_H$	Inertia constants of exciter, generator, toe low-pressure turbines, intermediate-pressure turbine and high-pressure turbine respectively
M_i	Inertia constant of the i^{th} rotating mass
P	Real power
P_A, P_A, P_I, P_H	Power of the stages of the turbine
Q	Reactive power
R_L	Resistance of the series capacitor compensated transmission line (Line1)
R_a	Armature resistance
$R_{fd}, R_{ld}, R_{lq}, R_{2q}$	Rotor and damp windings resistance respectively
S	Complex power delivered to the infinite bus in the IEEE first benchmark model
S	Laplace transformation operator
T_A, T_E, T_F	Time constant in excitation system
$T_{LB}, T_{LA}, T_{IP}, T_{HP},$	Input torques of two low-pressure turbines, intermediate-pressure turbine and high-pressure turbine respectively
$T_g, T_{ch}, T_{rh}, T_{co},$	Time constant in governor and turbine system
T_1 ,T_2	Time constant in supplementary controller
T_{m0}	Initial mechanical torque
U	Input vector
V_C	Voltage across the series capacitor of the compensator transmission line
V_L	Voltage across the inductance of the series capacitor compensated transmission line
$V_{Ld}, V_{Lq},$	Voltages across the inductance in the d-q reference frame

V_R	Voltages across the resistance of the series capacitor compensated transmission line
$V_{Rd,}$ $V_{Rq,}$	Voltages across the resistance in the d-q reference frame
$V_{a,}$ $V_{b,}$ $V_{c,}$	Three phase voltages on the AC side
V_b	Infinite bus voltage
V_{dc}	Voltage across the dc capacitor
V_s	AC system voltage
V_t	Generator terminal voltage
$V_{td,}$ $V_{tq,}$	Generator terminal voltages in the d-q reference frame
X	State vector
$\Psi_{d,}$ $\Psi_{q,}$	Stator flux linkages in d-q components
$\Psi_{fd,}$ $\Psi_{lq,}$ $\Psi_{lq,}$ $\Psi_{2q,}$	Rotor flux linkages in d-q components
δ	Generator power angle
$\delta_{E,}$ $\delta_{B,}$ $\delta_{A,}$ $\delta_{I,}$ $\delta_{H,}$	Rotor angles of exciter, two low-pressure turbines, intermediate-pressure turbine and high-pressure turbine respectively
ϕ	Phase angle of the current flowing from a VSC to an AC system
θ	Phase angle of the bus voltage
ω	Angular velocity
$\omega_{E,}$ $\omega_{B,}$ $\omega_{A,}$ $\omega_{I,}$ $\omega_{H,}$	Angular velocity of exciter, two low-pressure turbines, intermediate-pressure turbine and high-pressure turbine respectively
$\omega_e(f_e)$	Sub synchronous nature frequency
ω_{ref}	Reference angular velocity
$\omega_0\,(f_0)$	Synchronous frequency
Δ	Prefix to denote a small deviation in the initial operating point
$_0$	Suffix to denote the initial operating operation

Acknowledgement

All praise and glory is due to Allah, the lord, benefactor and cherisher of the entire world who supplied me with the courage, guidance and necessary knowledge to complete this research work. This thesis is the most significant scientific accomplishment in my life. It has indeed motivated me to explore more facts and obtain increased knowledge in the field of power system and I would like to continue the research in the future.

I would like to acknowledge those who all helped me to complete this work. The role of the university and the department has been very important and helpful for me during the whole period of research.

I would like to express my heartiest gratitude to my supervisor, Prof. Dr. Md. Shahid Ullah for his great supervision, inspiration and unbounded support for doing this thesis. I truly appreciate and value his guidance and encouragement from the beginning to the end of this thesis. I am indebted to him for all the help he has provided me, the precious time he spent in editing my many mistakes and making sure my thesis is always on track.

I am indebted to Mr. Ashik Ahmed, Asst. Prof. EEE department, IUT who always kept an eye on the progress of this work and his programming experience was of great benefit for me. I would like to express my deep appreciation and gratitude to him.

Finally my warmest tribute to my parents, beloved wife, all my family members, lots of my friends, seniors, juniors, colleagues and students who every time supported me by their prayers and well wishes for me.

Abstract

Subsynchronous Resonance (SSR) phenomenon is an important dynamic problem in power system which can lead to the failure of the power system and destruction to the rotor shaft. When series capacitive compensators in EHV transmission line are implemented together with a steam turbine-generator it can cause to the SSR occurrence. Damping of these SSR oscillations has to be ensured in an effective manner so that the system dynamics remains stable under a range of operating scenario. Various types of Flexible AC Transmission System (FACTS) controllers particularly SVC, TCSC, GCSC, STATCOM, SSSC, UPFC, IPFC have been used for this purpose in the past. Pulse Width Modulated Series Compensator (PWMSC) is a newly FACTS device, which can modulate the impedance of a transmission line through the variation of the duty cycle of a train of pulses with fixed frequency, resulting in improvement of system performance. The thesis starts with the study of the nonlinear and linear model of IEEE First benchmark Model (FBM) and performs the small signal analysis by inserting small disturbance in mechanical power input in the governor. The eigen value analysis shows that the different torsional modes are becoming unstable for different compensation levels. The critical compensation levels have been identified. There are four unstable torsional modes and Mode-1 exhibits the most severe undamping with 68.5% compensation level. The dynamic current injection model of PWMSC has been developed in the IEEE FBM and small signal analysis has been performed. A supplementary controller with lead block and reset block has been designed to control the parameters based on an eigen value based objective function. Genetic Algorithm (GA) is then used to solve the optimization problem. The results show that the properly tuned PWMSC can successfully damp out all the shaft torsional torques over a wide range of compensation levels. The maximum overshoots and settling times for different states are also satisfactory. The analysis has been performed at critical compensation levels so that all individual compensation levels are covered. This feature of PWMSC can be used to increase the limit of line power transfer in a multi-area power system in stable manner. The outcome confirms the effectiveness of the PWMSC in damping SSR oscillations in power system.

Chapter 1

Introduction

1.1 Background

The discovery of electricity is one of the greatest achievements of mankind. Today life without electricity is almost impossible. We need electricity at every moment and in every walk of life. Electricity is considered the soul or the life without which the entire world remains dead and dormant. The development of a nation completely depends on the total generation and the usage of electricity. For this reason the reliable and economic operation of electricity is the utmost important to the modern society.

In the modern power system the electricity is generated in a power station and supplied to the consumers. Generally the modern power generation plants are located hundred to thousand kilometers away from the load center due to the high cost of the land, limited availability of the resources and the social and environmental constrains. As power demand increases in many parts of the world, power transmission needs to be developed, as well. The building of more power lines may not be the best way, however, as transmission lines cost a lot of money, take considerable time to construct, and are subject to severe environmental constraints.

The power system is much more loaded than before. The large-scale power system interconnection is intended to make electric energy generation and transmission more economical and reliable. But due to this the power system is becoming more and more complex and different instability problems are arising. Instability means a condition denoting loss of synchronism. So the stability of an interconnected power system is its ability to return to normal or stable operation after having been subjected to some form of disturbance. To obtain and to maintain stability in a power system is very important in the field of power system. Accurate assessment of power system stability has become increasingly important as power systems are stressed to meet the demand of modern market operation [1].

Normally the power systems are nonlinear in nature and the operating conditions can vary over a wide range. The increasing size of generating units, loading of the transmission lines

and high speed excitation systems can become the transmission power limiting factor as these are the main causes affecting the small signal stability. Therefore, system requires a controller to damp out these oscillations. The need for the power flow control in electrical power system is thus evident.

With the advent of interconnection of large electric power systems, many new dynamic power system problems have emerged, which include the low-frequency oscillations of the interconnected large electric power systems, the subsynchronous torsional oscillations of turbines in a steam-electric power plant with capacitor-compensated transmission lines and many others [2].

Series capacitive compensators have been used for many years in Extra High Voltage (EHV) transmission line to compensate the excessive inductance of long transmission lines, in order to reduce the line voltage drop, improve its voltage regulation, minimize losses by optimizing load distribution between parallel transmission lines, and to increase the power transfer capability. Series capacitors are also installed in electrical power systems to improve its voltage stability as well. The introduction of series capacitor in a power system has brought the Subsynchronous Resonance (SSR) phenomena. When series capacitive compensators in transmission line are implemented together with a steam turbine-generator it can cause to the SSR occurrence [4-6].

The SSR phenomenon has resulted in the destruction of two generator shafts at the same Mohave power station on December 9, 1970, and again on October 26, 1971[7, 8]. Since then, considerable effort has been expended to find solutions to cure these damaging effects. Preliminary studies have confirmed that the Navajo Station can also be subjected to SSR effects if precautionary measures are not taken to prevent them. A special IEEE Power Engineering Society Task Force was formed to deal with SSR problems. The task force has proposed a "bench mark" model for computer simulation of the phenomena. The “First Bench Mark Model” (FBM) is used for the computer simulation of the power system for SSR study.

Subsynchronous resonance phenomena manifest themselves as induction generator effect and torsional interaction. The subsynchronous component of the generator rotor oscillation increases with time due to disturbance. Another phenomenon, known as hunting occurs when there is too much armature and/or line resistance [9]. Recent studies reveal that the SSR phenomenon is also present in case of renewable energy based generation system [10-11].

In early days, equipments like compensating capacitor, regulating transfer, Power System Stabilizer (PSS) were used to bring stability in power systems. The continuing rapid development of high-power semiconductor technology now makes it possible to control electric power system by means of power electronic devices. These devices constitute an emerging technology called FACTS (Flexible AC transmission System). FACTS technology has a number of benefits, such as greater power flow control, increased secure loading of existing transmission circuits, damping of power system oscillations, less environmental impact and, potentially, less cost than most alternative techniques of transmission system reinforcement. For the analysis of small signal stability accurate representation of system dynamics along with proper FACTS controller is essential.

Pulse Width Modulated Series Compensator (PWMSC) is the latest member in the FACTS family. It is possible to attain similar objectives in comparison with conventional FACTS devices. It has some advantages than other FACTS devices. In the PWMSC, the switches are forced to be turned on and off at a rate considerably higher than the fundamental frequency. The output wave is chopped and the width of the resulting pulse is modulated. Undesirable harmonics in the output waveform are shifted to the higher frequencies, and filtering requirements are much reduced. The sinusoidal PWMSC scheme remains one of the most popular because of its simplicity and effectiveness [12].

1.2 Literature Survey

SSR is a dynamic phenomenon in the power system which has certain special characteristics. The definitions of subsynchronous oscillation and SSR are given by the IEEE as [13, 14]:

"Subsynchronous oscillation is an electric power system condition where the electric network exchanges significant energy with a turbine-generator at one or more of the natural frequencies of the combined system below the synchronous frequency of the system following a disturbance from equilibrium. The above excludes the rigid body modes of the turbine-generator rotors."

"Subsynchronous Resonance (SSR) encompasses the oscillatory attributes of electrical and mechanical variables associated with turbine-generators when coupled to a series capacitor

compensated transmission system where the oscillatory energy interchange is lightly damped, undamped, or even negatively damped and growing."

1.2.1 SSR: Basic Phenomenon

Consider the simple power system shown in Figure 1.1. It consists of a large turbine-generator which is connected to an infinite bus system through a series capacitor compensated transmission line. The generator is driven by a multi-stage turbine, where the various stages of the turbine (HP, IP and LP) and the generator rotor (GEN) are coupled by elastic shafts.

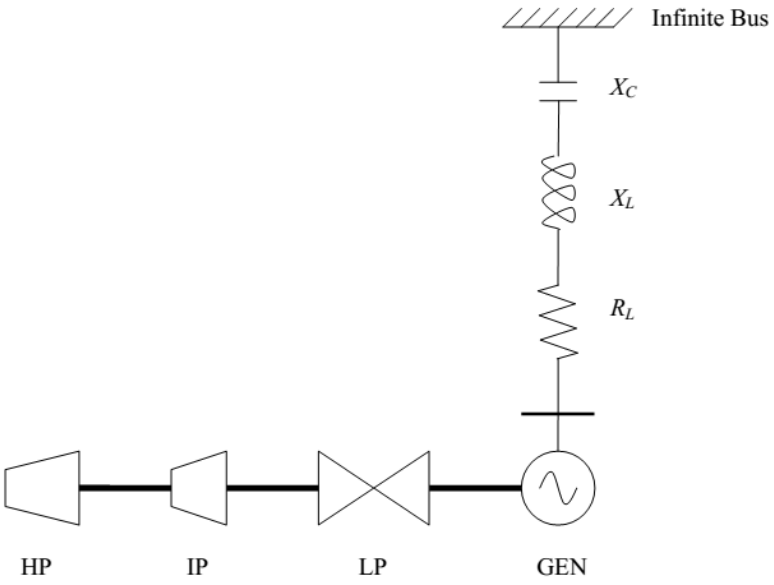

Figure 1.1: A series capacitor compensated power system.

The natural resonance frequency for the electrical system is given by

$$\omega_e = \frac{1}{\sqrt{(L_T)(C)}} = \frac{\omega_0}{\sqrt{(\omega_0 L_T)(\omega_0 C)}} = \omega_0 \sqrt{\frac{X_C}{X_{L_T}}} \quad \text{rad/s} \tag{1.1}$$

or

$$f_e = f_0 \sqrt{\frac{X_C}{X_{L_T}}} \quad \text{Hz} \tag{1.2}$$

where ω_0 is the system synchronous frequency ($\omega_0 = 2\pi f_0$, f_0 = 60 Hz) X_C is the capacitive reactance, and X_{L_T} is the total inductive reactance of the electric system, which comprises the generator subtransient reactance and the transmission line inductive reactance.

In practice, f_e is always below the synchronous frequency f_0 since the compensation levels of transmission line are usually less than 100%. For this reason, f_e is called the subsynchronous natural frequency of the electrical system.

The shaft system of the turbine-generator has (N-1) natural torsional frequencies where N is the number of the rotating masses. These torsional frequencies are functions of the inertia of the different masses and the stiffness of the connected shafts. Due to the physical properties of the shaft materials and the mechanical design of the turbine-generator shaft system, the torsional natural frequencies are also subsynchronous. Thus, the basic interaction between the electrical and mechanical systems is due to the closeness of f_e to the natural torsional frequencies of the turbine-generator shaft system. SSR can occur in the following three forms:

1. Torsional Interaction: This is due to an interaction and exchange of energy between the series compensated electrical system and the turbine-generator mechanical system. This can lead to growing shaft torque oscillations at one of the natural torsional frequencies of the turbine-generator shaft system. Torsional interaction can occur when the generator is connected to a series compensated electrical system that has one or more natural frequencies, which are the synchronous frequency complements of one or more of the spring-mass natural frequencies. Generally, shaft torques due to torsional interaction can be expected to build up at a relatively slow rate such that damaging torque levels would not be reached in less than a minute or so.

2. Induction Generator Effect: This is a pure electrical phenomenon which is due to the fact that, when subsynchronous currents flow in the armature circuit of a synchronous generator, the generator appears as a negative-resistance circuit at the prevailing subsynchronous frequencies. If the apparent resistance is greater than the inherent positive resistance of the circuit at one of the natural frequencies of the electrical circuit, growing subsynchronous voltages and currents will be expected in the system and at the generator. This could result in voltages and currents large enough to be damaging to the generator and power system equipment. In addition, if the subsynchronous currents in the generator armature are at the frequency corresponding to one of the turbine- generator spring-mass modes, large oscillatory shaft torques may result. As in the case of torsional interaction, a relatively slow oscillation growth rate would be expected.

3. Torque Amplification: this phenomenon occurs when a fault on a series compensated power system, and its subsequent clearing, results in a high-energy storage in the series capacitor banks, which then discharge their energy through a generator in the form of a current having a frequency that corresponds to one of the natural torsional frequencies of the turbine-generator mechanical system. Unlike torsional interaction and induction generator effect, the growth rate for torque amplification is high and oscillating shaft torques might be expected to reach a damaging level within 0.1 second. The ultimate hazard of SSR is a shaft fraction at full load and rated speed. The damage of such an occurrence cannot be accurately predicted, but extensive equipment damage could occur with a safety hazard to personnel. A more likely most-severe hazard would be crack initiation at the surface of one of the turbine-generator shafts, indicating fatigue and requiring shaft replacement, resulting in a unit outage of 90 days or more.

1.2.2 Flexible AC Transmission System

From the general point of view, the FACTS principle is mainly dependent on the advanced technologies of power electronic techniques and algorithms into the power system, to make it electronically controllable. FACTS Technology is concerned with the management of active and reactive power to improve the performance of electrical networks. The concept of FACTS technology embraces a wide variety of tasks related to both networks and consumers problems, especially related to power quality issues.

The availability of the modern semiconductor devices such as the Gate Turn-Off thyristor (GTO), and the Insulated Gate Bipolar Transistor (IGBT) [12], has led to the development of a new generation of power electric converters. These devices, unlike the conventional thyristors which have no intrinsic turn-off ability, are of the fully controlled type. The most common converters, which employ the self-commutating, high voltage, high current, and high switching frequency power electronic devices, are the Voltage Source Converters (VSCs).

A number of FACTS controllers which use VSCs as their basic building block have been already in operation in various parts of the world. The most popular controllers are: the Static Compensator (STATCOM) [15-16], the Static Synchronous Series Compensator (SSSC) [17-

18], the Unified Power Flow Controller (UPFC) [19-20], and the Voltage Source Converter High-Voltage Direct-Current (VSC HVDC) [21-23].

1.2.3 PWMSC

Fixed and controlled series compensators have been used for many years in transmission lines for compensating line reactance in order to increase power transfer capability and enhance the transient stability in power networks. One advantage of the series compensators is the use of a control scheme that varies effective series reactance. Thereinafter, this scheme can provide an effective means of active and reactive power flow control in a transmission line. Conventional series FACTS devices proposed in literature can be classified in two major groups:

1) Thyristor controlled reactance, and
2) Synchronous controllable voltage sources.

The first group is usually implemented with line commutated thyristors [24] while the second is based on force-commutated voltage source converters. However, in recent years new devices based on AC link converters have been proposed [25-27]. These do not require a DC link, and it is possible to reach similar objectives to those obtained by means of conventional FACTS devices. The series compensator considered in this paper is of the controlled reactance type which can be viewed as a PWM controlled capacitor. Such compensators have the advantage of being simpler in both power circuit structure and control.

This PWM-switched capacitor for series compensation is the dual of the shunt reactor switched by a PWM AC controller that is presented in [28]. A static phase-shifter is based on four switches.

PWM AC controller has also been discussed in literature [29]. In [25] the authors proposed the use of the PWM controlled capacitor to control active power on a transmission line with a simple structure that provides continuous control of the degree of series compensation by varying the duty cycle control.

A brief comparison of this PWMSC with the TCSC in small power system with three buses is presented in [26] where it is shown that the PWMSC is a smoother control alternative than the TCSC. A comparative evaluation between PWMSC and SSSC based on detailed

switching models is presented in [28] showing that the DC link converter requires about twice as much capacitive energy storage and about 66% additional semiconductor MVA rating rather than the AC link for the same application. Since no practical PWMSC has been built and installed on a real power system so far, an estimation of composed components cost for these two controllers are also considered in [28]. The authors show that the cost of SSSC is higher than that of PWMSC for that particular application. The paper also highlight that the use of AC capacitors enables PWMSC to operate at higher temperatures, in contrast to DC capacitors used in SSSC, which are quite vulnerable to high temperatures. The three-phase vector switching converter is proposed to develop FACTS controllers which can control power flow in transmission system. Authors have introduced a new FACTS device based on pulse width modulated ac link UPFC named Gamma controller. In [30-31], some studies of the effect of the AC link compensator on power system stability are presented. The formulation of power flow of the AC link compensators is analyzed at steady state performance in [30]. In these papers, it is shown that the compensator does not provide enough damping for certain contingencies. Based on these preliminary studies, a better current injection model for the PWMSC is proposed and studied in this paper [32].

1.2.4 Related Work and Scopes of the Thesis

Different methods are already employed by utilities for damping SSR oscillations including generator excitation control [3, 33], power system stabilizer [34, 35], static VAR compensator (SVC) [36-38] and static phase shifter [39]. In the recent years Flexible AC Transmission Systems (FACTS) controllers for instance Thyristor Controlled Series Capacitor (TCSC), Static Synchronous Series Compensator (SSSC), Unified Power Flow Controller (UPFC) and Gated Control Series Capacitors (GCSC) have been implemented to mitigate the SSR in power networks [40-43]. Among the FACTS device the TCSC is the most adaptable one [44] but both Thyristor Control Series Compensator (TCSC) and the GCSC, switches are gated at line frequencies. This results in the generations of low frequency line current harmonics. In addition the synchronization with the line frequency is required. SSR damping using a VSC based HVDC back-to-back system is performed in [45].

The drawbacks of SSSC, TCSC and GCSC can be mitigated or eliminated by replacing the ac controllers that switch at the line frequency with PWM ac controllers capable of switching at

frequencies significantly higher than line frequency, typically above 600 Hz for high power switches, such as GTOs, or higher for IGBTs. In [46] the three TCRs of a three –phase TCSC are replaced by three PWM ac controllers, employing four force-commutated switches per phase, or a total of 12 for the thee-phase unit. The synchronization with the ac mains may not be necessary if the switching frequency is high enough. The use of force-commuted switches allow operation at frequencies higher than that of the ac mains, thus resulting in the generation of high order harmonics only, around the switching frequencies and multiples.

Among the converter-based FACTS controllers, the PWMSC is regarded as one of the latest devices in the FACTS device family. It provides significant transient stability performance improvements over a wide range of power flow levels [47]. Its main features are a simple power structure, gating and control strategy [48]. One lead-lag controller has been used for controlling the system output. Optimization techniques can be used for obtaining the appropriate system parameters. Genetic Algorithm (GA) is one of the advance algorithms [49-52].

From the above literature review it is concluded that SSR is a severe dynamic problem in power system and the application of the PWMSC to the modern power system can solve the SSR problem and therefore lead to a more flexible, secure and economic operation of power system.

1.3 Thesis Objectives

The main objective of the thesis work is to investigate the feasibility of using PWMSC in the IEEE FBM to damp the SSR oscillations. The procedural steps to satisfy the objective are as follows:

1. Study the non-linear model of the IEEE First bench mark model (FBM) for SSR study.

2. Linearize the model using Taylor series expansion and obtain the state Matrix.

3. Develop the non-linear model of FBM with PWMSC for SSR study with associated control blocks and linearize the model using Taylor series expansion.

4. Use efficient parameter optimization algorithm for proper tuning of the controller gains.
5. Performance evaluation of the proposed PWMSC with tuned lead-lag controller for SSR damping in IEEE FBM system.

1.4 Outline of the Thesis

There are five chapters in this thesis. The main topics of each chapter are as follows:

Chapter 1 represents the background of the research study, literature survey, related works and thesis scopes and the objectives of the thesis. The total outline of the thesis is also presented in this chapter.

Chapter 2 presents a review of general power system stability, classification of stability and category of stability and provides current definitions of transient stability and small signal stability. Furthermore, the eigenvalue characteristics and participation factors are discussed elaborately. One of the advance optimization techniques, Genetic algorithm is also discussed.

Chapter 3 provides the small-signal analysis of subsynchronous resonance phenomenon without the controller. The computer simulation results are presented to show the eigenvalue and state of the modes for small signal analysis.

Chapter 4 describes the damping of subsynchronous resonance oscillations under small disturbances using PWMSC on system model. The computer simulation results are presented to show the eigenvalue and state of the modes for small signal analysis. Performance evaluation of the proposed PWMSC with tuned lead-lag controller for SSR damping in IEEE FBM system is done in this chapter for the critical compensation levels.

Chapter 5 concludes the whole work with a brief summary and some future suggestions.

“Appendices” part has got the list of values used in modeling, constants obtained in linearized model and values used for the system initial condition.

Chapter 2

General Stability Analysis of SMIB System

2.1 Introduction

In this chapter, we will study how to assess the stability of a power system, how to improve the stability and how to protect our system from moving to unstable system for subsynchronous resonance (SSR) oscillations. In order to do these issues, the present chapter includes a review of general concepts relating to power system stability devices in order to contextualize this research. The classification of stability problems in power grid along with the methods that have been proposed for its analysis is also summarized. For the optimal operation of the system a lead-lag controller is used as supplementary controller and optimized by optimization technique. Genetic Algorithm is used as optimization technique in this thesis, so a short discussion on Genetic Algorithm is presented at the end of this chapter.

2.2 Power System Stability

Several definitions for stability have been found in the literature [53-55]. Anderson et al [54] have mentioned that "**if the oscillatory response of a power system during the transient period following a disturbance is damped and the system settles in a finite time to a new steady operating condition, the system is called stable. If the system is not stable, it is considered to be unstable**".

Kundur [4] has defined it as "**the ability of the power system to maintain synchronism when subjected to a severe transient disturbance**". The resulting system response involves large excursions of generator rotor angles and is influenced by the non-linear power-angle relationship.

Singh [53] states it as "**the attribute of the system which enables it to develop restoring forces between the elements thereof, equal to or greater than the disturbing forces so as to restore a state of equilibrium between the elements**".

Classification of power system stability can be made based on the following considerations:

• The physical nature of the resulting mode of instability as indicated by the main system variable in which instability can be observed.

• The size of the disturbance considered which influences the method of calculation and prediction of stability.

• The devices, processes, and the time span that must be taken into consideration in order to assess stability.

Figure 2.1 gives the overall picture of the power system stability problem, identifying its categories and subcategories.

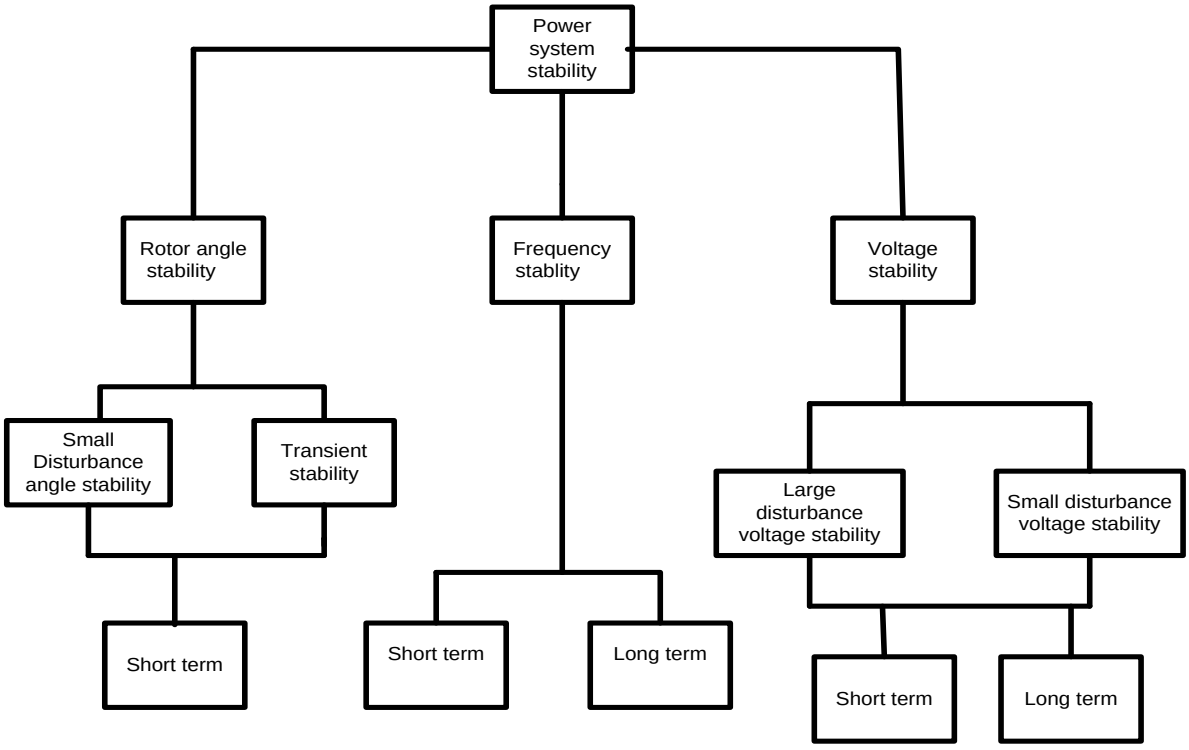

Figure 2.1: Classification of Power System Stability.

The stability problem involves the study of the electromechanical oscillations inherent in power systems. Under steady-state conditions, there is equilibrium between the input mechanical torque and the output electromagnetic torque of each generator, and the speed remains constant. If the system is perturbed, this equilibrium is upset, resulting in

acceleration or deceleration of the rotors of the machines according to the laws of motion of a rotating body. Instability results if the system cannot absorb the kinetic energy corresponding to these rotor speed differences. For any given situation, the stability of the system depends on whether or not the deviations in angular positions of the rotors result in sufficient restoring torques [56]. Loss of synchronism can occur between one machine and the rest of the system, or between groups of machines, with synchronism maintained within each group after separating from each other.

The change in electromagnetic torque of a synchronous machine following a perturbation can be resolved into two components:

• *Synchronizing torque component*, in phase with rotor angle deviation.

• *Damping torque component*, in phase with the speed deviation.

System stability depends on the existence of both components of torque for each of the synchronous machines.

2.2.1 Small Signal Stability

The small signal stability of a power system is concerned with the ability of the power system to maintain synchronism under small disturbances. The disturbances are considered to be sufficiently small that linearization of system equations is permissible for purposes of analysis. It depends only on the initial conditions and is of two types. Inadequate synchronizing torque results in non-oscillatory mode whereas insufficient damping torque causes rotor oscillations of increasing amplitude. The time frame of interest in small-disturbance stability studies is on the order of 10 to 20 seconds following a disturbance.

Transient stability is concerned with the ability of the power system to maintain synchronism when subjected to a severe disturbance, such as a short circuit on a transmission line. The resulting system response involves large excursions of generator rotor angles and is influenced by the nonlinear power-angle relationship. Unlike the small signal analysis it also depends on severity of the disturbance along with the initial operating states. Instability usually occurs due to insufficient synchronizing torque. The time frame of interest in transient stability studies is usually 3 to 5 seconds following the disturbance which may extend to 10–20 seconds for very large systems with dominant inter-area swings.

Examples of state variables of a power system are:

- synchronous and asynchronous machine rotor speeds
- synchronous machine load angles
- magnetic flux linkages
- controller state variables

If a disturbance causes a change in the value of one or more of these state variables, the system is driven from the equilibrium. If thereafter the system returns to its steady state, it is stable, whereas if the initial deviation from the steady state becomes ever larger, it is unstable. A further difference between transient stability and small signal stability is that if a steady state is reached after a disturbance leading to a transient phenomenon, i.e. a change in the system's topology, the new steady state can be different from the initial one. In contrast, if a system returns to a steady state after an incremental change in a state variable, this steady state is identical to the initial steady state, because no change in the network's topology has occurred.

2.2.2 Improving Rotor Angle Stability

According to [57] the rotor (power) angle stability of a power system can be enhanced, and its dynamic response improved, by correct system design and operation. For example, the following features help to improve stability:

- Use of protective equipment and circuit-breakers that ensure the fastest possible fault clearing;
- Use of single-pole circuit-breakers so that during single-phase faults only the faulted phase is cleared and the healthy phases remain intact;
- Use of a system configuration that is suitable for the particular operating conditions (e.g. avoiding long, heavily loaded transmission links);
- Ensuring an appropriate reserve in transmission capability;
- Avoiding operation of the system at low frequency and/or voltage;
- Avoid weakening the network by the simultaneous outage of a large number of lines and transformers.

Installation of the following devices/techniques has resulted in satisfactory improvement.

- Power System Stabilizers (PSS)
- Fast valving
- Braking Resistors
- Generator tripping
- Flexible AC Transmission system (FACTS) controllers

2.2.3 Characteristics of the Small Signal Stability Problems

Small signal stability problems may be either local or global in nature. Local problems involve a small part of the power system, and are usually associated with rotor angle oscillations of a single power plant against the rest of the power system. Such oscillations are called local plant mode oscillations. Stability (damping) of these oscillations depends on the strength of the transmission system as seen by the power plant, generator excitation control systems and plant output [4, 58-59]. Global problems are caused by interactions among large groups of generators and have widespread effects. They involve oscillations of a group of generators in one area swinging against a group of generators in another area. Such oscillations are called inter-area mode oscillations. Their characteristics are very complex and significantly differ from those of local plant mode oscillations. Load characteristics, in particular, have a major effect on the stability of inter-area modes [4, 58]. The time frame of interest in small-disturbance stability studies is on the order of 10 to 20 seconds following a disturbance.

2.3 Eigenvalues and Small Signal Stability

The main goal of this section is to figure out the correspondence between the eigenvalues of an electrical power system and its dynamic characteristics. First the linearization of the state equations of the power system will be discussed. After that, the correspondence between the eigenvalues of the state matrix which is the crucial part of the linearized description, and the time domain will be pointed out.

2.3.1 Linearization of State Equations for SSR

Modal Analysis

In this thesis the focus will be on modeling of IEEE first benchmark model for SSR study, which can be described by a set of First-order non-linear, ordinary algebraic-differential equations (DEA) of the following form [4, 59-60]:

$$\frac{dx_i}{dt} = f_i(x_1, x_2, \dots, x_n; z_1, z_2, \dots, z_m; u_1, u_2, \dots, u_r) \tag{2.1}$$

$$0 = g_i(x_1, x_2, \dots, x_n; z_1, z_2, \dots, z_m; u_1, u_2, \dots, u_r) \tag{2.2}$$

The mathematical model of a power system can be written as a set of DAE

$$\dot{x} = f(x, z, u) \tag{2.3}$$

$$y = g(x, z, u) \tag{2.4}$$

With

$$x = \begin{bmatrix} x_1 \\ x_2 \\ \vdots \\ x_n \end{bmatrix} \qquad z = \begin{bmatrix} z_1 \\ z_2 \\ \vdots \\ z_n \end{bmatrix} \qquad u = \begin{bmatrix} u_1 \\ u_2 \\ \vdots \\ u_n \end{bmatrix} \qquad f = \begin{bmatrix} f_1 \\ f_2 \\ \vdots \\ f_n \end{bmatrix} \qquad g = \begin{bmatrix} g_1 \\ g_2 \\ \vdots \\ g_n \end{bmatrix} \tag{2.5}$$

where

f is a vector containing n first-order non-linear differential equations

x is a vector containing n state variables

u is a vector containing r input variables

g is a vector containing n non-linear algebraic equations

z is a vector containing m algebraic variables

y is a vector containing m output variables

By assuming that the system in equation 2.3 is time invariant, i.e. the time derivatives of the state variables are not explicit functions of the time; *t* can be excluded from equation 2.3. In

small signal analysis, equations 2.3 and 2.4 can be linearized by a Taylor series expansion around an operating point (x_0, z_0, u_0) and the resulting linearized description of the system can be used to investigate its response to small variations in the input or state variables, starting at equilibrium point [4, 61-62]. Neglecting the terms of order two and above and eliminating the algebraic variables **z** just taking into account first-order terms, the system state matrix is obtained from derivations given below.

A procedure for small perturbations is established for *ith* component of vector **x.**

$$\dot{x}_1 = \dot{x}_{io} + \Delta\dot{x}_i = f_i[(x_0 + \Delta x_0), (u_0 + \Delta u_0)] \tag{2.6}$$

$$= f_i(x_0, u_0) + \frac{\partial f_i}{\partial u_i}\Delta x_i + \cdots + \frac{\partial f_i}{\partial u_n}\Delta x_n + \frac{\partial f_i}{\partial u_1}\Delta u_1 + \cdots + \frac{\partial f_i}{\partial u_r}\Delta u_r \tag{2.7}$$

From equation (2.3) it follows that

$$\dot{x}_{io} = f_i(x_0, u_0) \tag{2.8}$$

and therefore (2.7) can be written as

$$\Delta\dot{x}_i = \frac{\partial f_i}{\partial u_i}\Delta x_i + \cdots + \frac{\partial f_i}{\partial u_n}\Delta x_n + \frac{\partial f_i}{\partial u_1}\Delta u_1 + \cdots + \frac{\partial f_i}{\partial u_r}\Delta u_r \tag{2.9}$$

with $i = 1,2,\ldots,n$

The same can be done for the j^{th} component of y, with reference to (2.4),

$$\Delta\dot{y}_i = \frac{\partial g_j}{\partial x_1}\Delta x_1 + \cdots + \frac{\partial g_j}{\partial x_n}\Delta x_n + \frac{\partial g_j}{\partial u_1}\Delta u_1 + \cdots + \frac{\partial g_j}{\partial u_r}\Delta u_r \tag{2.10}$$

with $j = 1,2,\ldots,n$

The prefix Δ denotes a small deviation, thus

$\Delta x = x - x_0$ $\Delta y = y - y_0$ $\Delta u = u - u_0$

Doing this for all components of the vectors **x** and **y** gives the following linearized set of the state and output equations

$$\Delta\dot{\mathbf{x}} = \mathbf{A}\Delta\mathbf{x} + \mathbf{B}\Delta\mathbf{u} \tag{2.11}$$

$$\Delta\mathbf{y} = \mathbf{C}\Delta\mathbf{x} + \mathbf{D}\Delta\mathbf{u} \tag{2.12}$$

with

$$\boldsymbol{A} = \begin{bmatrix} \frac{\partial f_1}{\partial x_1} & \cdots & \frac{\partial f_1}{\partial x_n} \\ \vdots & \ddots & \vdots \\ \frac{\partial f_n}{\partial x_1} & \cdots & \frac{\partial f_n}{\partial x_n} \end{bmatrix} \qquad \boldsymbol{B} = \begin{bmatrix} \frac{\partial f_1}{\partial u_1} & \cdots & \frac{\partial f_1}{\partial u_r} \\ \vdots & \ddots & \vdots \\ \frac{\partial f_n}{\partial u_1} & \cdots & \frac{\partial f_n}{\partial u_r} \end{bmatrix}$$

$$\boldsymbol{C} = \begin{bmatrix} \frac{\partial g_1}{\partial x_1} & \cdots & \frac{\partial g_1}{\partial x_n} \\ \vdots & \ddots & \vdots \\ \frac{\partial g_m}{\partial x_1} & \cdots & \frac{\partial g_m}{\partial x_n} \end{bmatrix} \qquad \boldsymbol{D} = \begin{bmatrix} \frac{\partial g_1}{\partial u_1} & \cdots & \frac{\partial g_1}{\partial u_r} \\ \vdots & \ddots & \vdots \\ \frac{\partial g_m}{\partial u_1} & \cdots & \frac{\partial g_m}{\partial u_r} \end{bmatrix}$$

(2.13)

Thus, the matrices **A**, **B**, **C** and **D** contain the partial derivatives of the functions in **f** and **g** to the state variables **x** and the input variables **u**. Matrix **A** is the state matrix of the system. Equations ((2.11) and (2.12)) can be Laplace transformed to obtain the state equations in the frequency domain. Take the Laplace transform assuming zero initial conditions

$$s\,\Delta x(s) - \Delta x(0) = \mathbf{A}\,\Delta x(s) + \mathbf{B}\,\Delta u(s) \tag{2.14}$$

$$\Delta y(s) = \mathbf{C}\,\Delta x(s) + \mathbf{D}\,\Delta u(s) \tag{2.15}$$

A solution to the state equations can be obtained by rearranging the upper equation of (2.14) & (2.15) as follows

$$(s\mathbf{I} - \mathbf{A})\,\Delta x(0) + \mathbf{B}\,\Delta u(s) \tag{2.16}$$

I is the identity matrix and the values of s which satisfy

$$\det(s\mathbf{I} - \mathbf{A}) = 0 \tag{2.17}$$

are known as the eigenvalues of matrix A.

2.3.2 Eigenvalues

Eigenvalue is a scalar associated with a given linear transformation of a vector space and having the property that there is some nonzero vector which when multiplied by the scalar is equal to the vector obtained by letting the transformation operate on the vector; *especially* it is the root of the characteristic equation of a matrix.

2.3.3 Properties of Eigenvalues

In small signal stability analysis the properties of the system equations ((2.11), (2.12)) around operating point (x_0, $z_{0,}$ y_0), studied through an eigenvalue analysis of the state matrix **A**. The study determines the time domain response of the system to small perturbations, and therefore contains important information's on the dynamic behavior of the system under study condition called mode, which is obtained from **A** matrix**.**

For a system to be stable the real parts of all eigenvalues of the state matrix **A** has to be negative and must lie in the left half-plane of the complex plane. An eigenvalue with a negative real part ensures that oscillations will decay with time and will return to a steady state following a small disturbance. The opposite will occur if an eigenvalue has a positive real part. The amplitude of the modes will increase exponentially and the power system will be unstable at that operating point.

If **A** is real, complex eigenvalue occur in conjugate pairs, and each pair would correspond to an oscillatory mode. Figure 2.2 shows the possible natural modes of a system. The eigenvalues of **A** contain essential information about the mode's frequencies and their damping after a small disturbance. The real part component gives the damping and the imaginary component gives the frequency of oscillation.

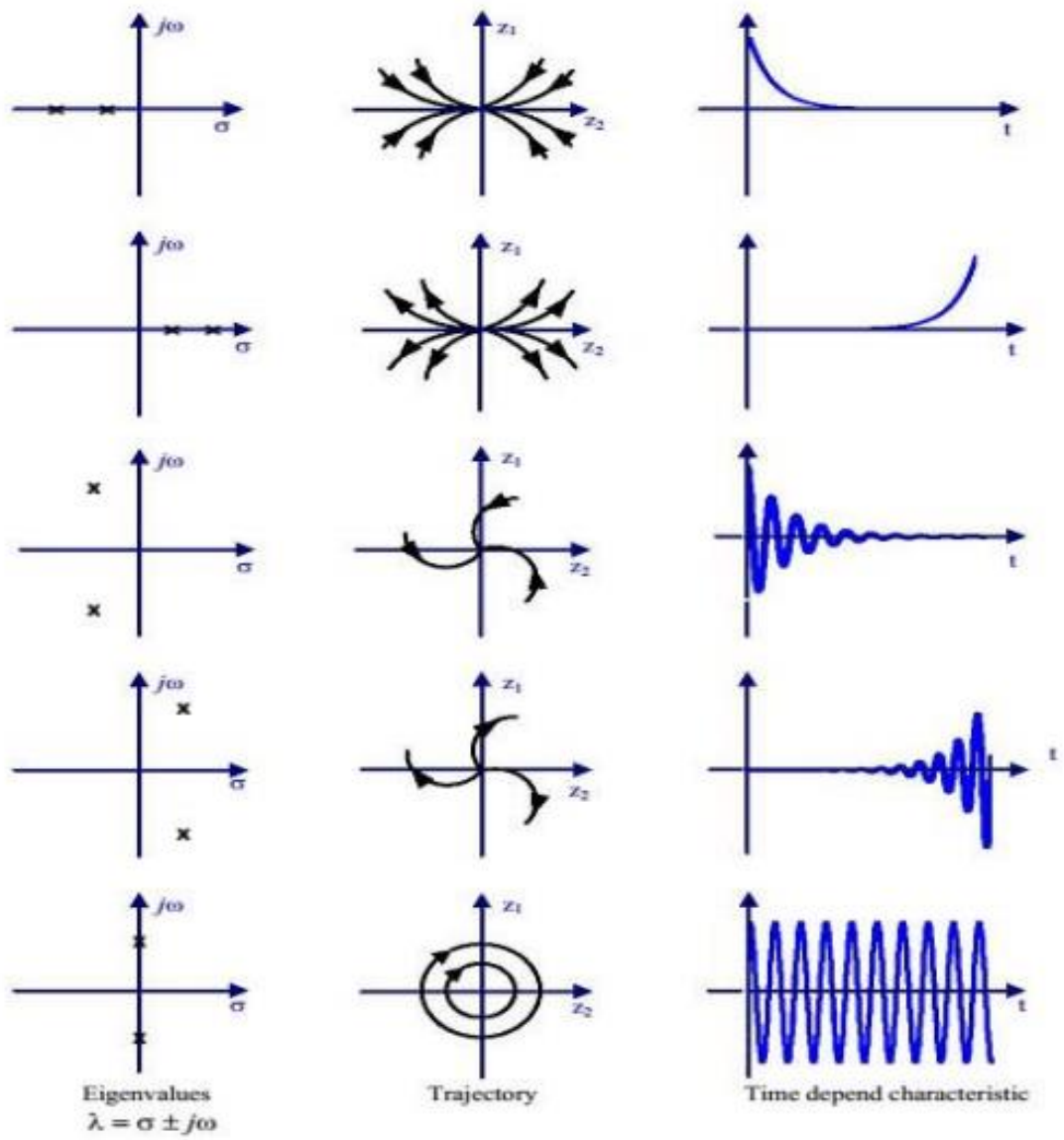

Figure 2.2: Possible combination of eigenvalues pairs (left) and their trajectories (middle) and time responses (right).

Stability behavior of the system model from Eigen value analysis is like this:

- **The Eigen values are real numbers.**

1. Eigen values both positive

Unstable: All trajectories in the neighborhood of the fixed point will be directed outwards and away from the fixed point.

2. Eigen values both negative

Stable: All trajectories in the neighborhood of the fixed point will be directed towards the fixed point.

3. Eigen values opposite sign

Unstable: Trajectories in the general direction of the negative eigen value's eigenvector will initially approach the fixed point but will diverge as they approach a region dominated by the positive (unstable) eigen value.

- **Eigen values are complex conjugates**

1. Real parts positive

Unstable: All trajectories in the neighborhood of the fixed point spiral away from the fixed point with ever increasing radius.

2. Real parts negative

Stable: All trajectories in the neighborhood of the fixed point spiral into the fixed point with ever decreasing radius.

2.3.4 Eigenvalues and Eigenvectors Formulation

It can be shown that for any eigenvalue λ, a left and right eigenvector $\mathbf{\Psi}$ and $\mathbf{\Phi}$ can be calculated, such that

$$\mathbf{A}\Phi = \lambda\Psi$$

$$\Psi\mathbf{A} = \lambda\Phi \tag{2.18}$$

$\mathbf{\Phi}$ is a vector with *n* rows and $\mathbf{\Psi}$ is a vector with *n* columns. According to the upper equation of ((2.11), (2.12)), if no inputs are applied, the system is described by

$$\Delta\dot{x} = \mathbf{A}\Delta x \tag{2.19}$$

In this equation, the states are coupled, which means that they influence each other. It is hence difficult to draw conclusions with respect to the system behavior. Therefore, the eigenvalues are put onto the diagonal of a matrix Λ, the transposed right eigenvectors are

turned into the columns of a matrix **Ψ**, and the left eigenvectors are turned into the columns of a matrix **Φ ,** after which the following transformation is applied

$$\Delta x = \Phi z \tag{2.20}$$

Substituting this into equation (2.18) gives

$$\Phi \dot{z} = \mathbf{A}\Phi z \tag{2.21}$$

When the individual eigenvalues in the upper equation of (2.18) are replaced by the diagonal matrix Λ and both sides of the equations are multiplied the inverse of **Φ**, the following is true

$$\mathbf{A}\Phi = \Phi A$$

$$\Phi^{-1}\mathbf{A}\Phi = \Lambda \tag{2.22}$$

Using the second equation together with (2.21), it can be seen that

$$\dot{z} = \mathbf{A}z \tag{2.23}$$

Because the matrix Λ is diagonal, it represents *n* uncoupled algebraic equations of the form

$$\dot{z}_i = \lambda_i z_i \tag{2.24}$$

An equation of this form can be easily transformed back to the time domain, yielding

$$z_i(t) = z_i(0)e^{\lambda_i t} \tag{2.25}$$

Again using the transformation in equation (2.20) results in

$$\Delta x(t) = \Phi z(t) \tag{2.26}$$

In which **z** contains the *n* equations as given in (2.25).

This can be written as

$$\Delta x(t) = \sum_{i=1}^{n} \Phi_i z_i(0)\, e^{\lambda_i t} \tag{2.27}$$

It can be shown that the inverse of the matrix **Φ**, containing the left eigenvectors as columns, is the matrix **Ψ**, containing the transposed right eigenvectors as columns.

Thus, using equation (2.26)

$$z(t) = \Psi \Delta x(t) \tag{2.28}$$

and with $t = 0$

$$z(0) = \Psi \Delta x(0) \tag{2.29}$$

The scalar product of Ψ_i and $\Delta x(0)$ can be replaced by C_i . With equation (2.28), this results in

$$\Delta x(t) = \sum_{i=1}^{n} \Phi_i z_i(0)\, e^{\lambda_i t} \tag{2.30}$$

Thus, the time response of the ith state variable is given by

$$\Delta x_i(t) = \Phi_{i1} c_1 e^{\lambda_1 t} + \cdots + \Phi_{in} c_n e^{\lambda_n t} \tag{2.31}$$

and it has been shown that the eigenvalues of the linearized system matrix determine the time domain response of the system to a perturbation, as was the aim of this discussion. If the eigenvalues are complex, in the case of real physical systems they always occur in pairs that are complex conjugates. Therefore, the imaginary parts cancel each other and equation (2.31) is real. Equation (2.31) clearly illustrates the well-known fact that the real part of an eigenvalue has to be negative for a system to be stable [4].

2.4 Damping Ratio and Oscillation Frequency

For the eigenvalues $\lambda = \sigma \pm j\omega$ of matrix A the damping ration σ is the defined as

$$\xi_i = -\frac{\sigma}{\sqrt{\sigma_i^2 + \omega_i^2}} \tag{2.32}$$

With $\xi \in [-1,1]$

The damping ratio ξ determines the rate of decay of the amplitude of the oscillation. The time constant τ of the amplitude decay is $\tau = 1/|\sigma|$ [4, 62]

The mechanical part of synchronous system is intrinsically prone to weakly damped oscillations; it doesn't affect the rotor speed oscillations. Therefor the damping of rotor speed oscillations comes from damper winding, the controller of the machines and the rest of power

system. However, the lower the frequency the less damping is provided by the damper winding. Because power system oscillations have frequencies in the order of few Hz and lower and rather small amplitude, so hardly any damping is provided by damper winding. Small signal stability is strongly related to the damping of system oscillations, which discussed by several researchers [63-66].

The oscillation frequency f of the i^{th} mode, in Hz, is defined as

$$f_i = \frac{\omega}{2\pi} \tag{2.33}$$

2.5 Participation Factors

Participation factors are non-dimensional scalars that measure the relative contribution of system modes to system states, and of system states to system modes, for linear system. Participation factors helps us to obtain the influence of state on modes, because then we will know which states machines should be controlled in order to increase damping of a certain problem.

The participation matrix **$\mathbf{P_f}$,** proposed in [67-68] is defined as:

$$\Psi_{jk}^{T}\Phi_{jk} = [\Psi_{1j} \quad \Psi_{2j} \quad \dots \quad \Psi_{nj}]\begin{bmatrix}\Phi_{j1}\\ \Phi_{j2}\\ \Phi_{j3}\\ \Phi_{j4}\end{bmatrix} \tag{2.34}$$

We may express the above vector product as a summation.

$$\Psi_{jk}^{T}\Phi_{jk} = \sum_{j=1}^{n}\Psi_{kj}\Phi_{jk} \tag{2.35}$$

After some steps we will obtain

$$\xi_k = \left[\Psi_{ki}^{T}x_j(0)\right]\left[\sum_{j=1}^{n}\Psi_{kj}\Phi_{jk}\right]e^{\lambda_k}t \tag{2.36}$$

Now we are in a position to make a definition of participation factor

$$P_{jk} = \Psi_{kj}\Phi_{jk} \tag{2.37}$$

Substitution of eq. (2.36) in eq. (2.37) results

$$\xi_k = \left[\Psi_{ki}^T x_j(0)\right]\left[\sum_{j=1}^{n} P_{fjk}\right] \tag{2.38}$$

The participation factor $\boldsymbol{P_{fjk}}$ indicates the participation (influence) of the j^{th} state in the k^{th} mode. The participation factor is extremely useful. Consider that through eigenvalue calculation and/or time-domain simulation it is learnt that mode k is a "problem mode," i.e., it is marginally damped or negatively damped. Then one can identify what to do about this is by inspecting the participation factors for this mode.

2.6 Optimization Theory

Optimization is the act of obtaining the best result under given circumstances. The word 'optimum' is taken to mean 'maximum' or 'minimum' depending on the circumstances. In design, construction, and maintenance of any engineering system, engineers have to take many technological and managerial decisions at several stages. The ultimate goal of all such decisions is either to minimize the effort required or to maximize the desired benefit. Since the effort required or the benefit desired in any practical situation can be expressed as a function of certain decision variables, so optimization can be defined as the process of finding the conditions that give the minimum or maximum value of a function, where the function represents the effort required or the desired benefit.

2.6.1 Advanced Technique of Optimization:

Many difficulties such as multi-modality, dimensionality and differentiability are associated with the optimization of large-scale problems. Traditional techniques such as steepest decent, linear programing and dynamic programing generally fail to solve such large-scale problems especially with nonlinear objective functions. Most of the traditional techniques require gradient information and hence it is not possible to solve non-differentiable functions with the help of such traditional techniques. Moreover, such techniques often fail to solve optimization problems that have many local optima. To overcome these problems, there is a need to develop more powerful optimization techniques which is called advanced technique of optimization. Research is still going on to find more effective optimization techniques.

Some of the well-known population-based advanced optimization techniques developed during last three decades are: Genetic Algorithms (GA) [31,69]which works on the principle of the Darwinian theory of the survival-of-the fittest and the theory of evolution of the living beings; Artificial Immune Algorithms (AIA) [70] which works on the principle of immune system of the human being; Particle Swarm Optimization (PSO) [71] which works on the principle of foraging behavior of the swarm of birds; Differential Evolution (DE) [72] which is similar to GA with specialized crossover and selection method; Bacteria Foraging Optimization (BFO) [73] which works on the principle of behavior of bacteria; Shuffled Frog Leaping (SFL) [74] which works on the principle of communication among the frogs, Artificial Bee Colony (ABC) [75] which works on the principle of foraging behavior of a honey bee; Biogeography-Based Optimization (BBO) [76] which works on the principle of immigration and emigration of the species from one place to the other; Gravitational Search Algorithm (GSA) [77] which works on the principle of gravitational force acting between the bodies and Grenade Explosion Method (GEM) [78] which works on the principle of explosion of grenade. These algorithms have been applied to many engineering optimization problems and proved effective to solve some specific kind of problems.

2.6.2 Genetic Algorithm

Among the other optimization techniques we have chosen genetic algorithm for our research. A genetic algorithm is a search technique used in finding true or approximate solutions to optimization and search problems. Genetic algorithms are categorized as global search heuristics. Genetic algorithms form particular class of evolutionary algorithms that use techniques inspired by evolutionary biology such as inheritance, mutation, selection and crossover (also called recombination). Genetic Algorithms are implemented as a computer simulation in which a population of abstract representations (called chromosomes or the genotype or the genome) of candidate solutions (called individuals, creatures, or prototypes) to an optimization problem evolves toward better solutions. Traditionally, solutions are represented in binary strings of 0s and 1s, but other encodings are also possible. The evolution usually starts from a population of randomly generated individuals. Genetic algorithms form on of the best ways to solve a problem for which a little is known. They are very general algorithms that work well in any search space. A genetic algorithm is able to create a high quality solution [79].

2.6.3 Fitness Function

A fitness function is a particular type of objective function that is used to summarize, as a single figure of merit, how close a given design solution is to achieve the set aims. In the GA each individual within the population is assigned a fitness value, which express how good the solution is at solving the problem. The fitness value probabilistically determines how successful the individual will be at propagating it genes (its code) to subsequent generations. Better solutions are assigned higher values of fitness than worse performing solutions.

2.6.4 Selection

The selection procedure implements the natural selection or the survival-of-the fittest principle and selects good individuals out of the current population for generating the next population according to the assigned fitness. For example: choosing two parents from the population for crossing. After deciding on an encoding, the next step is to decide how to perform selection. Darwin stated in his theory of evolution that best ones survive to create new offspring. Selection is a method that randomly picks chromosomes out of the population according to their evaluation function. The higher the fitness function, the more chance an individual will be selected. Four common methods for selection are: 1. Roulette Wheel selection, 2. Stochastic Universal sampling, 3. Normalized geometric selection and 4. Tournament selection. After selection, crossover and mutation recombine and alter parts of the individuals to generate new solutions.

2.6.5 Crossover

Crossover is a genetic recombination operator that combines two parents (chromosomes) to form children (offspring) for the next generation. The children are different from their parents but which inherit apportion of their parents' genetic materials. The main idea behind crossover is that the new chromosome may be better than both of parents (mates) if it takes best characteristics from each of the parents. Typically this operator is applied at a rate of 60% to 80% of the population, and the crossover point and each pair is randomly selected [80]. Various forms of crossover operator have been developed. The simplest form, single point crossover, is illustrated in figure 2.3. When using one-point crossover, only one crossover point is chosen at random. For example let there be two parents choses a random position in the genetic coding, and exchange genetic information to the right of this points, thus creating two new offspring.

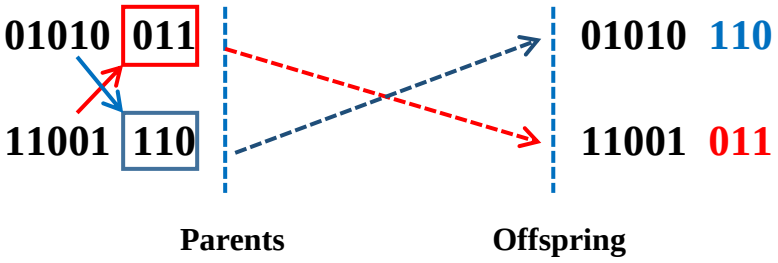

Figure 2.3: Single point crossover

2.6.6 Mutation

After crossover, the strings are subjected to mutation. Mutations are applying random changes to individual parents (chromosomes) to form children (offspring). It helps to keep diversity in the population by discovering new or recovering the lost genetic materials by searching the neighborhood solution space. Despite the fact that mutation can serve a vital role in a genetic algorithm, it prevents the algorithm to be trapped in a local minimum. For a binary encoding, this involves swapping gene 1 for gene 0 with small probability (typically at the rate of 0.1% to 10%) [80] of each bit in the chromosome as shown in the figure 2.4.

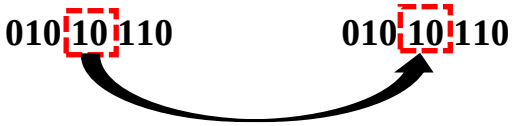

Figure 2.4: Binary mutation operator

2.7 Summary:

In this chapter the stability of a power system is discussed. Some basic working principle of Genetic Algorithm is studied as well. The linear model of the IEEE first benchmark model will be studied and the dynamic model of PWMSC and the linear model pf IEEE FBM will be developed in the upcoming chapters. The performance of the IEEE FBM with PWMSC and without PWMSC will also be evaluated by the eigen value analysis and the time domain simulation in the next chapters.

Chapter 3

Small-signal Analysis of Subsynchronous Resonance Phenomenon

3.1 Introduction

The differential and algebraic equations which describe the dynamic performance of the synchronous machine and the transmission network are, in general, nonlinear. For the purpose of stability analysis, these equations may be linearized by assuming that a disturbance is considered to be small. Small-signal analysis using linear techniques provides valuable information about the inherent dynamic characteristics of the power system and assists in its design. This chapter presents an analytical method useful in the study of small-signal analysis of subsynchronous resonance (SSR), establishes a linearized model for the power system, and performs the analysis of the SSR using the eigenvalue technique. It is believed that by studying the small-signal stability of the power system, the engineer will be able to find countermeasures to damp all subsynchronous torsional oscillations.

3.2 Small-Signal Analysis Study System

The system used in the small-signal analysis of SSR in this thesis is the IEEE first benchmark model for computer simulation of subsynchronous resonance [81]. This system, shown in Figure 3.1, consists of a single series-capacitor compensated transmission line connecting a large turbine-generator to a large system. The shaft system of the turbine-generator unit consists of a high-pressure turbine (HP), an intermediate-pressure turbine (IP), two low pressure turbines (LPA & LPB), the generator rotor (GEN), and its rotating exciter (EXC). The system data and the initial operating conditions of the system are given in Appendix A.

3.2.1 Power System Modeling

The nonlinear differential equations of the system under study are derived by developing individually the mathematical models which represent the various components of the system, namely the synchronous machine, the turbine-generator mechanical system, the governor

system, the excitation system, and the transmission line. Knowing the mutual interaction among these models, the whole system differential equations can be formed.

3.2.2 Modeling of the Synchronous Machine

Figure 3.2 shows a schematic diagram of a conventional synchronous machine [4, 82]. The stator circuit consists of a three-phase winding produces a sinusoidally space distributed magnetomotive force. The rotor of the machine carries the field (excitation) winding which is excited by a dc voltage. The electrical damping due to the eddy currents in the solid rotor and, if present, the damper winding is represented by three equivalent damper circuits; one on the direct axis (d-axis) and the other two on the quadrature axis (q-axis). The performance of the synchronous machine can be described by the equations given below in the d-q reference frame [4]. In these equations, the convention adopted for the signs of the voltages and currents are that *v* is the impressed voltage at the terminals and that the direction of positive current *i* corresponds to generation. The sign of the currents in the equivalent damper windings is taken positive when they flow in a direction similar to that of the positive field current.

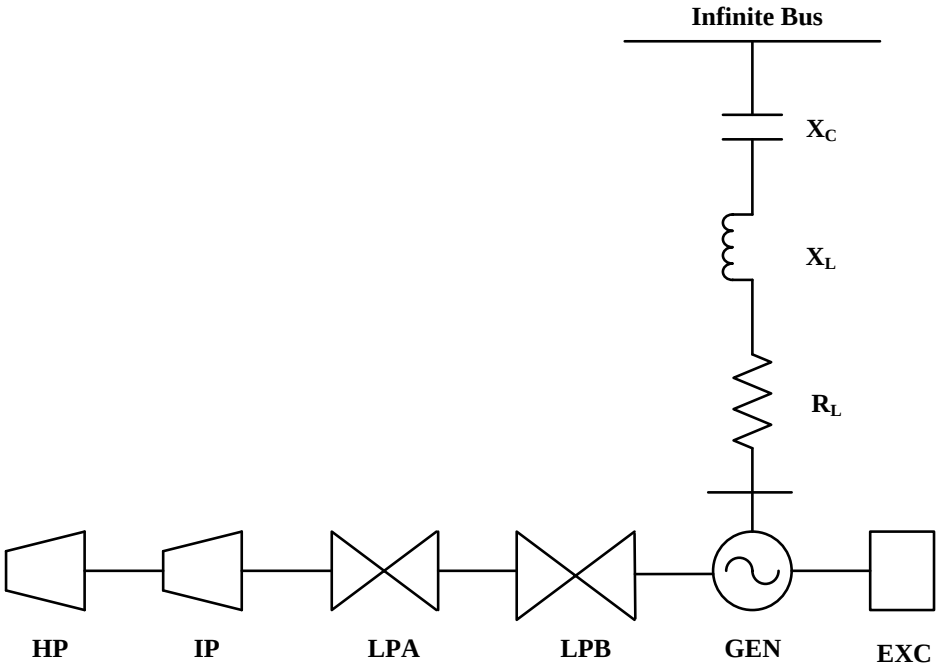

Figure 3.1: The IEEE first benchmark model for computer simulation of subsynchronous resonance.

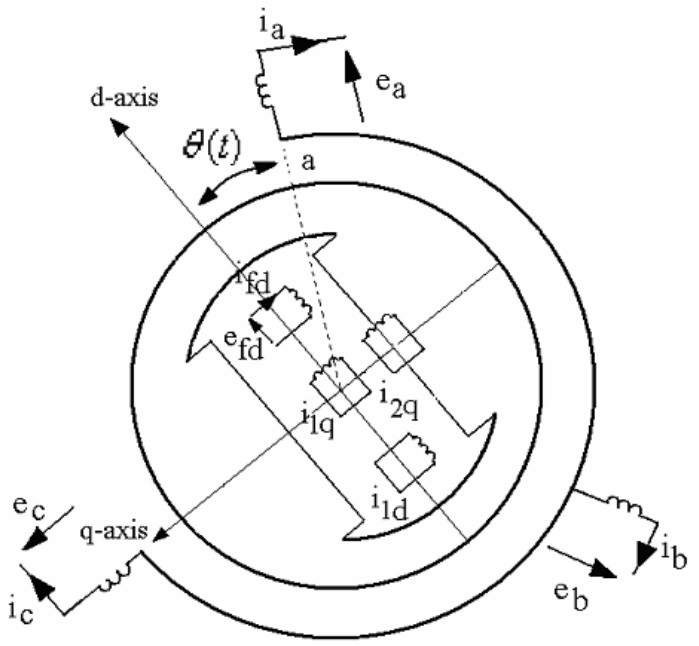

Figure 3.2: Schematic diagram of a conventional synchronous machine.

In this figure,

a, b, c: Stator three-phase winding

fd: Field (excitation) winding

e_{fd}: Field voltage

1d: d-axis damper winding

1q: The first q-axis damper winding

2q: The second q-axis damper winding

θ*(t)*: Angle by which the d-axis leads the magnetic axis of phase a winding, electrical rad.

With time *t* expressed in seconds, the angular velocity ω expressed in rad/s (ω_0 = 377 rad / sec) and the other quantities expressed in per unit, the stator equations become:

$$e_d = \frac{1}{\omega_0}\frac{d\Psi_d}{dt} - \frac{\omega}{\omega_0}\Psi_q - R_a i_d$$

$$e_q = \frac{1}{\omega_0}\frac{d\Psi_q}{dt} + \frac{\omega}{\omega_0}\Psi_d - R_a i_d$$

The rotor equations:

$$e_{fd} = \frac{1}{\omega_0}\frac{d\Psi_{fd}}{dt} + R_{fd}i_{fd}$$

$$0 = \frac{1}{\omega_0}\frac{d\Psi_{1d}}{dt} + R_{1d}i_{1d}$$

$$0 = \frac{1}{\omega_0}\frac{d\Psi_{1q}}{dt} + R_{1q}i_{1q}$$

$$0 = \frac{1}{\omega_0}\frac{d\Psi_{2q}}{dt} + R_{2q}i_{2q}$$

The stator flux linkage equations:

$$\Psi_d = -L_d\, i_d \; + \; L_{ad}i_{fd} + L_{ad}i_{1d}$$

$$\Psi_q = -L_d\, i_d \; + \; L_{ad}i_{fd} + L_{ad}i_{1d}$$

The rotor flux linkage equations:

$$\Psi_{fd} = -L_{ffd}\, i_{fd} \; + \; L_{ad}i_{1d} - L_{ad}i_d$$

$$\Psi_{1d} = -L_{ad}\, i_{fd} \; + \; L_{11d}i_{1d} - L_{ad}i_d$$

$$\Psi_{1q} = -L_{11q}\, i_{1q} \; + \; L_{aq}i_{2q} - L_{aq}i_q$$

$$\Psi_{2q} = -L_{aq}\, i_{1q} \; + \; L_{22q}i_{2q} - L_{aq}i_q$$

The air-gap torque equation:

$$T_e = -\Psi_d\, i_q \; - \; \Psi_q i_d$$

The overall differential equations which describe the transient performance of the synchronous machine are given by the following matrix equation:

$$\left[\frac{dX_{syn}}{dt}\right] = \left[At_{syn}\right]\left[X_{syn}\right] + \left[Bt_{syn}\right]\begin{bmatrix} V_{td} \\ V_{tq} \\ e_{fd} \end{bmatrix} \qquad (3.1)$$

Where

$$\left[X_{syn}\right] = [\, i_d \quad i_q \quad i_{fd} \quad i_{1q} \quad i_{1d} \quad i_{2q}\,]^T$$

$$\left[At_{syn}\right] = [L]^{-1}\,[Qt]$$

$$\left[Bt_{syn}\right] = [L]^{-1}\,[Rt]$$

$$[L] = \begin{bmatrix} -L_d & 0 & L_{ad} & 0 & L_{ad} & 0 \\ 0 & -L_q & 0 & L_{aq} & 0 & L_{aq} \\ -L_{ad} & 0 & L_{ffd} & 0 & L_{ad} & 0 \\ 0 & -L_{aq} & 0 & L_{11q} & 0 & L_{aq} \\ -L_{ad} & 0 & L_{ad} & 0 & L_{11d} & L_{aq} \\ 0 & -L_{aq} & 0 & L_{aq} & 0 & L_{22q} \end{bmatrix} \tag{3.2}$$

$$[Qt] = \begin{bmatrix} \omega_0 R_a & -\omega L_q & 0 & \omega L_{aq} & 0 & \omega L_{aq} \\ \omega L_d & \omega_0 R_a & -\omega L_{ad} & 0 & -\omega L_{ad} & 0 \\ 0 & 0 & -\omega_0 R_{ffd} & 0 & 0 & 0 \\ 0 & 0 & 0 & -\omega_0 R_{1q} & 0 & 0 \\ 0 & 0 & 0 & 0 & -\omega_0 R_{1d} & 0 \\ 0 & 0 & 0 & L_{aq} & 0 & -\omega_0 R_{2d} \end{bmatrix}$$

$$[Rt] = \begin{bmatrix} \omega_0 & 0 & 0 \\ 0 & \omega_0 & 0 \\ 0 & 0 & \omega_0 \\ 0 & 0 & 0 \\ 0 & 0 & 0 \\ 0 & 0 & 0 \end{bmatrix}$$

here subscript ^{T} means matrix transpose.

Linearized and rearranged Equation (3.1) is written as

$$\left[\frac{d\Delta X_{syn}}{dt}\right] = \left[A_{syn}\right]\left[\Delta X_{syn}\right] + \left[B_{syn}\right]\left[\Delta U_{syn}\right] \tag{3.3}$$

where

$$\left[\Delta X_{syn}\right] = [\Delta i_d \quad \Delta i_q \quad \Delta i_{fd} \quad \Delta i_{1q} \quad \Delta i_{1d} \quad \Delta i_{2q}\,]^T$$

$$\left[\Delta U_{syn}\right] = [\Delta V_{td} \quad \Delta V_{tq} \quad \Delta e_{fd} \quad \Delta\omega]^T$$

$$\left[A_{syn}\right] = [L]^{-1}\,[Q]$$

$$\left[B_{syn}\right] = [L]^{-1}\,[R]$$

$[L]$: same as in equation (3.2) (3.4)

$$[Q] = \omega_0 \begin{bmatrix} R_a & -L_q & 0 & L_{aq} & 0 & L_{aq} \\ L_d & R_a & -L_{ad} & 0 & -L_{ad} & 0 \\ 0 & 0 & -R_{ffd} & 0 & 0 & 0 \\ 0 & 0 & 0 & -R_{1q} & 0 & 0 \\ 0 & 0 & 0 & 0 & -R_{1d} & 0 \\ 0 & 0 & 0 & L_{aq} & 0 & -R_{2d} \end{bmatrix}$$

$$[R] = \begin{bmatrix} \omega_0 & 0 & 0 & \Psi_{q0} \\ 0 & \omega_0 & 0 & -\Psi_{q0} \\ 0 & 0 & \omega_0 & 0 \\ 0 & 0 & 0 & 0 \\ 0 & 0 & 0 & 0 \\ 0 & 0 & 0 & 0 \end{bmatrix}$$

3.2.3 Modeling of the Transmission line

A series capacitor-compensated transmission line [3, 83] may be represented by the *RLC* circuit shown in Figure 3.3. In the voltage phasor diagram shown in Figure 3.4, the rotor angle δ is the angle (in elec. Rad) by which the q-axis leads the reference voltage V_b. The differential equations for the circuit elements, after applying Park's transformation [4], can be expressed in the d-q reference frame by the following matrix expressions.

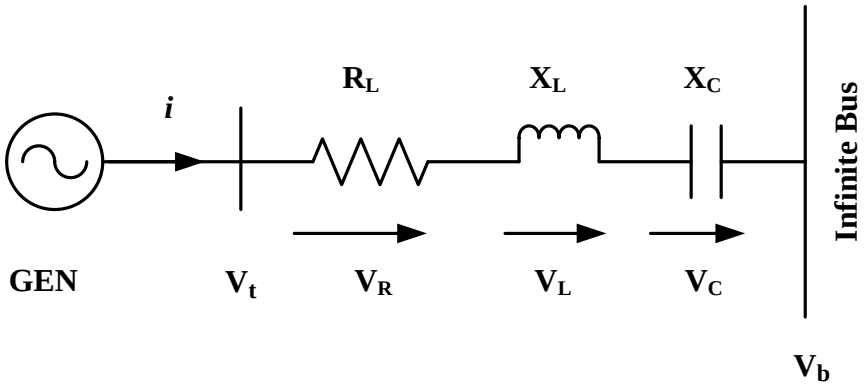

Figure 3.3: A series capacitor-compensated transmission line.

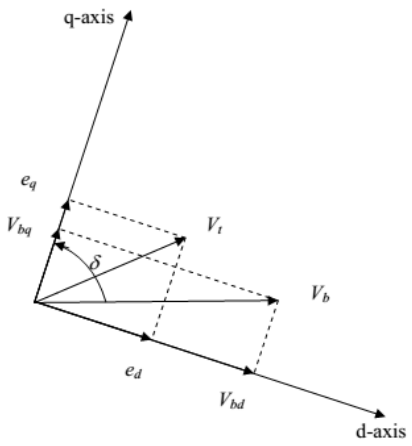

Figure 3.4: Voltage phasor diagram.

The voltage across the resistance:

$$\begin{bmatrix} V_{Rd} \\ V_{Rq} \end{bmatrix} = \begin{bmatrix} R_L & 0 \\ 0 & R_L \end{bmatrix} \begin{bmatrix} i_d \\ i_q \end{bmatrix} \tag{3.5}$$

The voltage across the inductance:

$$\begin{bmatrix} V_{Ld} \\ V_{Lq} \end{bmatrix} = \begin{bmatrix} 0 & -\frac{\omega}{\omega_0} X_L \\ \frac{\omega}{\omega_0} X_L & 0 \end{bmatrix} \begin{bmatrix} i_d \\ i_q \end{bmatrix} + \begin{bmatrix} \frac{X_L}{\omega_0} & 0 \\ 0 & \frac{X_L}{\omega_0} \end{bmatrix} \begin{bmatrix} \frac{di_d}{dt} \\ \frac{di_q}{dt} \end{bmatrix} \tag{3.6}$$

The voltage across the inductance:

$$\begin{bmatrix} \frac{dV_{Cd}}{dt} \\ \frac{dV_{Cq}}{dt} \end{bmatrix} = \begin{bmatrix} \omega_0 X_C & 0 \\ 0 & \omega_0 X_C \end{bmatrix} \begin{bmatrix} i_d \\ i_q \end{bmatrix} + \begin{bmatrix} 0 & \omega \\ -\omega & 0 \end{bmatrix} \begin{bmatrix} V_{Cd} \\ V_{Cq} \end{bmatrix} \tag{3.7}$$

The overall equations of the transmission line can be written as

$$\begin{bmatrix} \frac{dV_{Cd}}{dt} \\ \frac{dV_{Cq}}{dt} \\ V_{td} \\ V_{tq} \end{bmatrix} = [Att] \begin{bmatrix} V_{Cd} \\ V_{Cq} \end{bmatrix} + [Rt1] \begin{bmatrix} \frac{di_d}{dt} \\ \frac{di_q}{dt} \end{bmatrix} + [Rt2] \begin{bmatrix} i_d \\ i_q \end{bmatrix} + [Btt][V_b] \tag{3.8}$$

where

$$[Att] = \begin{bmatrix} 0 & \omega \\ -\omega & 0 \\ 1 & 0 \\ 0 & 1 \end{bmatrix}$$

$$[Rt1] = \begin{bmatrix} 0 & 0 \\ 0 & 0 \\ \frac{X_L}{\omega_0} & 0 \\ 0 & \frac{X_L}{\omega_0} \end{bmatrix}$$

$$[Rt2] = \begin{bmatrix} \omega_0 X_C & 0 \\ 0 & \omega_0 X_C \\ R_L & -\frac{\omega}{\omega_0} X_L \\ \frac{\omega}{\omega_0} X_L & R_L \end{bmatrix} \tag{3.9}$$

$$[Btt] = \begin{bmatrix} 0 \\ 0 \\ sin\delta \\ cos\delta \end{bmatrix}$$

The linearized form of Equation (3.8) is given by

$$\begin{bmatrix} \frac{d\Delta V_{Cd}}{dt} \\ \frac{d\Delta V_{Cq}}{dt} \\ \Delta V_{td} \\ \Delta V_{tq} \end{bmatrix} = [At] \begin{bmatrix} \Delta V_{Cd} \\ \Delta V_{Cq} \end{bmatrix} + [R1] \begin{bmatrix} \frac{d\Delta i_d}{dt} \\ \frac{d\Delta i_q}{dt} \end{bmatrix} + [R2] \begin{bmatrix} \Delta i_d \\ \Delta i_q \end{bmatrix} + [Bt] \begin{bmatrix} \Delta\omega \\ \Delta\delta \end{bmatrix} \tag{3.10}$$

where

$$[At] = \begin{bmatrix} 0 & \omega_0 \\ -\omega_0 & 0 \\ 1 & 0 \\ 0 & 1 \end{bmatrix}$$

$$[R1] = \begin{bmatrix} 0 & 0 \\ 0 & 0 \\ \frac{X_L}{\omega_0} & 0 \\ 0 & \frac{X_L}{\omega_0} \end{bmatrix}$$

$$[R2] = \begin{bmatrix} \omega_0 X_C & 0 \\ 0 & \omega_0 X_C \\ R_L & -X_L \\ X_L & R_L \end{bmatrix} \tag{3.11}$$

$$[Bt] = \begin{bmatrix} V_{Cq0} & 0 \\ -V_{Cd0} & 0 \\ -\frac{X_L}{\omega_0} i_{q0} & V_{bq0} \\ \frac{X_L}{\omega_0} i_{d0} & V_{bd0} \end{bmatrix}$$

3.2.4 Modeling of the Turbine-Generator Mechanical System

The turbine-generator mechanical system [3, 4], shown in Figure 3.5, consists of a high-pressure turbine (HP), an intermediate-pressure turbine (IP), two low-pressure turbines (LPA & LPB), the generator rotor (GEN) and the exciter (EXC). They together constitute a linear six-mass-spring system.

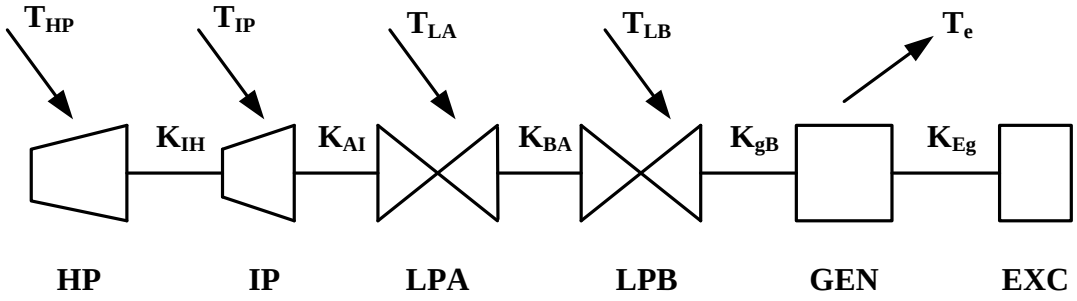

Figure 3.5: Structure of a typical six-mass shaft system model.

Assuming that *M* is the inertia constant in seconds, *D* is the damping coefficient in p.u. torque/p.u. speed for each rotating mass and *K* is a stiffness in p.u. torque/rad for each shaft section, the equations of the i_{th} mass of an N-mass spring system shown in Figure 3.6 are given by

$$\frac{M_i}{\omega_0} \frac{d\omega_i}{dt} = T_i + K_{i-1,i} (\delta_{i-1} - \delta_i) - K_{i,i+1} (\delta_i - \delta_{i+1}) - \frac{D_i}{\omega_0} (\omega_i - \omega_0) \tag{3.12}$$

$$\frac{d\delta_i}{dt} = \omega_i - \omega_0 \tag{3.13}$$

where

$$K_{i-1,i}\big|_{i=1} = 0, \qquad K_{i,i+1}\big|_{i=N} = 0, \qquad i = 1, 2, \ldots, N \tag{3.14}$$

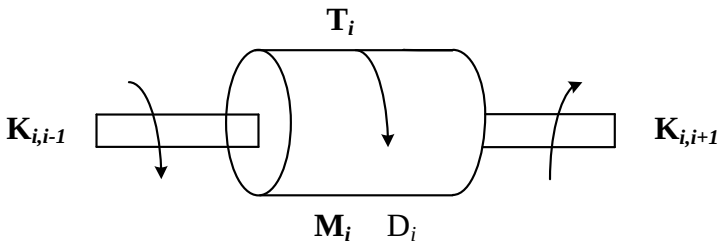

Figure 3.6: The i[th] mass of an N-mass spring system.

When Equations (3.12) to (3.14) are applied to the linear six-mass-spring system of Figure 3.5, the shaft system equations are written as:

$$\frac{M_E}{\omega_0}\frac{d\omega_E}{dt} = K_{Eg}\,(\delta - \delta_E) - \frac{D_E}{\omega_0}\,(\omega_E - \omega_0)$$

$$\frac{d\delta_E}{dt} = \omega_E - \omega_0$$

$$\frac{M_g}{\omega_0}\frac{d\omega}{dt} = -T_e + K_{gB}\,(\delta_B - \delta) - K_{Eg}\,(\delta - \delta_E) - \frac{D_g}{\omega_0}\,(\omega - \omega_0)$$

$$\frac{d\delta}{dt} = \omega - \omega_0$$

$$\frac{M_B}{\omega_0}\frac{d\omega_B}{dt} = \frac{\omega_0}{\omega_B}P_A + K_{BA}\,(\delta_A - \delta_B) - K_{gB}\,(\delta_B - \delta) - \frac{D_B}{\omega_0}\,(\omega_B - \omega_0)$$

$$\frac{d\delta_B}{dt} = \omega_B - \omega_0$$

$$\frac{M_A}{\omega_0}\frac{d\omega_A}{dt} = \frac{\omega_0}{\omega_A}P_A + K_{AI}\,(\delta_I - \delta_A) - K_{BA}\,(\delta_A - \delta_B) - \frac{D_A}{\omega_0}\,(\omega_A - \omega_0)$$

$$\frac{d\delta_A}{dt} = \omega_A - \omega_0$$

$$\frac{M_I}{\omega_0}\frac{d\omega_I}{dt} = \frac{\omega_0}{\omega_I}P_I + K_{IH}\,(\delta_H - \delta_I) - K_{AI}\,(\delta_I - \delta_A) - \frac{D_I}{\omega_0}\,(\omega_I - \omega_0)$$

$$\frac{d\delta_I}{dt} = \omega_I - \omega_0$$

$$\frac{M_H}{\omega_0}\frac{d\omega_H}{dt} = \frac{\omega_0}{\omega_H}P_H - K_{IH}\,(\delta_H - \delta_I) - \frac{D_H}{\omega_0}\,(\omega_H - \omega_0)$$

$$\frac{d\delta_H}{dt} = \omega_H - \omega_0$$

The overall shaft equations are given by the following matrix equation

$$\left[\frac{dX_{ms}}{dt}\right] = [At_{ms}][X_{ms}] + [Bt_{ms}][U_{ms}] \tag{3.15}$$

where

$$[X_{ms}] = [\delta_E \quad \delta \quad \delta_B \quad \delta_A \quad \delta_I \quad \delta_H \quad \omega_E \quad \omega \quad \omega_B \quad \omega_A \quad \omega_I \quad \omega_H]^T$$

$$[U_{ms}] = [\omega_0 \quad P_H \quad P_I \quad P_A \quad T_e]^T$$

$$[At_{ms}] = \begin{bmatrix} 0_{6\times6} & I_{6\times6} \\ As1 & As2 \end{bmatrix}$$

$[As1]$

$$= \omega_0 \begin{bmatrix} -\frac{K_{Eg}}{M_E} & \frac{K_{Eg}}{M_E} & 0 & 0 & 0 & 0 \\ \frac{K_{Eg}}{M_g} & -\frac{K_{gB}+K_{Eg}}{M_g} & \frac{K_{gB}}{M_g} & 0 & 0 & 0 \\ 0 & \frac{K_{gB}}{M_B} & -\frac{K_{BA}+K_{gB}}{M_B} & \frac{K_{BA}}{M_B} & 0 & 0 \\ 0 & 0 & \frac{K_{BA}}{M_A} & -\frac{K_{AI}+K_{BA}}{M_A} & \frac{K_{BA}}{M_A} & 0 \\ 0 & 0 & 0 & \frac{K_{AI}}{M_I} & -\frac{K_{HI}+K_{AI}}{M_I} & \frac{K_{HI}}{M_I} \\ 0 & 0 & 0 & 0 & \frac{K_{HI}}{M_H} & -\frac{K_{HI}}{M_H} \end{bmatrix}$$

$$[As2] = \omega_0 \begin{bmatrix} -\frac{D_E}{M_E} & 0 & 0 & 0 & 0 & 0 \\ 0 & -\frac{D_g}{M_g} & 0 & 0 & 0 & 0 \\ 0 & 0 & -\frac{D_B}{M_B} & 0 & 0 & 0 \\ 0 & 0 & 0 & -\frac{D_A}{M_A} & 0 & 0 \\ 0 & 0 & 0 & 0 & -\frac{D_I}{M_I} & 0 \\ 0 & 0 & 0 & 0 & 0 & -\frac{D_H}{M_H} \end{bmatrix} \tag{3.16}$$

$$[Bt_{ms}] = \begin{bmatrix} -1_{6\times1} & 0_{6\times1} & 0_{6\times1} & 0_{6\times1} & 0_{6\times1} \\ \frac{D_E}{M_E} & 0 & 0 & 0 & 0 \\ \frac{D_g}{M_g} & 0 & 0 & 0 & -\frac{\omega_0}{M_g} \\ \frac{D_B}{M_B} & 0 & 0 & \frac{{\omega_0}^2}{\omega_B M_B} & 0 \\ \frac{D_A}{M_A} & 0 & 0 & \frac{{\omega_0}^2}{\omega_A M_A} & 0 \\ \frac{D_I}{M_I} & 0 & \frac{{\omega_0}^2}{\omega_I M_I} & 0 & 0 \\ \frac{D_H}{M_H} & \frac{{\omega_0}^2}{\omega_H M_H} & 0 & 0 & 0 \end{bmatrix}$$

Here, the $[\boldsymbol{I}_{nxn}]$ is an *n* by *n* identity matrix, 0_{mxn} is an *m* by *n* matrix with all elements zero, and $-1_{6\times1}$ is a 6 by 1 matrix with all elements -1.

Linearizing and rearranging Equation (3.15) yields to

$$\left[\frac{d\Delta X_{ms}}{dt}\right] = [A_{ms}][\Delta X_{ms}] + [B_{ms}][\Delta U_{ms}] \tag{3.17}$$

where

$$[\Delta X_{ms}] = [\Delta\delta_E \quad \delta\Delta \quad \Delta\delta_B \quad \Delta\delta_A \quad \Delta\delta_I \quad \Delta\delta_H \quad \Delta\omega_E \quad \Delta\omega \quad \Delta\omega_B \quad \Delta\omega_A \quad \Delta\omega_I \quad \Delta\omega_H]^T$$

$$[\Delta U_{ms}] = [\Delta T_e \quad \Delta P_H \quad \Delta P_I \quad \Delta P_A]^T$$

$$[A_{ms}] = \begin{bmatrix} 0_{6\times6} & I_{6\times6} \\ As21 & As22 \end{bmatrix}$$

[As21] is the same with [As1] in equation (3.16)

$$[As22] = \begin{bmatrix} -\frac{D_E}{M_E} & 0 & 0 & 0 & 0 & 0 \\ 0 & -\frac{D_g}{M_g} & 0 & 0 & 0 & 0 \\ 0 & 0 & -\frac{T_{m0}F_B+D_B}{M_B} & 0 & 0 & 0 \\ 0 & 0 & 0 & -\frac{T_{m0}F_A+D_A}{M_A} & 0 & 0 \\ 0 & 0 & 0 & 0 & -\frac{T_{m0}F_I+D_I}{M_I} & 0 \\ 0 & 0 & 0 & 0 & 0 & -\frac{T_{m0}F_H+D_H}{M_H} \end{bmatrix}$$

$$[B_{ms}] = \begin{bmatrix} 0_{7\times1} & 0_{7\times1} & 0_{7\times1} & 0_{7\times1} \\ -\frac{1}{M_g} & 0 & 0 & 0 \\ 0 & 0 & 0 & \frac{1}{M_B} \\ 0 & 0 & 0 & \frac{1}{M_A} \\ 0 & 0 & \frac{1}{M_I} & 0 \\ 0 & \frac{1}{M_H} & 0 & 0 \end{bmatrix}$$

3.2.5 Governor and Turbine System

The block diagram of the four-stage turbine and the associated electro-hydraulic governor [84] is shown in Figure 3.7. The corresponding data are given in Appendix A.

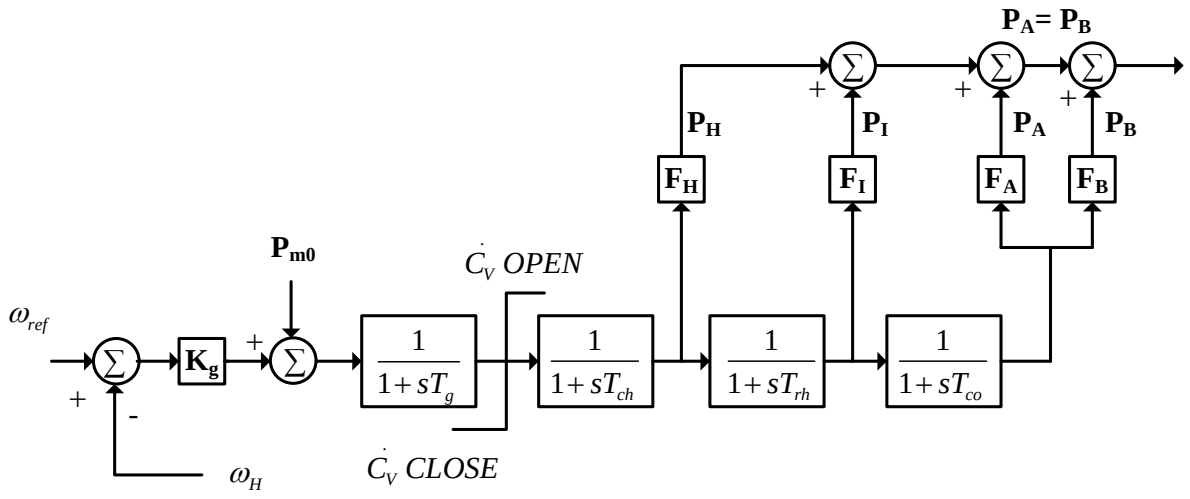

Figure 3.7: Block diagram of the governor and the turbine.

The corresponding state-space equation can be derived from the block diagram and is given by

$$\left[\frac{dX_g}{dt}\right] = [At_g][X_g] + [Bt_g]\begin{bmatrix} \omega_0 \\ P_{m0} \\ \omega_H \end{bmatrix} \tag{3.18}$$

where

$$[X_g] = [C_V \quad P_H \quad P_I \quad P_A]^T$$

$$[At_g] = \begin{bmatrix} -\frac{1}{T_g} & 0 & 0 & 0 \\ \frac{F_H}{T_{ch}} & -\frac{1}{T_{ch}} & 0 & 0 \\ 0 & \frac{F_I}{F_H T_{rh}} & -\frac{1}{T_{rh}} & 0 \\ 0 & 0 & \frac{F_A}{F_I T_{co}} & -\frac{1}{T_{co}} \end{bmatrix}$$

$$[Bt_g] = \begin{bmatrix} \frac{K_g}{T_g \omega_0} & \frac{1}{T_g} & -\frac{K_g}{T_g \omega_0} \\ 0 & 0 & 0 \\ 0 & 0 & 0 \\ 0 & 0 & 0 \end{bmatrix}$$

The linearized form of Equation (3.18) is given by

$$\left[\frac{\Delta dX_g}{dt}\right] = [A_g][\Delta X_g] + [B_g]\begin{bmatrix} \Delta P_{m0} \\ \Delta \omega_H \end{bmatrix} \tag{3.19}$$

where

$$[\Delta X_g] = [\Delta C_V \quad \Delta P_H \quad \Delta P_I \quad \Delta P_A]^T$$

$$[A_g] = \begin{bmatrix} -\frac{1}{T_g} & 0 & 0 & 0 \\ \frac{F_H}{T_{ch}} & -\frac{1}{T_{ch}} & 0 & 0 \\ 0 & \frac{F_I}{F_H T_{rh}} & -\frac{1}{T_{rh}} & 0 \\ 0 & 0 & \frac{F_A}{F_I T_{co}} & -\frac{1}{T_{co}} \end{bmatrix} \tag{3.20}$$

$$[B_g] = \begin{bmatrix} \frac{1}{T_g} & -\frac{K_g}{T_g \omega_0} \\ 0 & 0 \\ 0 & 0 \\ 0 & 0 \end{bmatrix}$$

3.2.6 Excitation System

The block diagram representation of the excitation system used in this study [3,4] is shown in Figure 3.8 and the corresponding data are given in Appendix A.

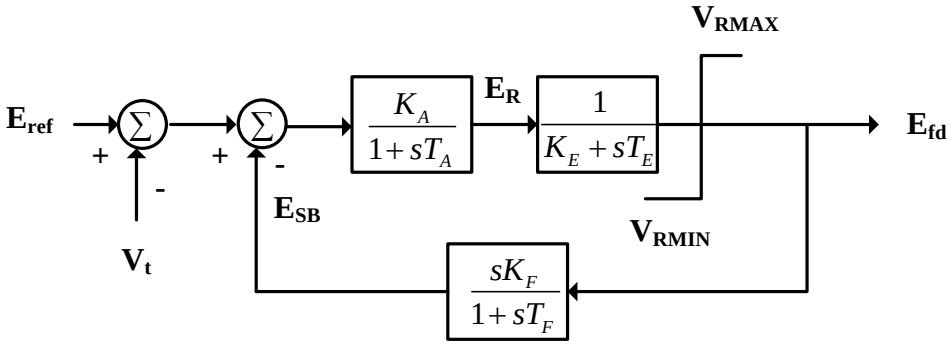

Figure 3.8: Block diagram of the excitation system.

Utilizing the relationship between the excitation system output voltage and the field voltage given by $E_{fd} = \frac{L_{ad}}{R_{fd}}\, e_{fd}$, the state-space equation of the excitation system can be derived from its block diagram and is given by

$$\left[\frac{dX_v}{dt}\right] = [At_v][X_v] + [Bt_v]\begin{bmatrix} V_t \\ E_{ref} \end{bmatrix} \tag{3.21}$$

where

$$[X_v] = [e_{fd} \quad E_R \quad E_{SB}]^T$$

$$[At_v] = \begin{bmatrix} -\frac{K_E}{T_E} & \frac{1}{T_E}\frac{R_{fd}}{L_{ad}} & 0 \\ 0 & -\frac{1}{T_A} & -\frac{K_A}{T_A} \\ -\frac{K_E K_F}{T_E T_F}\frac{L_{ad}}{R_{fd}} & \frac{K_F}{T_F T_E} & -\frac{1}{T_F} \end{bmatrix} \tag{3.22}$$

$$[Bt_v] = \begin{bmatrix} 0 & 0 \\ -\frac{K_A}{T_A} & \frac{K_A}{T_A} \\ 0 & 0 \end{bmatrix}$$

Linearized Equation (3.21) is written as

$$\left[\frac{d\Delta X_v}{dt}\right] = [A_v][\Delta X_v] + [B_v]\begin{bmatrix} \Delta V_t \\ \Delta E_{ref} \end{bmatrix} \tag{3.23}$$

where

$$[\Delta X_v] = [\Delta e_{fd} \quad \Delta E_R \quad \Delta E_{SB}]^T$$

$$[A_v] = \begin{bmatrix} -\frac{K_E}{T_E} & \frac{1}{T_E}\frac{R_{fd}}{L_{ad}} & 0 \\ 0 & -\frac{1}{T_A} & -\frac{K_A}{T_A} \\ -\frac{K_E K_F}{T_E T_F}\frac{L_{ad}}{R_{fd}} & \frac{K_F}{T_F T_E} & -\frac{1}{T_F} \end{bmatrix} \tag{3.24}$$

$$[B_v] = \begin{bmatrix} 0 & 0 \\ -\frac{K_A}{T_A} & \frac{K_A}{T_A} \\ 0 & 0 \end{bmatrix}$$

3.3 Small Signal Model of a Single Machine Infinite Bus System

The overall model of the system under study can be derived by performing the following mathematical manipulations for the interactions among the various components of the system [83].

The electrical parts of the system: combining Equation (3.3) and (3.10) to form the following equations

$$\begin{bmatrix} \frac{d\Delta X_{syn}}{dt} \\ \frac{d\Delta V_{Cd}}{dt} \\ \frac{d\Delta V_{Cq}}{dt} \end{bmatrix} = [Amt] \begin{bmatrix} \Delta X_{syn} \\ \Delta V_{Cd} \\ \Delta V_{Cq} \end{bmatrix} + [Bmt] \begin{bmatrix} \Delta e_{fd} \\ \Delta\omega \\ \Delta\delta \end{bmatrix} \tag{3.25}$$

$$\begin{bmatrix} \Delta V_{td} \\ \Delta V_{tq} \end{bmatrix} = [Ci] \begin{bmatrix} \Delta X_{syn} \\ \Delta V_{Cd} \\ \Delta V_{Cq} \end{bmatrix} + [Di] \begin{bmatrix} \Delta e_{fd} \\ \Delta\omega \\ \Delta\delta \end{bmatrix} \tag{3.26}$$

The mechanical parts of the system: combining Equations (3.17), (3.19) and (3.23) to form the following equations

$$\begin{bmatrix} \frac{d\Delta X_{ms}}{dt} \\ \frac{d\Delta X_g}{dt} \\ \frac{d\Delta X_v}{dt} \end{bmatrix} = [Ap1] \begin{bmatrix} \Delta X_{ms} \\ \Delta X_g \\ \Delta X_v \end{bmatrix} + [Ap2] \begin{bmatrix} \Delta T_e \\ \Delta V_t \end{bmatrix} + [Bp] \begin{bmatrix} \Delta P_{m0} \\ \Delta E_{ref} \end{bmatrix} \tag{3.27}$$

There are, however, two non-state variables ΔT_e and ΔV_t that must be eliminated.

The linearized form of the air-gap torque Equation (3.24) is given by

$$\Delta T_e = [Tedq0]\left[\Delta X_{syn}\right] \tag{3.28}$$

where

$$[Tedq0] = \begin{bmatrix} i_{q0}(L_q - L_d) & i_{d0}(L_q - L_d) + i_{fd0}L_{ad} & i_{q0}L_{ad} & -i_{d0}L_{aq} & i_{q0}L_{ad} & -i_{d0}L_{aq} \end{bmatrix} \tag{3.29}$$

The linearized terminal voltage equation ${V_t}^2 = {V_{td}}^2 + {V_{tq}}^2$ is given by

$$\Delta V_t = \begin{bmatrix} \frac{V_{td0}}{V_{t0}} & \frac{V_{tq0}}{V_{t0}} \end{bmatrix} \begin{bmatrix} \Delta V_{td} \\ \Delta V_{tq} \end{bmatrix} \tag{3.30}$$

Combining Equations (3.26), (3.28) and (3.30) to form the following equation

$$\begin{bmatrix} \Delta T_e \\ \Delta V_t \end{bmatrix} = [Cmt] \begin{bmatrix} \Delta X_{syn} \\ \Delta V_{Cd} \\ \Delta V_{Cq} \end{bmatrix} + [Dmt] \begin{bmatrix} \Delta e_{fd} \\ \Delta\omega \\ \Delta\delta \end{bmatrix} \tag{3.31}$$

The overall system equations derived by combining Equation (3.25), (3.27) and (3.31) are written by

$$\left[\frac{d\Delta X}{dt}\right] = [A][\Delta X] + [B][\Delta U] \tag{3.32}$$

where

$$[\Delta X] = [\Delta\delta_E \quad \Delta\delta \quad \Delta\delta_B \quad \Delta\delta_A \quad \Delta\delta_I \quad \Delta\delta_H \quad \Delta\omega_E \quad \Delta\omega \quad \Delta\omega_B \quad \Delta\omega_A \, \Delta\omega_I \quad \Delta\omega_H \ldots$$

$$\Delta C_V \quad \Delta P_H \; \Delta P_I \quad \Delta P_A \quad \Delta e_{fd} \quad \Delta E_R \quad \Delta E_{SB} \quad \Delta i_d \quad \Delta i_q \quad \Delta i_{fd} \quad \Delta i_{1q} \ldots$$

$$\Delta i_{1d} \quad \Delta i_{2q} \quad \Delta V_{Cd} \quad \Delta V_{Cq}]^{\mathrm{T}}$$

$$[\Delta U] = [\Delta P_{m0} \quad \Delta E_{ref}]^{\mathrm{T}} \tag{3.33}$$

The complete electrical and mechanical model of a one-machine, infinite-bus system for SSR study is a 27th order system.

The detail manipulations for forming the overall system equations are shown in Appendix B.

3.4 Effect of Series Capacitor Compensation on SSR

The six-mass model of the turbine-generator shaft system shown in Figure 3.5 has five torsional modes in addition to the rigid body mode (mode 0). Mode 0, signifies that the six masses oscillate in unison without a shaft twist and Mode N has the N^{th} lowest frequency and a mode shape with N phase reversals. The total number of modes including Mode 0 is equal to the number of inertial elements in the spring-mass model. The negative damping (undamping) due to the torsional interaction for the turbine-generator is evaluated using eigenvalue analysis by varying the degree of series compensation from to 0 to 100%. The percentage of compensation is defined as

$$\%\, compensation = \frac{X_C}{X_L} \times 100 \tag{3.34}$$

The results of this variation in compensation level are shown in Figure 3.9 and the system eigenvalues for the critical compensation levels are given in Table 3.1 and

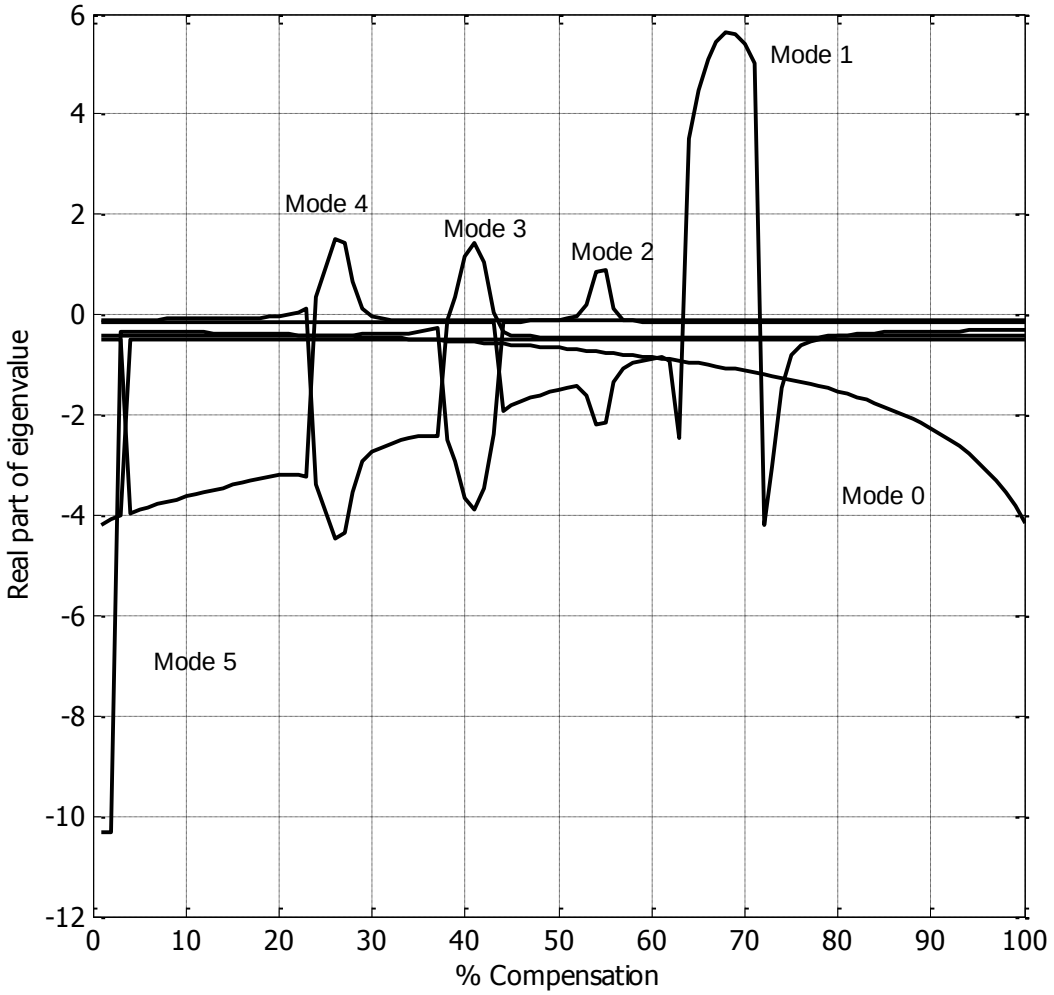

Figure 3.9: The real part of SSR mode eigenvalues as a function of the percentage compensation

The real part of the eigenvalues for the percentage compensation from 0 to 100 is plotted for five torsional modes in addition to the rigid body mode (mode 0) in the figure 3.9. It has been observed that for modes 1 to 4 each has one critical compensation level where the eigenvalues reach their maximum positive values. The critical points are 26.5%, 41.1%, 54.7% and 68.4%. These critical points are taken for SSR study and the performance of PWMSC is evaluated at these critical points.

Table 3.1: Eigenvalues of SSR modes (Mode 1-5), rigid body mode (Mode 0), electrical mode and the other modes.

Modes	State variables	% Compensation Level			
		26.5%	41.1%	54.7	68.4
Mode 5	δ_H, ω_H	- 0.48 ± 298.28i	- 0.48 ± 298.28i	- 0.48 ± 298.28i	- 0.48 ± 298.28i
Mode 4	δ_I, ω_I	**1.56 ± 202.73i**	- 0.12 ± 202.77i	- 0.12 ± 202.85i	- 0.11 ± 202.88i
Mode 3	δ_A, ω_A	- 0.40 ± 160.77i	**1.42 ± 160.35i**	- 0.44 ± 160.44i	- 0.44 ± 160.53i
Mode 2	δ_E, ω_E	- 0.14 ± 127.07i	- 0.14 ± 127.11i	**0.96 ± 126.85i**	- 0.15 ± 126.96i
Mode 1	δ_B, ω_B	- 0.20 ± 99.22i	- 0.18 ± 99.46i	- 0.13 ± 100.13i	**5.64 ± 98.58i**
Mode 0	δ, ω	- 0.43 ± 8.45i	- 0.55 ± 9.36i	- 0.75 ± 10.39i	- 1.07 ± 11.72i
Elec.	V_{Cd}, V_{Cq}	- 4.49 ± 202.88i	- 3.86 ± 160.43i	- 2.26 ± 126.79i	- 5.82 ± 98.86i
Other Modes	i_d, i_q	- 4.97 ± 551.23i	- 5.07 ± 594.02i	- 5.13 ± 627.38i	- 5.19 ± 657.00i
	i_{1d}, i_{1q}	- 96.63 ± 1.50i	- 96.86 ± 1.58i	- 97.07 ± 1.59i	- 97.23 ± 1.54i
	i_{2q}	- 32.72	- 32.98	- 33.30	- 33.76
	E_R	- 26.67	- 26.70	- 26.75	- 26.82
	C_V	- 10.29	- 10.27	- 10.24	- 10.19
	e_{fd}	- 5.08	- 5.47	- 5.92	- 6.53
	P_H	- 2.37	- 2.39	- 2.41	- 2.43
	P_A	- 1.68	- 1.68	- 1.67	- 1.67
	P_I	- 0.14	- 0.14	- 0.14	- 0.14
	i_{fd}	- 0.60	- 0.63	- 0.65	- 0.68
	E_{SB}	- 0.89	- 0.89	- 0.90	- 0.91

In the Table 3.1 all the eigenvalues for the four critical compensation levels are presented and the SSR modes (Mode 1-5), rigid body mode (Mode 0), electrical mode are identified. Examining Figure 3.9 and Table 3.1 yields to the following observations:

- There are four unstable torsional modes (Modes 1, 2, 3, and 4). Each of these modes has its largest SSR interaction when the real part of its eigenvalue is a maximum.

- Mode 1 exhibits the most severe undamping with a peak at 68.4% series compensation.
- Mode 5 damping is seen to have a small constant negative value over the whole range of series compensation.
- The frequency of the electrical mode (capacitor) decreases with the increase of the compensation level, which is below the synchronous frequency and, therefore, may excite the torsional oscillation modes.
- The frequency of the generator current components increases with the degree of capacitor compensation, but it is usually above the synchronous frequency.
- The other eigenvalue modes listed in Table 3.1 are stable, like the generator windings, the excitation system, and the governor system and the turbine.

3.5 Summary

This chapter presented the investigations of the subsynchronous resonance phenomenon under small disturbances. These investigations are conducted on the IEEE first benchmark model which consists of a large turbine-generator connecting to an infinite bus system through a series capacitor compensated transmission line. In order to develop the linear system model, the nonlinear differential equations of each component of the system are derived and then linearized. These set of linearized equations were grouped and mathematically manipulated in order to obtain the overall system model in a state-space form. The effect of the series capacitor compensation on SSR was investigated using eigenvalue analysis. The results of these investigations have provided the critical compensation levels in the system under investigations.

Chapter 4

Dynamic Modeling of PWMSC and Performance Evaluation for SSR Damping

4.1 Introduction

A problem of interest in power industry is the mitigation of power system oscillations. SSR oscillations may be excited by small or large disturbance in the power system. SSR oscillations resulting from small (minute) disturbances are usually small. However, they can build up with time to large values causing shaft failure. On the other hand, large power system disturbances, such as short circuits, induce large growing SSR torsional oscillations in the turbine-generator shaft system. These oscillations may exceed the endurance limit of the turbine-generator shaft and, hence, cause a shaft fatigue in a period of a few seconds. These oscillations are related to the dynamics of system power transfer and often exhibit poor damping. The electromechanical oscillations in power system can be damped out by using a newly developed PWM based series compensator. Such compensators have the advantage of being simpler in both power circuit structure and control. A digital time-domain simulation study case of the power system with PWMSC during a small disturbance in the governor side is presented in this chapter and the comparative analysis is also presented at the end of this chapter.

4.2 PWMSC

4.2.1 Basic Model of PWMSC

Fixed series capacitors have been used for a long time for increasing power transfer in long lines and providing a higher utilization level of limited transmission systems. They are also most economical solutions for this purpose. However, the control of series compensation using thyristor switches has been introduced for fast power flow control only 15–20 years ago. A newly developed AC link converter based series compensation, a FACTS controller, is presented in [32]. The PWM controlled series compensator offers a method of variable

series compensation. It is known that transmission lines loading may be restricted by system dynamics stability. The PWMSC is a powerful new tool to help relieve these constraints. Furthermore, its controller can be designed to modify line reactance and provide enough damping to system oscillation modes. Figure 4.1 displays a realization of schematic diagram of the PWM series compensator which is embedded into a transmission line [85].

The PWM controlled series compensator consists of: (a) series injection transformers (b) compensation capacitors and (c) PWM controlled switches S_a , S_b , S_c , S_a', $S_b'$and S_c'. In Figure 4.1, the three switches S_a, S_b , S_c with the same switching function in a complementary way to those in S_a', $S_b'$and S_c' switches. The switching period divides the circuit in two switching states. When S_a, S_b and S_c are on, the capacitors are connected to the system through a series injection transformer.

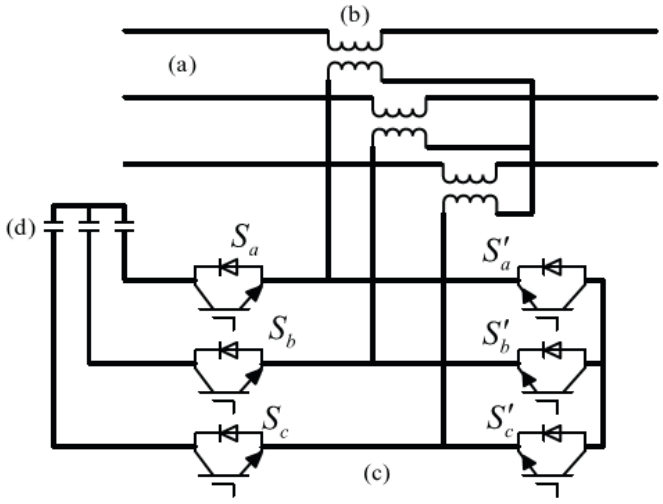

Figure 4.1: PWMSC controller (a) Transmission line; (b) Series injection transformer; (c) PWM switches; (d) Compensating capacitors.

When S_a', $S_b'$and S_c' are on, the series injection transformer is shorted, thereby isolating the capacitors from the line. When impedance is low at the primary winding, the primary behaves as a conductor. A little impedance is added by the transformer, but it can be neglected. In this structure, the bank of capacitors is connected in Y to the PWM AC converter [86, 87]. The compensator serves for continuous control of the degree of series compensation by varying the duty cycle of a single asynchronous train of fixed frequency pulses. The duty cycle (D) of the AC link converter is defined as the ratio of the on-period of switches S_a', $S_b'$and S_c' with respect to the total switching period.

4.2.2 Operation of PWMSC

The PWMSC is assumed to be connected between buses *i* and *j* in a transmission line as shown in Figure 4.2, where the PWMSC is operated like a continuously capacitive controllable reactance. However, for the purpose of developing a control strategy, it is useful to have a proper model representation for the PWMSC.

The main switches (S_a, S_b and S_c) of the AC link converter are controlled with the train of pulses with fixed frequency and variable duty cycle (*D*). When main switches are on, the capacitors are connected to transmission line. Therefore, instantaneous voltage that appears at the primary of the inserting transformer (V_S) is given by the voltage drop across the transformer leakage reactance plus a voltage proportional of voltage across the bank of capacitors, according to the turns ratio of the transformers. Switches S_a', $S_b'$and S_c' are controlled with the complementary signal so as to provide a freewheeling path for currents at the secondary of the coupling transformer when the main switches are off. During this operation, the secondary of the coupling transformers are short-circuited and the voltage that appears at the primaries (V_S) is only the voltage drop across the transformer leakage reactance. Therefore, characteristic of the PWMSC at the primary transformer is essentially that of a controllable reactance. Inserting reactance can vary from slightly inductive to capacitive, depending on the duty cycle (*D*) of the PWM AC link converter. Mathematical expressions in the next section that describe reactance characteristics of the PWMSC and the injected reactance into the system are derived in the following section.

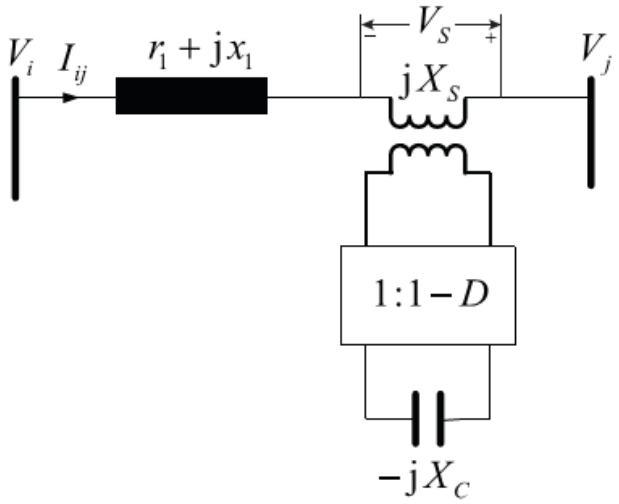

Figure 4.2: Single line diagram of PWMSC.

4.2.3 Mathematical Analysis of PWMSC

For analyzing the PWMSC, a single phase equivalent model, shown in Figure 4.2, is used. The primary series transformer is represented by a leakage reactance (X_T) in series with an ideal transformer at transmission line. In the secondary, there is a PWM AC link converter and a bank of capacitors with reactance X_C. The equivalent and injected impedances at transmission line may be calculated with state space averaging techniques as follows:

$$X_{eq} = X_{ij} + X_T + X_S \tag{4.1}$$

$$X_S = -n^2(1-D)^2 X_C \tag{4.2}$$

The n is the turns ratio of the transformer and X_{ij} is the reactance of the transmission line. Equations (4.1) and (4.2) show that the effective impedance depends on the duty cycle of the AC link switches; hence, this duty cycle provides a means of realizing the desired controllable impedance, power flow at line and power oscillations control. For more understanding, the variation of the PWMSC based injected reactance with duty cycle of the AC link is shown in Figure 4.3. In this figure, it is assumed that the designed PWMSC provides a series capacitive reactance of 0.35 p.u. for a line with 1 p.u. reactance. The leakage reactance of the series transformer is taken as 0.03 p.u. on the system base.

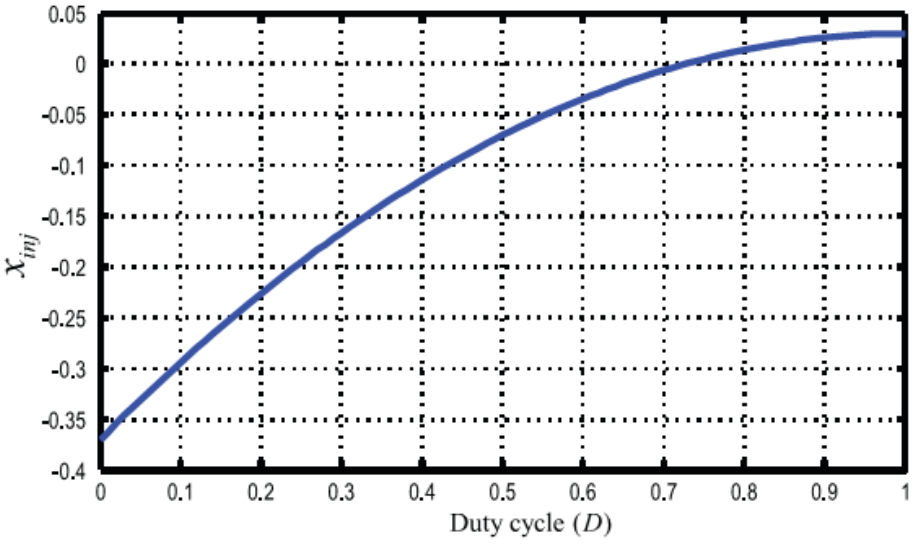

Figure 4.3: Variation of the PWMSC based injected reactance with duty cycle.

Equations (4.1) and (4.2) and Figure 4.3 imply that the injected reactance using PWMSC can be varied continuously between two extreme values.

4.2.4 PWMSC Current Injection Model

In order to effectively investigate the impact of series compensators on power systems effectively, appropriate models of these devices are very important. In this thesis, current injection model of PWMSC is used to study the effects of PWMSC on SSR oscillations in power system.

The installation of PWMSC changes the system bus admittance matrix Y_{bus} to an unsymmetrical matrix [88]. When the PWMSC is used for time domain simulations of multi-machine power systems, the modification of Y_{bus} is required at each stage. This method has the disadvantage that a constant factorized Y_{bus} cannot be repeatedly used when the PWMSC variable reactance is changeable in the process of transient stability calculation. For this reason, a current injection model of PWMSC is developed to avoid using the modification of Y_{bus} at each stage. The current injection model, which can be used for small signal stability and transient stability studies, is obtained by replacing the voltage across the PWMSC with the current source. By using equivalent injected currents at terminal buses to simulate a PWMSC no modification of Y_{bus} is required at each stage. This method has the advantages of fast computational speed and low computer storage compared with that of modifying Y_{bus} technique. Also, this model is helpful for understanding the effect and performance of the PWMSC on system damping enhancement [89].

A PWMSC connected between nodes *i* and *j* in a transmission line as shown in Figure 4.4, where the PWMSC is simplified like a continuously capacitive controllable reactance and its equivalent circuit is represented in Figure 4.5. In Figures 4.4 and 4.5, $V_i \angle\theta_i$ and $V_j \angle\theta_j$ are complex voltages at nodes *i* and *j*, and $V_S = -jX_S I_{se}$ represents voltage across the PWMSC .

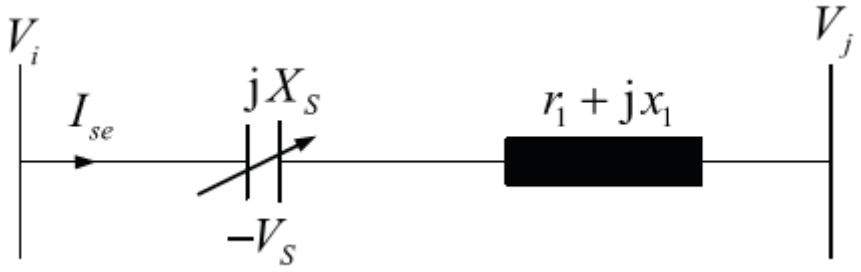

Figure 4.4: PWMSC located in a transmission line.

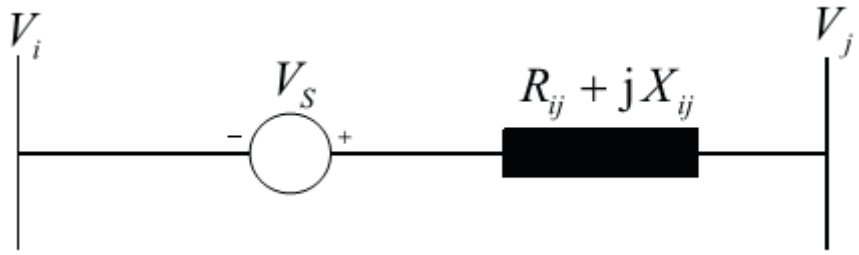

Figure 4.5: PWMSC equivalent circuit.

Figure 4.4 implies as follows:

$$I_{se} = \frac{V_i - V_j}{R_{ij} + j(X_{ij} + X_s)} \tag{4.3}$$

$$I_{se} = \frac{V_i - V_j}{R_{ij} + j(X_{ij} + X_T - n^2(1-D)^2 X_c)} \tag{4.4}$$

The current injection model of the PWMSC is obtained by replacing the voltage across the PWMSC by an equivalent current source, I_s, in Figure 4.6. Then:

$$I_s = \frac{V_s}{R_{ij} + jX_{ij}} = -\frac{jX_s I_{se}}{R_{ij} + jX_{ij}} \tag{4.5}$$

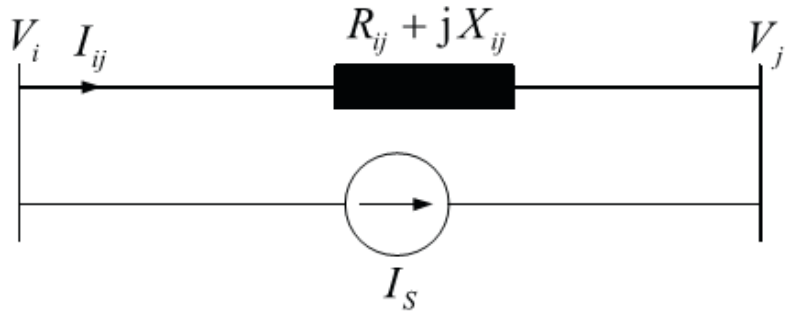

Figure 4.6: Replacing voltage across the PWMSC by a current source.

Current source model of the PWMSC is shown in Figure 4.7. Current injections into nodes i and j are calculated as follows:

$$I_{si} = \frac{j(X_T - n^2(1-D)^2 X_c)}{R_{ij} + j(X_{ij} + X_T - n^2(1-D)^2 X_c)} \cdot \frac{V_i - V_j}{R_{ij} + jX_{ij}} \tag{4.6}$$

$$I_{sj} = -I_{si} \tag{4.7}$$

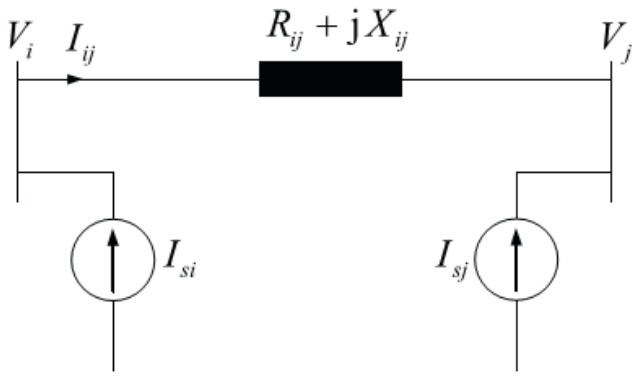

Figure 4.7: Current injection model for PWMSC.

4.3 System under Study with PWMSC

The single line diagram of PWMSC installed IEEE first benchmark model under investigation is shown in Figure 4.8. It consists of a turbine generator which is connected via a transformer to a large AC system through a series compensated transmission line. The FACTS device PWMSC is connected with the series capacitor.

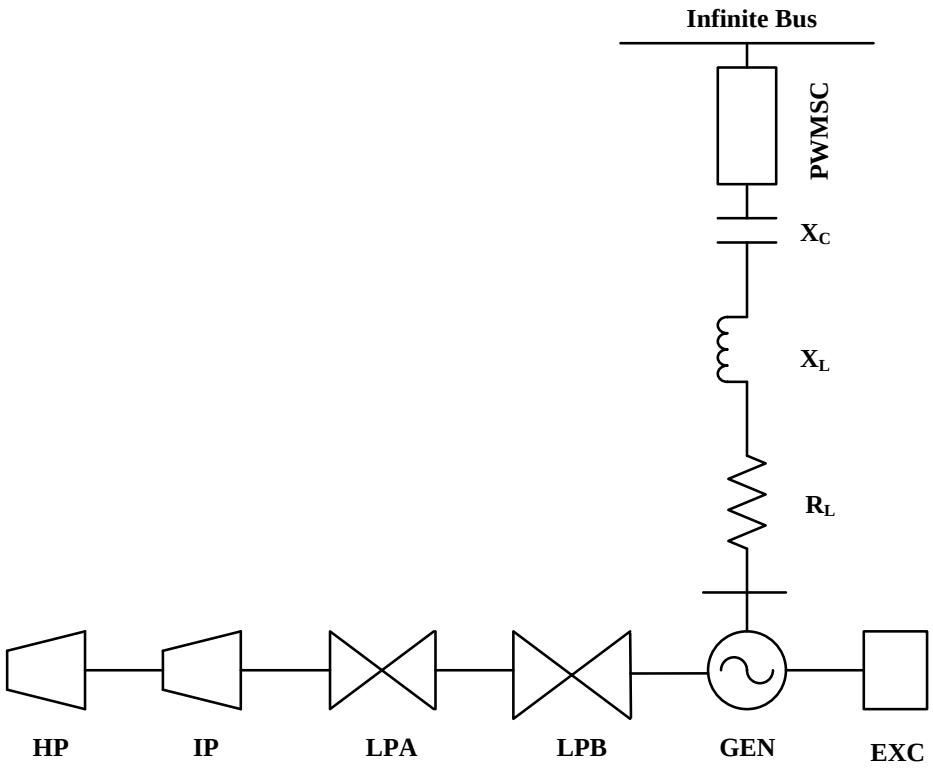

Figure 4.8: The PWMSC installed IEEE benchmark model under study

In order to develop the mathematical model for the system, the differential equations of the turbine-generator, the turbine-generator mechanical system and the series capacitor compensated transmission line given in Chapter 3 are used here again.

The PWMSC is installed in the transmission line. So the transmission line will be remodeled and the differential equations will be integrated with the system state matrix.

4.3.1 Modeling of PWMSC Installed Transmission Line

The PWMSC installed series capacitor-compensated transmission line may be represented by the RLC circuit shown in Figure 4.9. The differential equations for the circuit elements, after applying Park's transformation, can be expressed in the d-q reference frame by the following matrix expressions.

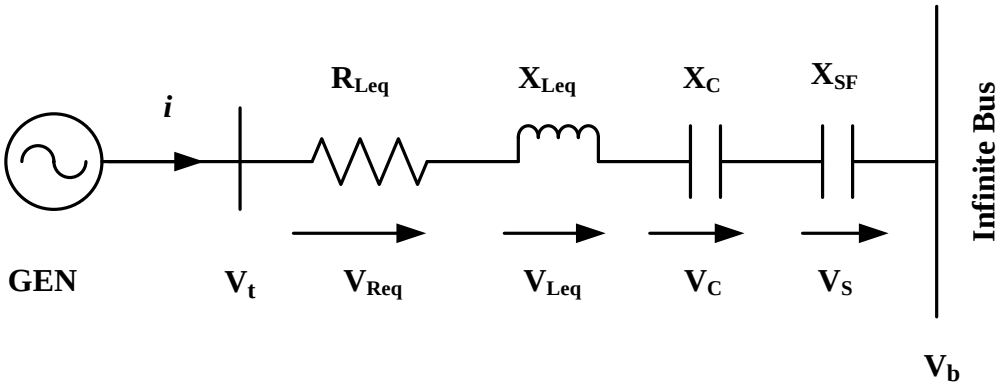

Figure 4.9: A series capacitor-compensated transmission line with PWMSC

The voltage across the resistance:

$$\begin{bmatrix} V_{Rd} \\ V_{Rq} \end{bmatrix} = \begin{bmatrix} R_L & 0 \\ 0 & R_L \end{bmatrix} \begin{bmatrix} i_d \\ i_q \end{bmatrix} \tag{4.8}$$

The voltage across the inductor:

$$\begin{bmatrix} V_{Ld} \\ V_{Lq} \end{bmatrix} = \begin{bmatrix} 0 & -\frac{\omega}{\omega_0} X_L \\ \frac{\omega}{\omega_0} X_L & 0 \end{bmatrix} \begin{bmatrix} i_d \\ i_q \end{bmatrix} + \begin{bmatrix} \frac{X_L}{\omega_0} & 0 \\ 0 & \frac{X_L}{\omega_0} \end{bmatrix} \begin{bmatrix} \frac{di_d}{dt} \\ \frac{di_q}{dt} \end{bmatrix} \tag{4.9}$$

The voltage across the line capacitor:

$$\begin{bmatrix} \frac{dV_{Cd}}{dt} \\ \frac{dV_{Cq}}{dt} \end{bmatrix} = \begin{bmatrix} \omega_0 X_C & 0 \\ 0 & \omega_0 X_C \end{bmatrix} \begin{bmatrix} i_d \\ i_q \end{bmatrix} + \begin{bmatrix} 0 & \omega \\ -\omega & 0 \end{bmatrix} \begin{bmatrix} V_{Cd} \\ V_{Cq} \end{bmatrix} \tag{4.10}$$

The voltage across the equivalent capacitor of PWMSC:

$$\begin{bmatrix} \frac{dV_{Sd}}{dt} \\ \frac{dV_{Sq}}{dt} \end{bmatrix} = \begin{bmatrix} \omega_0 X_S & 0 \\ 0 & \omega_0 X_S \end{bmatrix} \begin{bmatrix} i_d \\ i_q \end{bmatrix} + \begin{bmatrix} 0 & \omega \\ -\omega & 0 \end{bmatrix} \begin{bmatrix} V_{Sd} \\ V_{Sq} \end{bmatrix} \tag{4.11}$$

The overall equations of the transmission line can be written as

$$\begin{bmatrix} \frac{dV_{Cd}}{dt} \\ \frac{dV_{Cq}}{dt} \\ \frac{dV_{Sd}}{dt} \\ \frac{dV_{Sq}}{dt} \\ V_{td} \\ V_{tq} \end{bmatrix} = [Att] \begin{bmatrix} V_{Cd} \\ V_{Cq} \\ V_{Sd} \\ V_{Sq} \end{bmatrix} + [Rt1] \begin{bmatrix} \frac{di_d}{dt} \\ \frac{di_q}{dt} \end{bmatrix} + [Rt2] \begin{bmatrix} i_d \\ i_q \end{bmatrix} + [Btt][V_b] \tag{4.12}$$

where

$$[Att] = \begin{bmatrix} 0 & \omega & 0 & 0 \\ -\omega & 0 & 0 & 0 \\ 0 & 0 & 0 & \omega \\ 0 & 0 & -\omega & 0 \\ 1 & 0 & 1 & 0 \\ 0 & 1 & 0 & 1 \end{bmatrix}$$

$$[Rt1] = \begin{bmatrix} 0 & 0 \\ 0 & 0 \\ 0 & 0 \\ 0 & 0 \\ \frac{X_{Leq}}{\omega_0} & 0 \\ 0 & \frac{X_{Leq}}{\omega_0} \end{bmatrix}$$

$$[Rt2] = \begin{bmatrix} \omega_0 X_C & 0 \\ 0 & \omega_0 X_C \\ \omega_0 X_{SF} & 0 \\ 0 & \omega_0 X_{SF} \\ R_{Leq} & -\frac{\omega}{\omega_0} X_{Leq} \\ \frac{\omega}{\omega_0} X_{Leq} & R_{Leq} \end{bmatrix} \tag{4.13}$$

$$[Btt] = \begin{bmatrix} 0 \\ 0 \\ 0 \\ 0 \\ sin\delta \\ cos\delta \end{bmatrix}$$

The linearized form of Equation (4.12)is given by

$$\begin{bmatrix} \frac{d\Delta V_{Cd}}{dt} \\ \frac{d\Delta V_{Cq}}{dt} \\ \frac{d\Delta V_{Sd}}{dt} \\ \frac{d\Delta V_{Sq}}{dt} \\ \Delta V_{td} \\ \Delta V_{tq} \end{bmatrix} = [AtP] \begin{bmatrix} \Delta V_{Cd} \\ \Delta V_{Cq} \\ \Delta V_{Sd} \\ \Delta V_{Sq} \end{bmatrix} + [R1P] \begin{bmatrix} \frac{d\Delta i_d}{dt} \\ \frac{d\Delta i_q}{dt} \end{bmatrix} + [R2P] \begin{bmatrix} \Delta i_d \\ \Delta i_q \end{bmatrix} + [BtP] \begin{bmatrix} \Delta\omega \\ \Delta\delta \end{bmatrix} \tag{4.14}$$

Where

$$[AtP] = \begin{bmatrix} 0 & \omega_0 & 0 & 0 \\ -\omega_0 & 0 & 0 & 0 \\ 0 & 0 & 0 & \omega_0 \\ 0 & 0 & -\omega_0 & 0 \\ 1 & 0 & 1 & 0 \\ 0 & 1 & 0 & 1 \end{bmatrix}$$

$$[R1P] = \begin{bmatrix} 0 & 0 \\ 0 & 0 \\ 0 & 0 \\ 0 & 0 \\ \frac{X_{Leq}}{\omega_0} & 0 \\ 0 & \frac{X_{Leq}}{\omega_0} \end{bmatrix}$$

$$[R2P] = \begin{bmatrix} \omega_0 X_C & 0 \\ 0 & \omega_0 X_C \\ \omega_0 X_{SF} & 0 \\ 0 & \omega_0 X_{SF} \\ R_{Leq} & -\frac{\omega}{\omega_0} X_{Leq} \\ \frac{\omega}{\omega_0} X_{Leq} & R_{Leq} \end{bmatrix} \tag{4.15}$$

$$[BtP] = \begin{bmatrix} V_{Cq0} & 0 \\ -V_{Cd0} & 0 \\ V_{Sq0} & 0 \\ -V_{Sd0} & 0 \\ -\frac{X_{Leq}}{\omega_0} i_{q0} & V_{bq0} \\ \frac{X_{Leq}}{\omega_0} i_{d0} & V_{bd0} \end{bmatrix} \tag{4.16}$$

4.3.2 Dynamic control model of PWMSC

Figure 4.10 shows a schematic diagram of the dynamic control model of PWMSC for typical oscillatory stability studies. It can be noticed that following a similar modeling approach, as in the case of another series compensator, line reactance is assumed to be controlled through the duty cycle *D*. This model does not consider power oscillation damping controller. The model includes an input signal and a reference signal X_{Sref} which is the initial value of the series compensator. These inputs are summed to produce an error signal which is fed into a first-order lag block. The lag block is associated with the duty cycle control and natural response of the PWMSC, and is represented by a single time constant T_{PWMSC}. The output of the lag block X_S has windup limits associated with it. The ultimate reactance value is used to modify the line impedance of the series compensated branch during the calculation of the network solution [90, 91].

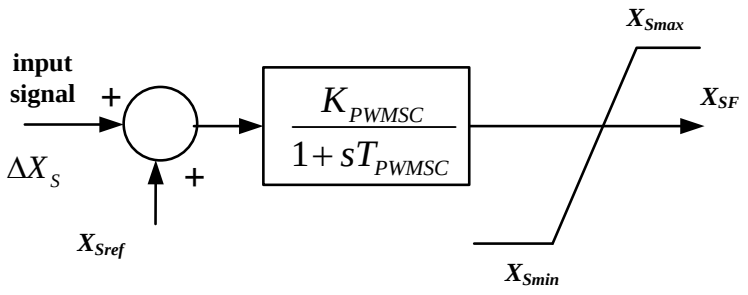

Figure 4.10: The dynamic control model of PWMSC.

4.3.3 Supplementary Controller Design

The idea of supplementary excitation is to apply a signal through the excitation system to increase the damping torque of the generator in the power system. Figure 4.11 shows the transfer function of a lead-lag controller whose output controls the reactance of the PWMSC. Various input signals can be used for the supplementary excitation design: the speed deviation Δω, the accelerating power ΔPa, or the system frequency Δf . As it is known that the generator speed contains components of all the torsional modes [92], it is selected as the stabilizing signal in the supplementary signal in the supplementary controller design.

Design a Phase Lead Compensation: The phase lead compensation may be realized by operational amplifiers, and the simplest transfer function may be chosen in the form of

$$G_C = \left(\frac{1+sT_1}{1+sT_2}\right)^k, \qquad k = 1 \text{ or } 2,\ T_1 > T_2 \tag{4.17a}$$

There is a phase angle limit that a compensation block can provide, and T_2 cannot be too small. For a T_2 chosen as 0.2s and T_1 as $10T_2$, the phase lead provided by each compensation block is about 34° for $s = j2\pi$ rad/s corresponding to 1 Hz.

Design a Reset Block for u_E: The supplementary excitation control should be activated only when the low-frequency oscillation begins to develop, and it should be automatically terminated when the system oscillation ceases. It should not interfere with the regular function of excitation during steady-state operation at the system frequency. A reset block is therefore necessary, which may have the form of

$$G_{RESET} = \frac{sT}{1+sT} \tag{4.17b}$$

Since the reset block should not have any effect on phase shift or gain at the oscillating frequency, it can be achieved by choosing a large T value, so that sT is much larger than unity.

Figure 4.11 shows the block diagram of a supplementary excitation control with one compensation block and one reset block. The supplementary excitation will not have any effect on the steady state of the system, since in steady state

$$s\Delta\omega = 0 \tag{4.17c}$$

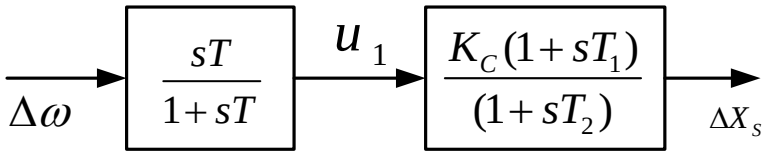

Figure 4.11: Transfer function lead-lag controller

The linearized equation of PWMSC with lead-lag controller is derived as follows

$$\begin{bmatrix} \frac{d\Delta u_1}{dt} \\ \frac{d\Delta X_S}{dt} \\ \frac{d\Delta X_{SF}}{dt} \end{bmatrix} = \begin{bmatrix} C_1 \\ C_2 \\ C_3 \end{bmatrix} \begin{bmatrix} \Delta X_{syn} \\ \Delta X_{ms} \\ du_1 \\ dX_S \\ dX_{SF} \end{bmatrix} \tag{4.17d}$$

Where

$$C_1 = \Big[-\frac{Kw_0}{M_g} i_{q0}(L_q - L_d) \quad -\frac{Kw_0}{M_g}\{i_{d0}(L_q - L_d) + i_{fd0}L_{ad}\} \quad -\frac{Kw_0}{M_g} i_{q0}L_{ad} \quad \frac{Kw_0}{M_g} i_{d0}L_{aq} \dots$$

$$-\frac{Kw_0}{M_g} i_{q0}L_{ad} \quad \frac{Kw_0}{M_g} i_{d0}L_{aq} \quad \frac{Kw_0}{M_g} K_{gE} \quad -\frac{Kw_0}{M_g}(K_{gB} + K_{gE}) \quad \frac{Kw_0}{M_g} K_{gB} \quad 0 \quad 0 \quad 0 \quad 0 \dots$$

$$-\frac{KD_g}{M_g} \quad 0 \quad 0 \quad 0 \quad 0 \quad -\frac{1}{T_\omega} \quad 0 \quad 0 \Big]$$

$$C_2 = \Big[-\frac{T_1}{T_2}\frac{Kw_0}{M_g} i_{q0}(L_q - L_d) \quad -\frac{T_1}{T_2}\frac{Kw_0}{M_g}\{i_{d0}(L_q - L_d) + i_{fd0}L_{ad}\} \quad -\frac{T_1}{T_2}\frac{Kw_0}{M_g} i_{q0}L_{ad} \dots$$

$$\frac{T_1}{T_2}\frac{Kw_0}{M_g} i_{d0}L_{aq} \quad -\frac{T_1}{T_2}\frac{Kw_0}{M_g} i_{q0}L_{ad} \quad \frac{T_1}{T_2}\frac{Kw_0}{M_g} i_{d0}L_{aq} \quad \frac{T_1}{T_2}\frac{Kw_0}{M_g} K_{gE} \dots$$

$$-\frac{T_1}{T_2}\frac{Kw_0}{M_g}(K_{gB} + K_{gE}) \quad \frac{T_1}{T_2}\frac{Kw_0}{M_g} K_{gB} \quad 0 \quad 0 \quad 0 \quad 0 \quad -\frac{T_1}{T_2}\frac{KD_g}{M_g} \quad 0 \quad 0 \quad 0 \quad 0 \dots$$

$$-\left(\frac{1}{T_2} - \frac{T_1}{T_2}\frac{1}{T_\omega}\right) \quad -\frac{1}{T_2} \quad 0 \Big]$$

$$C_3 = \Big[0_{1\times 19} \quad \frac{K_{PWMSC}}{T_{PWMSC}} \quad -\frac{1}{T_{PWMSC}} \Big]$$

4.4 Overall System Model

The overall model of the system under study can be derived by performing the following mathematical manipulations for the interactions among the various components of the system [83].

The electrical parts of the system: combining Equation (3.3) and (4.14) to form the following equations

$$\begin{bmatrix} \frac{d\Delta X_{syn}}{dt} \\ \frac{d\Delta V_{Cd}}{dt} \\ \frac{d\Delta V_{Cq}}{dt} \\ \frac{d\Delta V_{Sd}}{dt} \\ \frac{d\Delta V_{Sq}}{dt} \end{bmatrix} = [Amt\_PWMSC] \begin{bmatrix} \Delta X_{syn} \\ \Delta V_{Cd} \\ \Delta V_{Cq} \\ \Delta V_{Sd} \\ \Delta V_{Sq} \end{bmatrix} + [Bmt\_PWMSC] \begin{bmatrix} \Delta e_{fd} \\ \Delta\omega \\ \Delta\delta \end{bmatrix} \tag{4.18}$$

$$\begin{bmatrix} \Delta V_{td} \\ \Delta V_{tq} \end{bmatrix} = [Ci\_PWMSC] \begin{bmatrix} \Delta X_{syn} \\ \Delta V_{Cd} \\ \Delta V_{Cq} \\ \Delta V_{Sd} \\ \Delta V_{Sq} \end{bmatrix} + [Di\_PWMSC] \begin{bmatrix} \Delta e_{fd} \\ \Delta\omega \\ \Delta\delta \end{bmatrix} \tag{4.19}$$

The mechanical parts of the system: combining Equations (3.17), (3.19) and (3.23) to form the following equations

$$\begin{bmatrix} \frac{d\Delta X_{ms}}{dt} \\ \frac{d\Delta X_{g}}{dt} \\ \frac{d\Delta X_{v}}{dt} \end{bmatrix} = [Ap1] \begin{bmatrix} \Delta X_{ms} \\ \Delta X_{g} \\ \Delta X_{v} \end{bmatrix} + [Ap2] \begin{bmatrix} \Delta T_e \\ \Delta V_t \end{bmatrix} + [Bp] \begin{bmatrix} \Delta P_{m0} \\ \Delta E_{ref} \end{bmatrix} \tag{4.20}$$

There are, however, two non-state variables ΔT_e and ΔV_t that must be eliminated.

The linearized form of the air-gap torque Equation (3.24) is given by

$$\Delta T_e = [Tedq0][\Delta X_{syn}] \tag{4.21}$$

where

$$[Tedq0] = \begin{bmatrix} i_{q0}(L_q - L_d) & i_{d0}(L_q - L_d) + i_{fd0}L_{ad} & i_{q0}L_{ad} & -i_{d0}L_{aq} & i_{q0}L_{ad} & -i_{d0}L_{aq} \end{bmatrix} \tag{4.22}$$

The linearized terminal voltage equation ${V_t}^2 = {V_{td}}^2 + {V_{tq}}^2$ is given by

$$\Delta V_t = \begin{bmatrix} \frac{V_{td0}}{V_{t0}} & \frac{V_{tq0}}{V_{t0}} \end{bmatrix} \begin{bmatrix} \Delta V_{td} \\ \Delta V_{tq} \end{bmatrix} \tag{4.23}$$

Combining Equations (19) (21) (23) (2.26), (2.28) and (3.30) to form the following equation

$$\begin{bmatrix} \Delta T_e \\ \Delta V_t \end{bmatrix} = [Cmt\_PWMSC] \begin{bmatrix} \Delta X_{syn} \\ \Delta V_{Cd} \\ \Delta V_{Cq} \\ \Delta V_{Sd} \\ \Delta V_{Sq} \end{bmatrix} + [Dmt\_PWMSC] \begin{bmatrix} \Delta e_{fd} \\ \Delta\omega \\ \Delta\delta \end{bmatrix} \tag{4.24}$$

The overall system equations derived by combining Equation (4.18), (4.20) and (4.24) are written by

$$\left[\frac{d\Delta X}{dt}\right] = [A][\Delta X] + [B][\Delta U] \tag{4.25}$$

where

$$[\Delta X] = [\Delta\delta_E \quad \Delta\delta \quad \Delta\delta_B \quad \Delta\delta_A \quad \Delta\delta_I \quad \Delta\delta_H \quad \Delta\omega_E \quad \Delta\omega \quad \Delta\omega_B \quad \Delta\omega_A \, \Delta\omega_I \quad \Delta\omega_H \ \ldots$$

$$\Delta C_V \quad \Delta P_H \ \Delta P_I \quad \Delta P_A \quad \Delta e_{fd} \quad \Delta E_R \quad \Delta E_{SB} \quad \Delta i_d \quad \Delta i_q \quad \Delta i_{fd} \quad \Delta i_{1q} \ \ldots$$

$$\Delta i_{1d} \quad \Delta i_{2q} \quad \Delta V_{Cd} \quad \Delta V_{Cq} \quad \Delta V_{Sd} \quad \Delta V_{Sq} \quad u_1 \quad \Delta X_S \quad \Delta X_{SF}]^{\mathrm{T}}$$

$$[\Delta U] = [\Delta P_{m0} \quad \Delta E_{ref}]^{\mathrm{T}} \tag{4.26}$$

The complete electrical and mechanical model of a one-machine, infinite-bus system for SSR study with PWMSC is a 32nd order system.

The detail manipulations for forming the overall system equations are shown in Appendix C.

4.5 The Controller Gains Using the Genetic Algorithm Approach

Genetic algorithm (GA) can be applied in the tuning of the supplementary controller gains for optimization. It will help the optimal control performance in the PWMSC. To select the best compensator parameters that enhance the power system dynamic performance the most, an eigenvalue based objective function is considered as given below-

$$J = - \min (\text{real (eigenvalues)} / \text{abs (eigenvalues)}) \quad (4.27)$$

So the objective here is to maximize the minimum of the damping ratio for a certain parameter set. Maximizing the minimum damping ratio will help the cause of improving the system overall damping. The supplementary controller parameter are bounded in the following manner-

$$10 > T_1 > 0.01$$

$$10 > T_2 > 0.01$$

$$10 > K_C > 1$$

The searching method developed in this work using a GA technique for the lead-lag controller's gains and time constants tuning and adjustment is described by a flowchart with the following steps:

Step1: Initialization: - Start the process by randomly generating (N–1) individuals of the initial population, where each individual is a candidate solution of the problem. The numerical values that each gain may assume are constrained by low boundary and high boundary values, in p.u., as described in the following

$$low\ boundary \leq gain's\ value \leq high\ boundary$$

The set of gains obtained by the poles placement procedure composes one of the individuals of the initial population.

The set of gains of the two loop generic lead-lag controller to be obtained forms one of the individuals of the initial population.

Table 4.1: Chromosome structure

T_1	T_2	K_C

Step 2: Evaluation: - Calculate the fitness value of each individual in the generation. The fitness value of individuals is given by:

$$g = -min\left\{\frac{-real(\lambda_i)}{abs(\lambda_i)}\right\} \quad (4.28)$$

$$for\ i = 1,2,3,\dots,N,\dots$$

Where, g is the fitness value, λ_i are the eigenvalues and i is the number of eigenvalues of the closed loop system. In optimization the aim is to minimize g in order to shift all the eigenvalues as far to the left of the left hand side of the complex plane as possible.

Step 3: New generation: - After the initial evaluation is concluded, the genetic operators are applied to obtain new individuals in the search space of the optimal solution. The search space of the optimal solution is consist of cross over and mutation.

Step 4: Stopping criteria: - If one of the stopping criteria is satisfied, then stop, else go to Step2. Here, the stopping criteria may be the maximal number of iterations, or the fitness value of best smaller than a specified negative value.

Step 5: Updating velocities and positions: - if the convergence or termination criterion is not satisfied, the iterative process returns to step 2. The flow chart is given below-

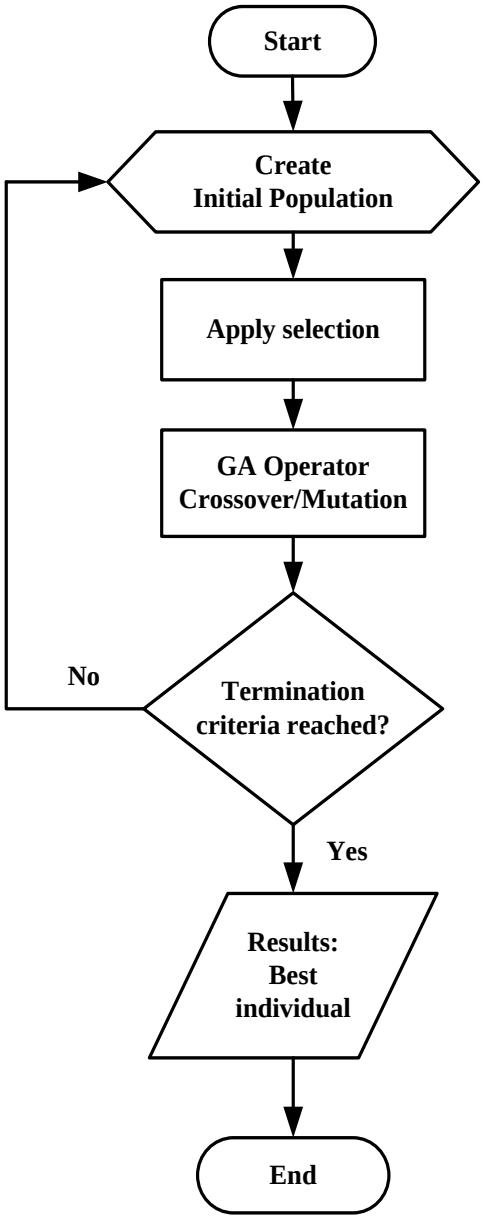

Figure 4.12: Genetic Algorithm flow chart for obtaining controller parameters

4.6 Simulation of SSR under Small Disturbance in PWMSC Installed System

In order to demonstrate the dynamic performance of the study system a pulse type disturbance is initiated in the governor side at t = 0.2 seconds and is cleared at t = 0.5. The simulation is performed for the four critical compensation levels as 26.5%, 41.1%, 54.7% and 68.4%.

4.6.1 Damping Subsynchronous Torsional Oscillations at 26.5% Compensation level

The PWMSC gain and time constants and the supplementary controller parameters obtained by using the genetic optimization technique are shown in the Table 4.2.

Table 4.2: Controller parameters at 26.5% compensation level

PWMSC	
$K_{PWMSC} = 10$	$T_{PWMSC} = 10$
Supplementary controller	
$T_1 = 0.0938$	$T_2 = 0.0100$
$T_w = 1$	$K_C = 1.7438$

Table 4.3: Eigenvalues of SMIB system with PWMSC and without PWMSC for the 26.5% Compensation level

Modes	26.5% Compensation level	
	Without PWMSC	With PWMSC
Mode 5	- 0.48 ± 298.28i	- 0.48 ± 298.28i
Mode 4	**1.56 ± 202.73i**	- 0.12 ± 202.90i
Mode 3	- 0.40 ± 160.77i	-0.44 ± 160.57i
Mode 2	- 0.14 ± 127.07i	-0.15 ± 127.00i
Mode 1	- 0.20 ± 99.22i	-0.22 ± 97.89i
Mode 0	- 0.43 ± 8.45i	-1.56 ± 13.82i
Elec.	- 4.49 ± 202.88i	-2.59 ± 69.95i
Other modes	- 4.97 ± 551.23i - 96.63 ± 1.50i - 32.72 - 26.67 - 10.29 - 5.08 - 2.37 - 1.68 - 0.14 - 0.60 - 0.89	- 9.58 ± 686.53i - 0.00 ± 377.00i - 97.39 ± 1.41i - 100.00 - 34.66 - 26.93 - 10.11 - 7.57 - 2.45 - 1.66 - 0.14 - 0.71 - 0.92 - 0.10 - 01.00

Stability can also be checked by seeing the eigenvalue of the system matrix derived from the system model. The eigenvalues obtained from our proposed model is shown in the Table 4.3. It has been found that Mode 4 is unstable without PWMSC at 26.5% compensation level. After introducing PWMSC this Mode 4 becomes stable and at Mode 0 the stability improved.

The time response of different state variables with and without PWMSC in the system for 26.5% compensation level is shown in the Figure 4.13 to 4.21.

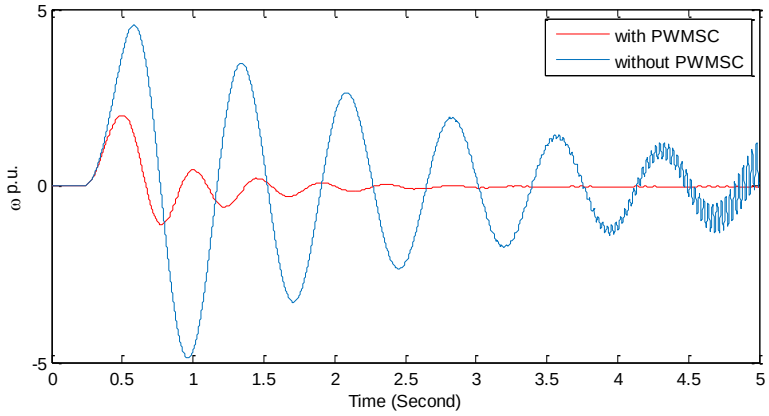

Figure 4.13: Time response of the generator (GEN) angular speed variation with PWMSC and without PWMSC at 26.5% compensation level.

It has been found from the Figure 4.13 that the generator (GEN) angular speed variation without PWMSC has the highest peak of 4.8 p.u. and the instability increases severely after 3.7s. The response with PWMSC starts to rise after 0.3s and rises upto 2.3 p.u. and become completely stable after around 3s.

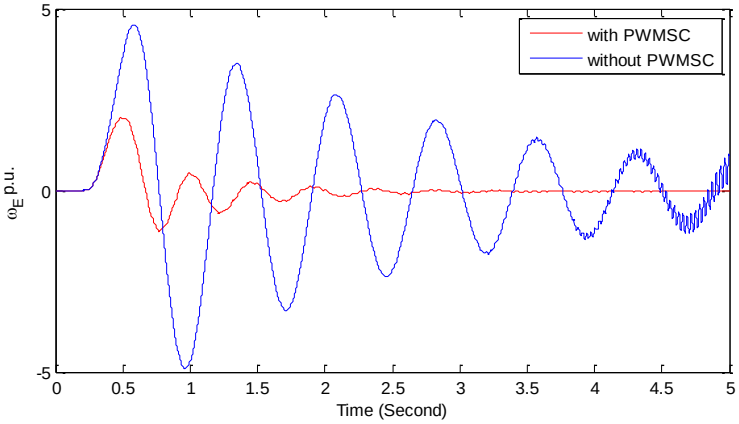

Figure 4.14: Time response of the exciter (EXC) angular speed variation with PWMSC and without PWMSC at 26.5% compensation level.

It has been found that (Figure 4.14) the exciter (EXC) angular speed variation without PWMSC has the highest peak of 4.8 p.u. and the instability increases severely after 4.0s. The response with PWMSC starts to rise after 0.3s and rises upto 2.3 p.u. and become completely stable after around 3s.

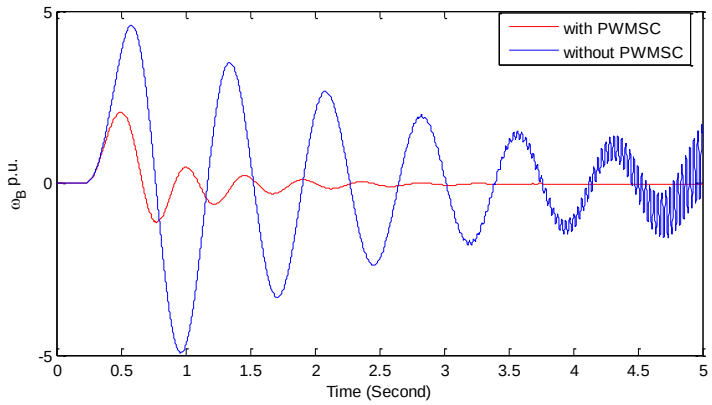

Figure 4.15: Time response of the low pressure stage (LPB) angular speed variation with PWMSC and without PWMSC at 26.5% compensation level.

It has been found that (Figure 4.15) the low pressure stsge (LPB) angular speed variation without PWMSC has the highest peak of 4.8 p.u. and the instability increases severely after 3.0s. The response with PWMSC starts to rise after 0.3s and rises upto 2.3 p.u. and become completely stable after around 3s.

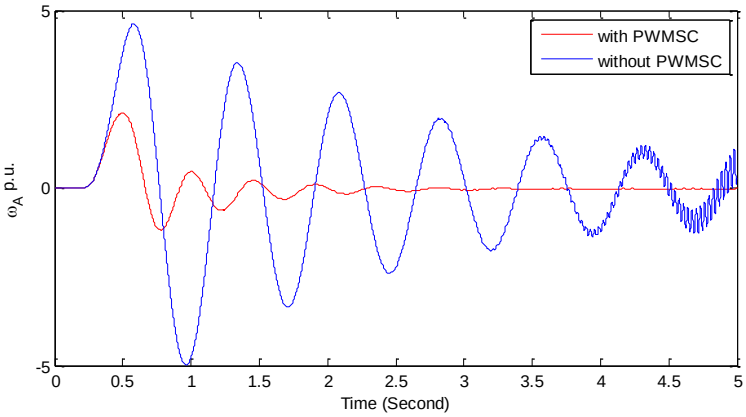

Figure 4.16: Time response of the low pressure stage (LPA) angular speed variation with PWMSC and without PWMSC at 26.5% compensation level.

It has been found that (Figure 4.16) the low pressure stsge (LPA) angular speed variation without PWMSC is unstable and has the highest peak of 4.8 p.u. and after 4s the instability

increases. The PWMSC successfully damp out the oscillations after around 3s.The response with PWMSC starts to rise after 0.3s and rises upto 2.3 p.u..

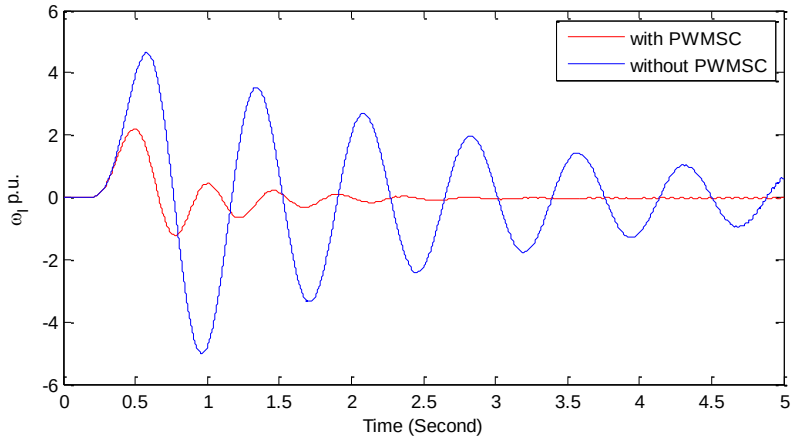

Figure 4.17: Time response of the intermediate pressure stage (IP) angular speed variation with PWMSC and without PWMSC at 26.5% compensation level.

It has been found that (Figure 4.17) the intermediate stage (IP) angular speed variation without PWMSC has the highest peak of 5.0 p.u. and the signal is gradually dampin but with a high settling time. The response with PWMSC starts to rise after 0.2s and rises upto 2 p.u. and become completely stable after around 2.5s.

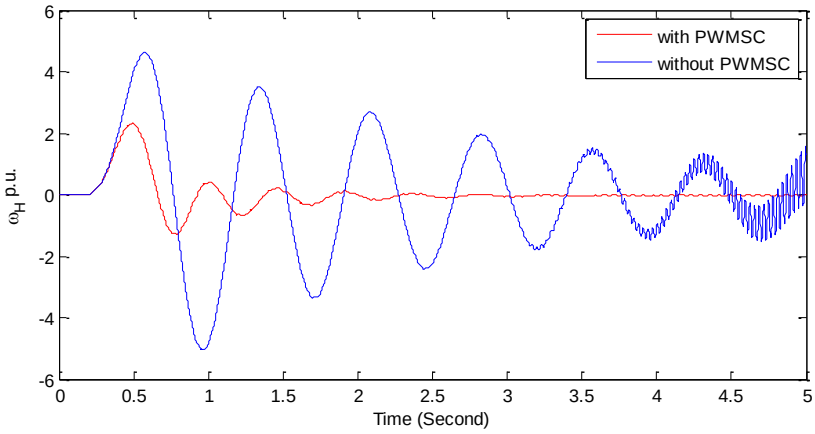

Figure 4.18: Time response of the High Pressure stage (HP) angular speed variation with PWMSC and without PWMSC at 26.5% compensation level.

It has been found that (Figure 4.18) the High Pressure stage (HP) angular speed variation without PWMSC has the highest peak of 4.4 p.u. and the instability increases severely after

3.5s. The response with PWMSC starts to rise after 0.3s and rises upto 2.1 p.u. and become completely stable after around 2.5s.

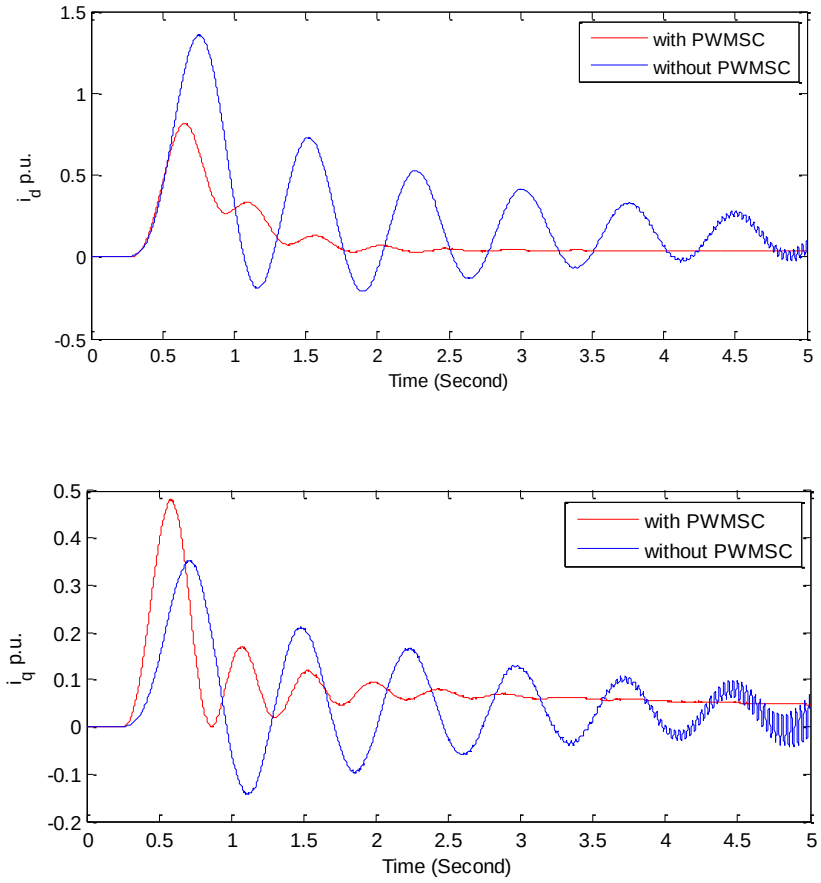

Figure 4.19: Time response of the generator stator currents in the d-q reference frame of the system with PWMSC and without PWMSC at 26.5% compensation level.

It has been found that (Figure 4.19) the stator current component in d-axis rises higher than the q-axis current. But both i_d and i_q response become stable after using PWMSC in the system.

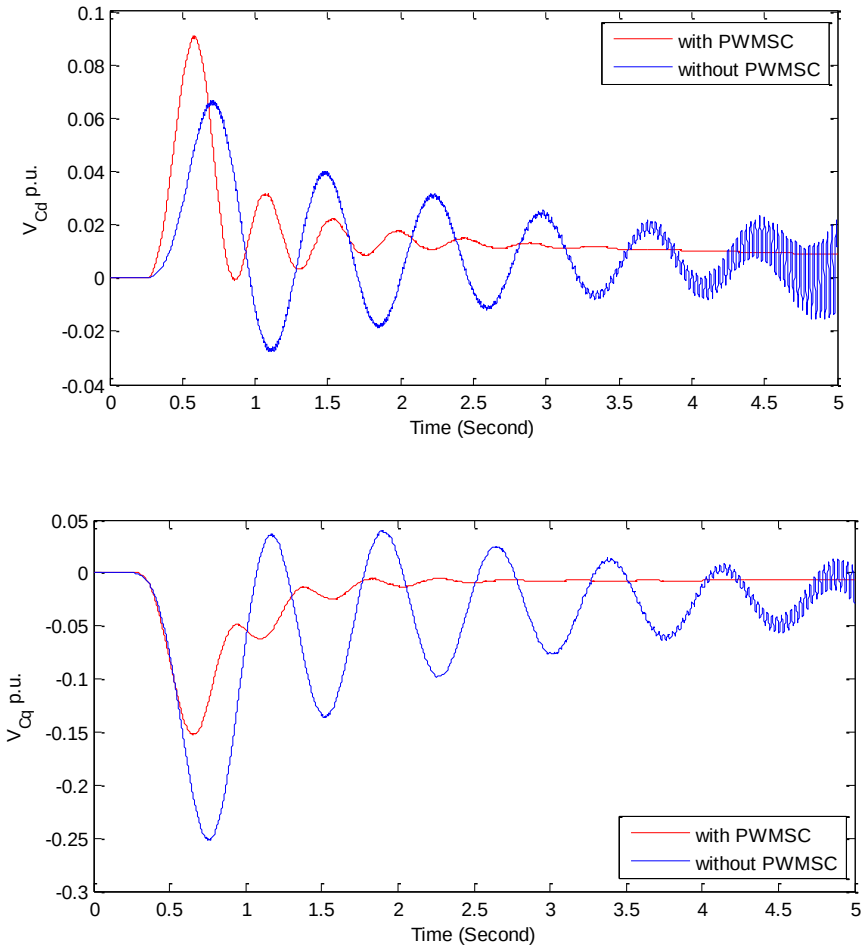

Figure 4.20: Time response of the series compensator capacitor voltage in the d-q reference frame of the system with PWMSC and without PWMSC at 26.5% compensation level.

It has been found that (Figure 4.20) the capacitor voltage component in d-axis is more unstable than the q-axis. But both V_{cd} and V_{cq} response become stable after using PWMSC in the system.

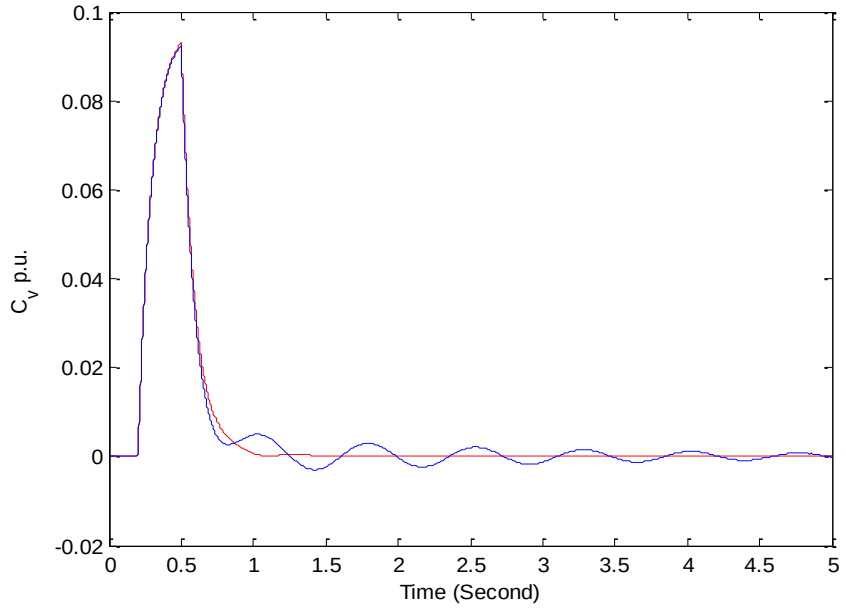

Figure 4.21: Time response of the governor valve control (C_v) with PWMSC and without PWMSC for 26.5% compensation level.

It has been found that (Figure 4.21) the governor valve is open from 0.2s to 0.7s and then oscillates with small amplitude for the system without PWMSC. But after using PWMSC the governor valve become stable after 0.7s.

4.6.2 Damping Subsynchronous Torsional Oscillations at 41.1% Compensation Level

The PWMSC gain and time constants and the supplementary controller parameters obtained from the genetic optimization techniques are shown in the Table 4.4.

Table 4.4: Controller parameters at 41.1% compensation level

PWMSC	
$K_{PWMSC} = 10$	$T_{PWMSC} = 10$
Supplementary controller	
$T_1 = 1.8339$	$T_2 = 0.01$
$T_w = 1$	$K = 1$

Table 4.5: Eigenvalues of SMIB system with PWMSC and without PWMSC for the 41.1% compensation level

Modes	41.1% Compensation level	
	Without PWMSC	With PWMSC
Mode 5	- 0.48 ± 298.28i	- 0.48 ± 298.28i
Mode 4	- 0.12 ± 202.77i	- 0.12 ± 202.90i
Mode 3	**1.42 ± 160.35i**	- 0.44 ± 160.57i
Mode 2	- 0.14 ± 127.11i	- 0.15 ± 127i
Mode 1	- 0.18 ± 99.46i	- 0.23 ± 97.91i
Mode 0	- 0.55 ± 9.36i	- 1.58 ± 13.88i
Elec.	- 3.86 ± 160.43i	- 2.54 ± 69.35i
Other modes	- 5.07 ± 594.02i - 96.86 ± 1.58i - 32.98 - 26.70 - 10.27 - 5.47 - 2.39 - 1.68 - 0.14 - 0.63 - 0.89	- 9.58 ± 687.11i - 97.38 ± 1.41i - 0.00 ± 377.00i - 0.10 - 100. - 1.00 - 34.68 - 26.93 - 0.10.11 - 0.07.60 - 0.02.45 - 0.01.66 - 0.00.14 - 0.00.71 - 0.00.92

It has been found that (Table 4.5) Mode 3 is unstable without PWMSC at 41.1% compensation level. After introducing PWMSC this Mode 3 becomes stable and at Mode 0 the stability increased. The controller parameters for the optimal operation of PWMSC are obtained by genetic algorithm and shown in the Table 4.4.

The time response of different state variables with and without PWMSC in the system for 41.1% compensation level is shown in the Figure 4.22 to 4.30.

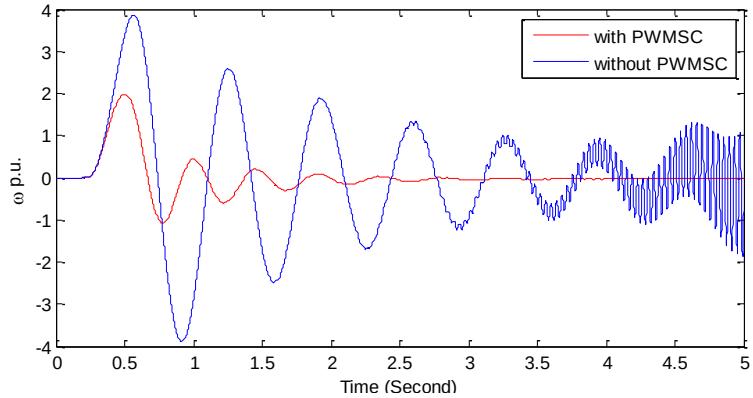

Figure 4.22: Time response of the generator (GEN) angular speed variation with PWMSC and without PWMSC at 41.1% compensation level.

It has been found from the Figure 4.22 that the generator (GEN) angular speed variation without PWMSC has the highest peak of 3.9 p.u. and the instability increases severely after 3.0s. The response with PWMSC starts to rise after 0.35s and rises upto 2.0 p.u. and become completely stable after around 2.7s.

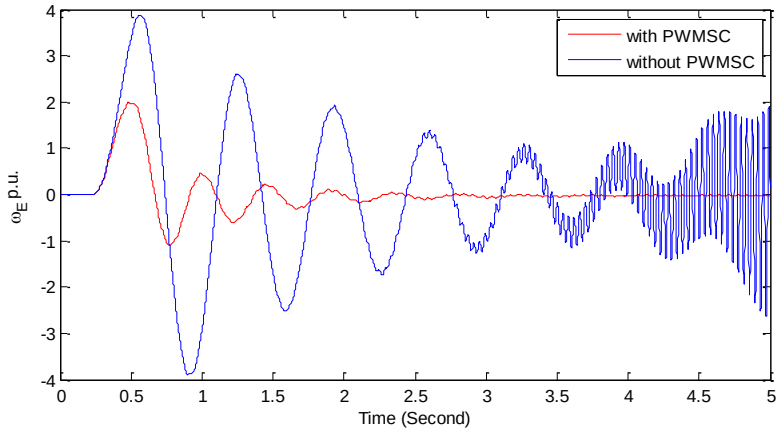

Figure 4.23: Time response of the exciter (EXC) angular speed variation with PWMSC and without PWMSC at 41.1% compensation level.

It has been found that (Figure 4.23) the exciter (EXC) angular speed variation without PWMSC has the highest peak of 3.9 p.u. and the instability increases severely after 2.5s. The response with PWMSC starts to rise after 0.3s and rises upto 2.0 p.u. and become completely stable after around 2.5s.

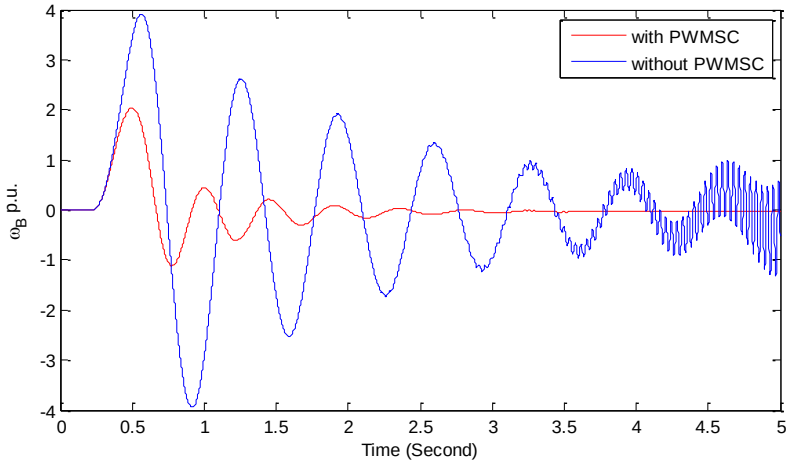

Figure 4.24: Time response of the low pressure stage (LPB) angular speed variation with PWMSC and without PWMSC at 41.1% compensation level.

It has been found that (Figure 4.24) the low pressure stsge (LPB) angular speed variation without PWMSC has the highest peak of 4.0 p.u. and the instability increases severely after 3.0s. The response with PWMSC starts to rise after 0.25s and rises upto 2.0 p.u. and become completely stable after around 3s.

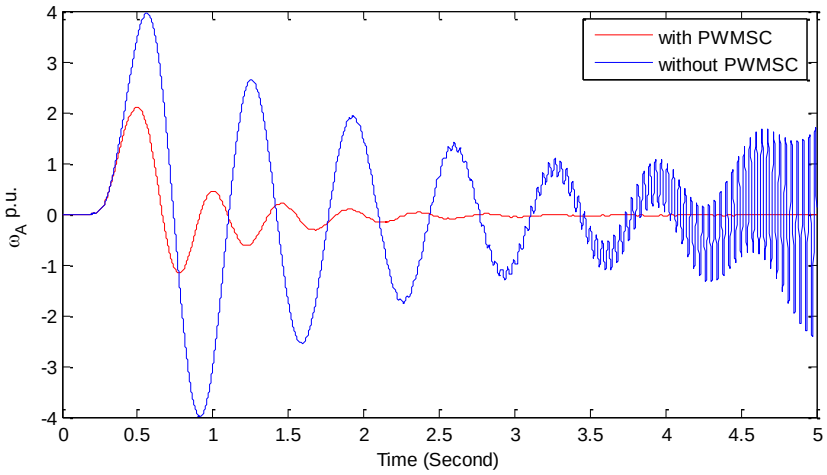

Figure 4.25: Time response of the low pressure stage (LPA) angular speed variation with PWMSC and without PWMSC at 41.1% compensation level.

It has been found that (Figure 4.25) the low pressure stsge (LPA) angular speed variation without PWMSC is unstable and has the highest peak of 4.0 p.u. and after 3s the instability increases. The PWMSC successfully damp out the oscillations after around 2.5s.The response with PWMSC starts to rise after 0.2s and rises upto 2.0 p.u..

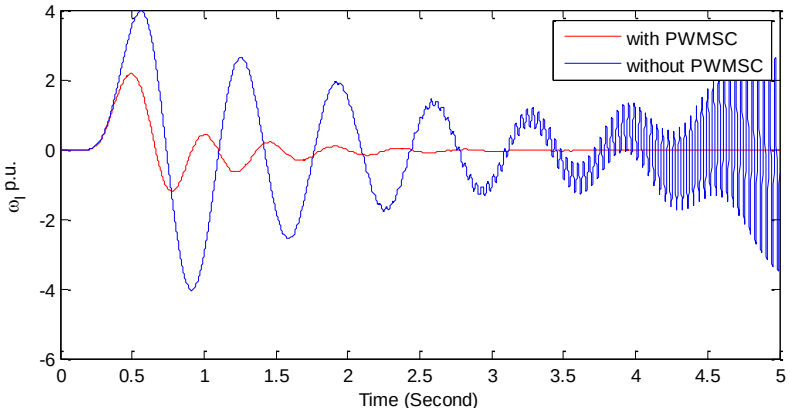

Figure 4.26: Time response of the intermediate pressure stage (IP) angular speed variation with PWMSC and without PWMSC at 41.1% compensation level.

It has been found that (Figure 4.26) the intermediate stage (IP) angular speed variation without PWMSC has the highest peak of 4.0 p.u. and the signal is growing more unstable after 2.5s. The response with PWMSC starts to rise after 0.2s and rises upto 2 p.u. and become completely stable after around 2.5s.

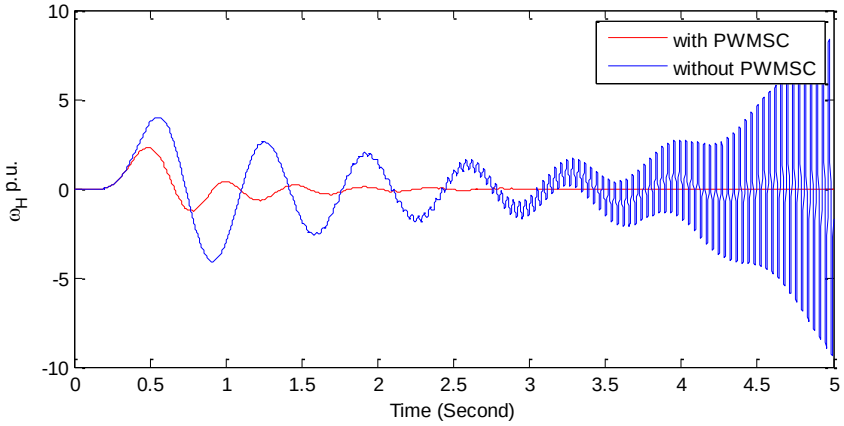

Figure 4.27: Time response of the High Pressure stage (HP) angular speed variation with PWMSC and without PWMSC at 41.15% compensation level.

It has been found that (Figure 4.27) the High Pressure stage (HP) angular speed variation without PWMSC has the highest peak of 4.6 p.u. and the instability increases severely after 2.5s. The response with PWMSC starts to rise after 0.3s and rises upto 2.5 p.u. and become completely stable after around 2.5s.

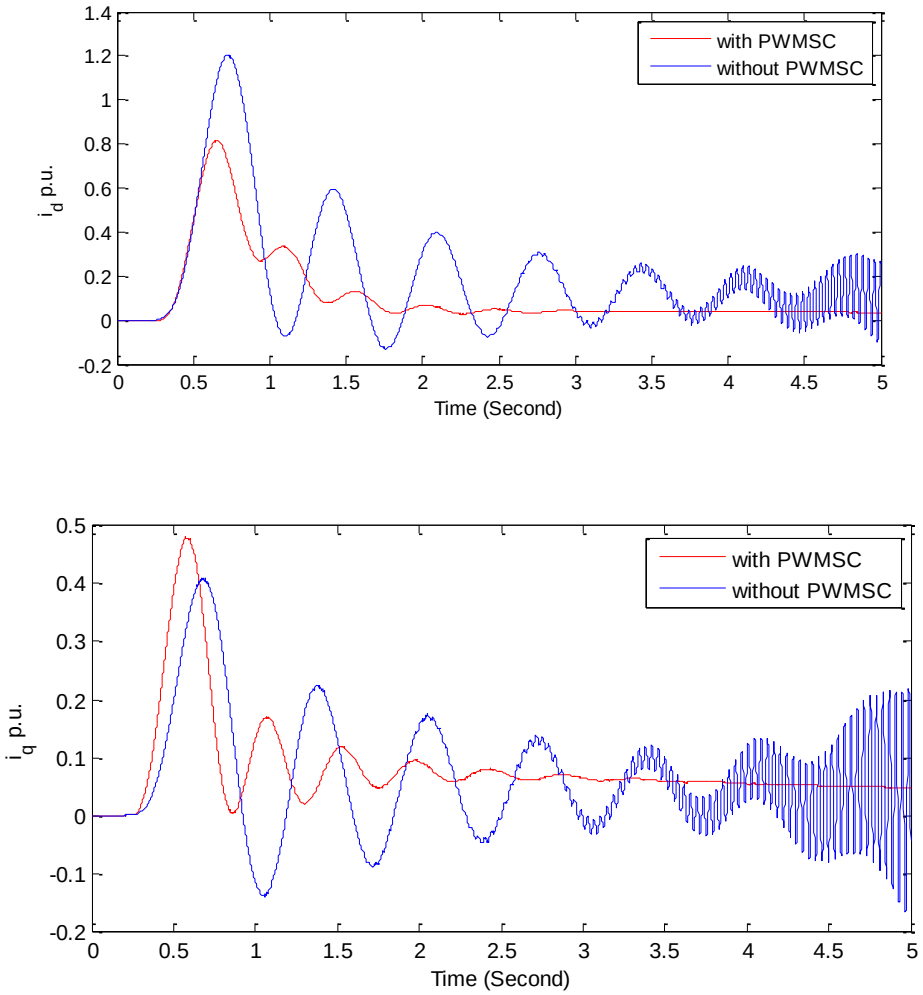

Figure 4.28: Time response of the generator stator currents in the d-q reference frame of the system with PWMSC and without PWMSC at 41.1% compensation level.

It has been found that (Figure 4.28) the stator current component in d-axis rises higher than the q-axis current. But both i_d and i_q response become stable after using PWMSC in the system.

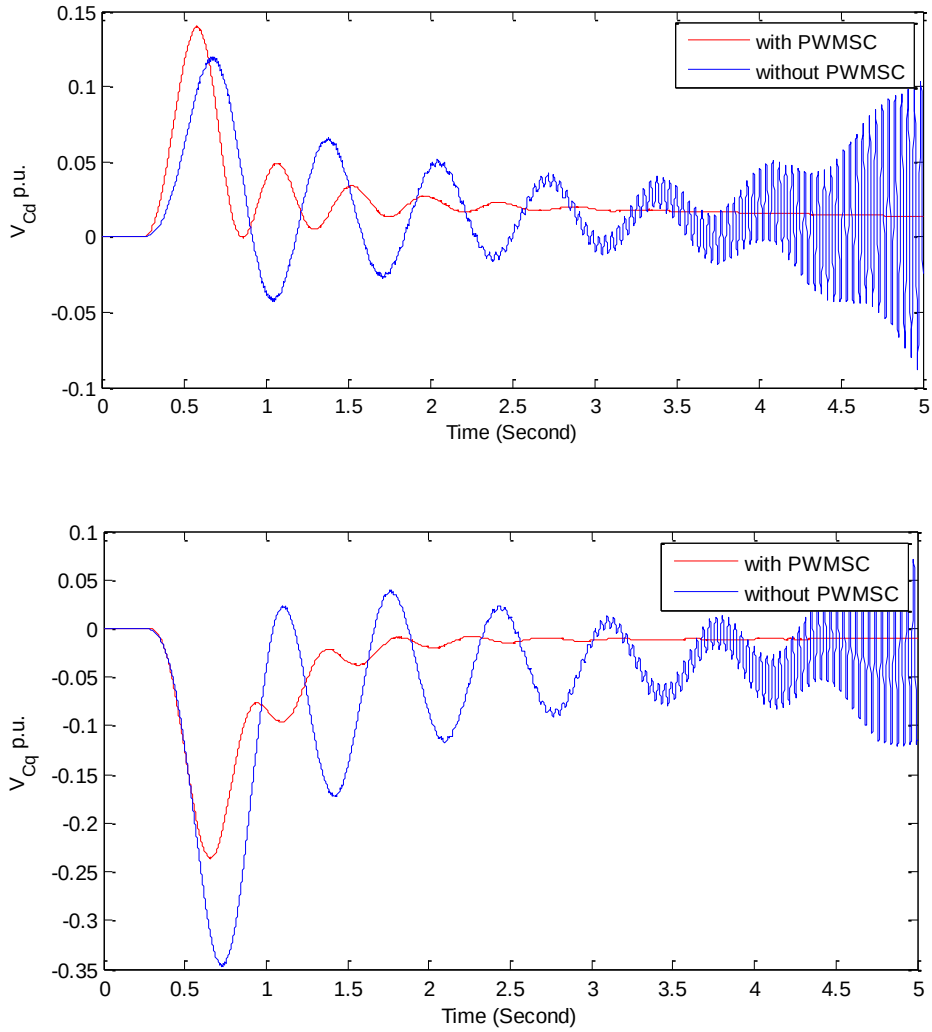

Figure 4.29: Time response of the series compensator capacitor voltage in the d-q reference frame of the system with PWMSC and without PWMSC at 26.5% compensation level.

It has been found that (Figure 4.29) the capacitor voltage component in d-axis is more unstable than the q-axis. But both V_{cd} and V_{cq} response become stable after using PWMSC in the system.

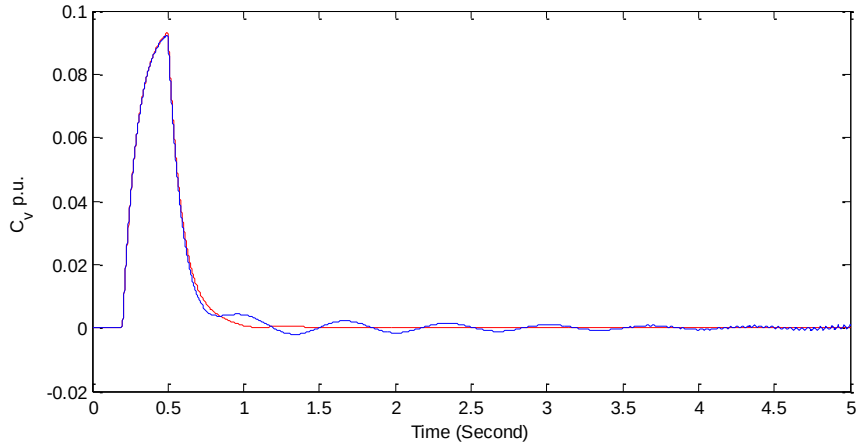

Figure 4.30: Time response of the governor valve control (C_v) with PWMSC and without PWMSC for 41.1% compensation level.

It has been found that (Figure 4.30) the governor valve is open from 0.2s to 0.65s and then oscillates with small amplitude for the system without PWMSC. But after using PWMSC the governor valve become stable after 0.7s.

4.6.3 Damping Subsynchronous Torsional Oscillations at 54.7% Compensation Level

The PWMSC gain and time constants and the supplementary controller parameters obtained from the genetic optimization techniques are shown in the Table 4.6.

Table 4.6: Controller parameters at 54.7% compensation level

PWMSC	
$K_{PWMSC} = 10$	$T_{PWMSC} = 10$
Supplementary controller	
$T_1 = 0.01$	$T_2 = 0.01$
$T_w = 1$	$K = 1$

Table 4.7: Eigenvalues of SMIB system with PWMSC and without PWMSC for the 54.7% compensation level

Modes	54.7% Compensation level	
	Without PWMSC	With PWMSC
Mode 5	- 0.48 ± 298.28i	- 0.48 ± 298.28i
Mode 4	- 0.12 ± 202.85i	- 0.12 ± 202.91i
Mode 3	- 0.44 ± 160.44i	- 0.44 ± 160.58i
Mode 2	**0.96 ± 126.85i**	- 0.15 ± 127.01i
Mode 1	- 0.13 ± 100.13i	- 0.27 ± 98.25i
Mode 0	- 0.75 ± 10.39i	- 2.01 ±15.20i
Elec.	- 2.26 ± 126.79i	-1.49 ± 57.25i
Other modes	- 5.13 ± 627.38i - 97.07 ± 1.59i - 33.30 - 26.75 - 10.24 - 5.92 - 2.41 - 1.67 - 0.14 - 0.65 - 0.90	- 9.60 ± 6.98.83i - 97.32 ± 1.30i - 0.00 ± 377.00i - 0.10 - 100.00 - 1.00 - 35.20 - 27.02 - 10.03 - 8.28 - 2.46 -1.66 - 0.14 - 0.72 - 0.92

The eigenvalues obtained from our proposed model is shown in the Table 4.7. It has been found that Mode 2 is unstable without PWMSC at 54.7% compensation level. After introducing PWMSC this Mode 2 becomes stable and at Mode 0 the stability increased.

The time response of different state variables with and without PWMSC in the system for 41.1% compensation level is shown in the Figure 4.31 to 4.39.

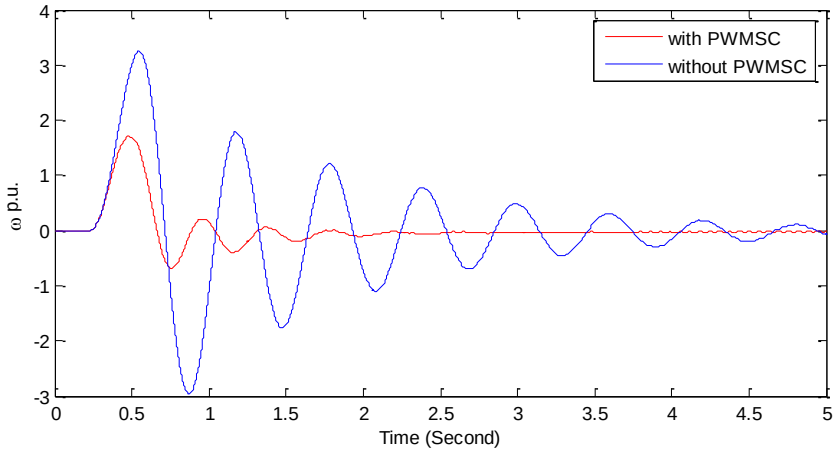

Figure 4.31: Time response of the generator (GEN) angular speed variation with PWMSC and without PWMSC at 54.7% compensation level.

It has been found from the Figure 4.31 that the generator (GEN) angular speed variation without PWMSC has the highest peak of 3.2 p.u. and the signal damps out gradually with time. The response with PWMSC starts to rise after 0.30s and rises upto 1.8 p.u. and become completely stable after around 2.5s.

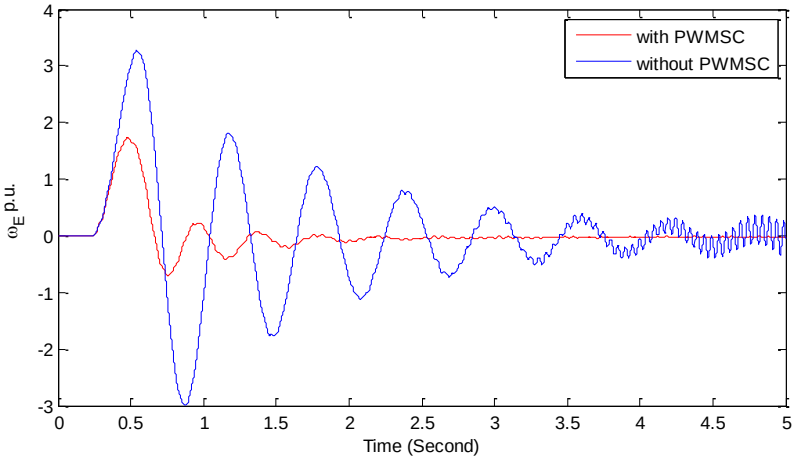

Figure 4.32: Time response of the exciter (EXC) angular speed variation with PWMSC and without PWMSC at 54.7% compensation level.

It has been found that (Figure 4.32) the exciter (EXC) angular speed variation without PWMSC has the highest peak of 3.2 p.u. and the system oscillations damp out gradually. The response with PWMSC starts to rise after 0.25s and rises upto 1.7 p.u. and become completely stable after around 2.5s.

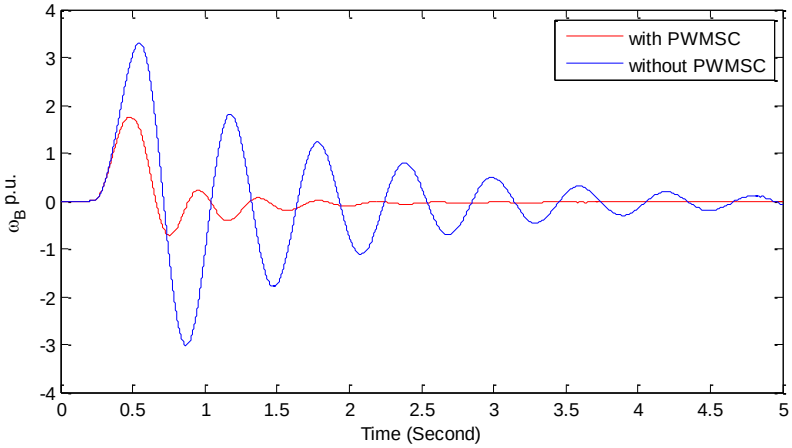

Figure 4.33: Time response of the low pressure stage (LPB) angular speed variation with PWMSC and without PWMSC at 54.7% compensation level.

It has been found that (Figure 4.33) the low pressure stsge (LPB) angular speed variation without PWMSC has the highest peak of 3.4 p.u. and the oscillations damp out gradually. But the system has a higher settling time. The response with PWMSC starts to rise after 0.3s and rises upto 1.7 p.u. and become completely stable after around 2.5s.

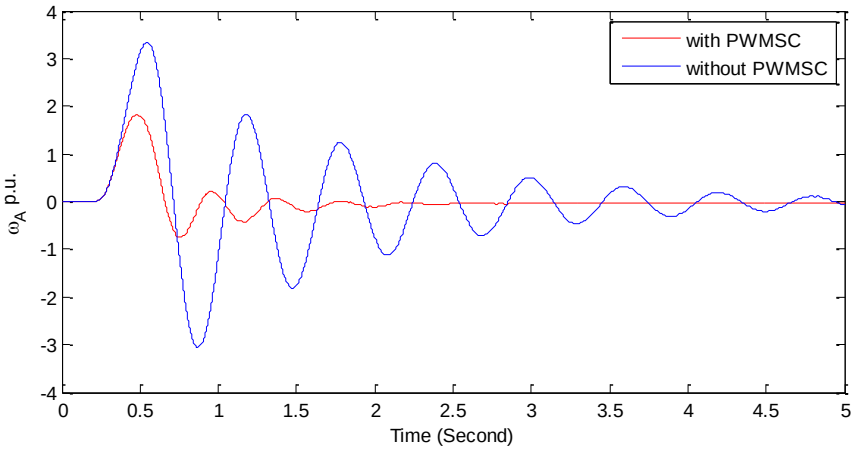

Figure 4.34: Time response of the low pressure stage (LPA) angular speed variation with PWMSC and without PWMSC at 54.7% compensation level.

It has been found that (Figure 4.34) the low pressure stsge (LPA) angular speed variation without PWMSC is unstable and has the highest peak of 3.2 p.u. and and the oscillations damp out slowly. The PWMSC successfully damp out the oscillations after around 2s.The response with PWMSC starts to rise after 0.2.5s and rises upto 1.8 p.u..

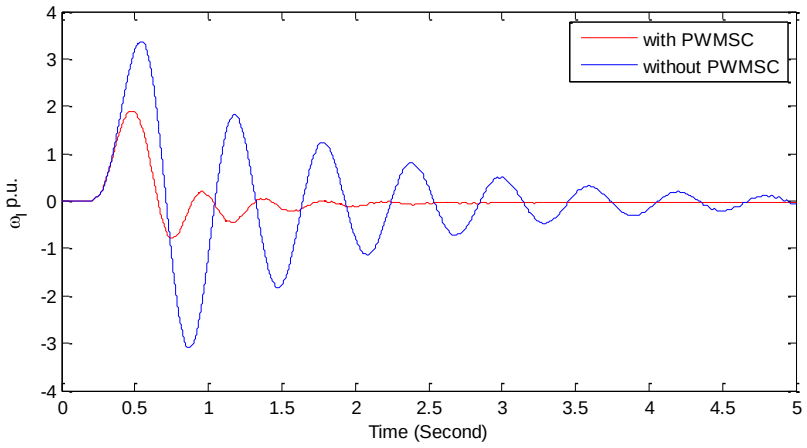

Figure 4.35: Time response of the intermediate pressure stage (IP) angular speed variation with PWMSC and without PWMSC at 54.7% compensation level.

It has been found that (Figure 4.35) the intermediate stage (IP) angular speed variation without PWMSC has the highest peak of 3.2 p.u. and the signal is gradually damping with a higher settling time. The response with PWMSC starts to rise after 0.2s and rises upto 3.2 p.u. and become completely stable after around 2.5s.

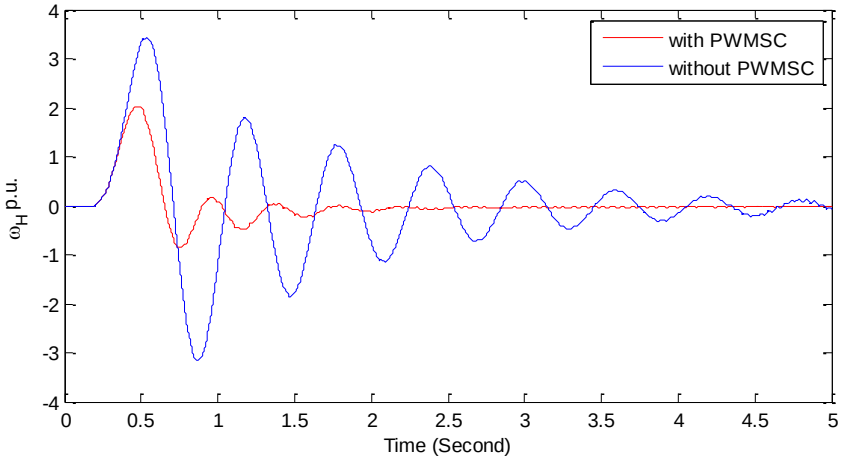

Figure 4.36: Time response of the High Pressure stage (HP) angular speed variation with PWMSC and without PWMSC at 54.7% compensation level.

It has been found that (Figure 4.36) the High Pressure stage (HP) angular speed variation without PWMSC has the highest peak of 3.6 p.u. and the oscillations damps out slowly with higher settling time.. The response with PWMSC starts to rise after 0.25s and rises upto 2.0 p.u. and become completely stable after around 2.0s.

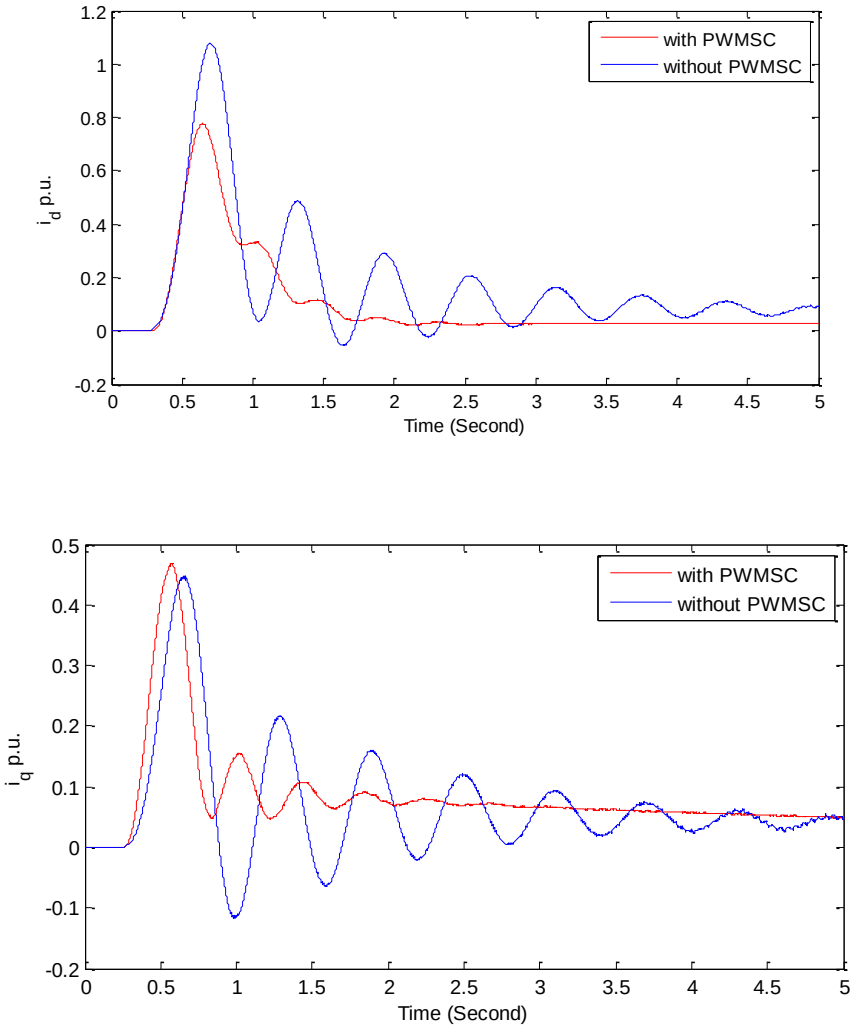

Figure 4.37: Time response of the generator stator currents in the d-q reference frame of the system with PWMSC and without PWMSC at 54.7% compensation level.

It has been found that (Figure 4.37) the stator current component in d-axis rises higher than the q-axis current. But both i_d and i_q response become stable after using PWMSC in the system.

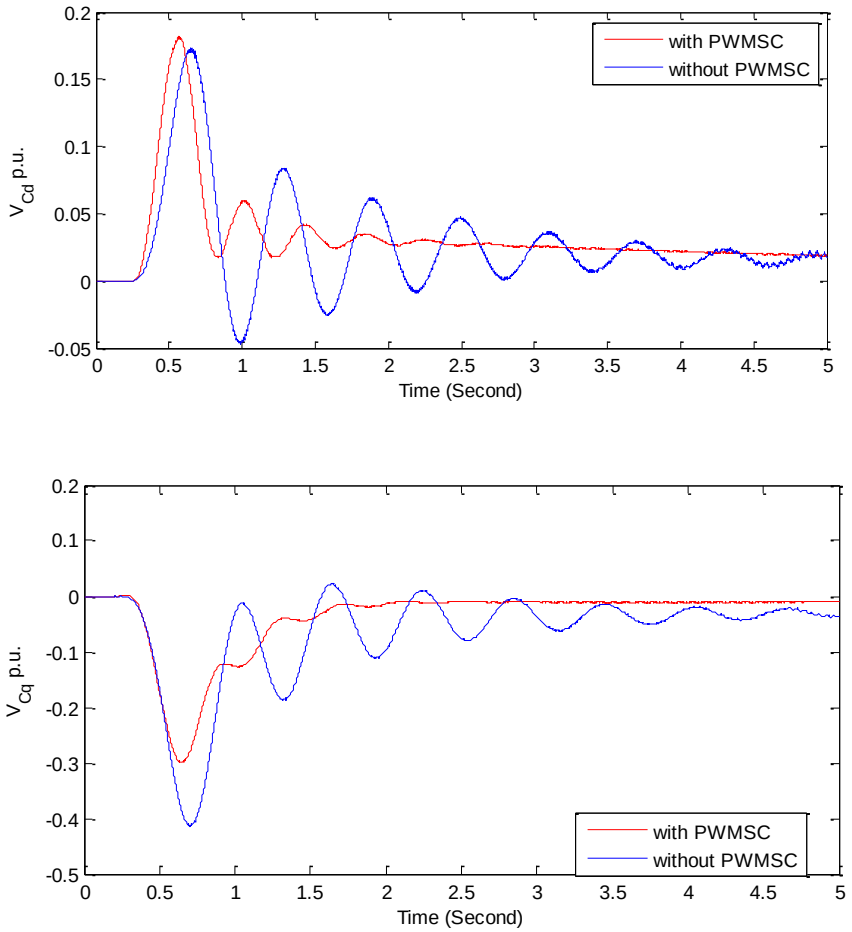

Figure 4.38: Time response of the series compensator capacitor voltage in the d-q reference frame of the system with PWMSC and without PWMSC at 54.7% compensation level.

It has been found that (Figure 4.38) the capacitor voltage component in d-axis is more unstable than the q-axis. But both V_{cd} and V_{cq} response become stable after using PWMSC in the system.

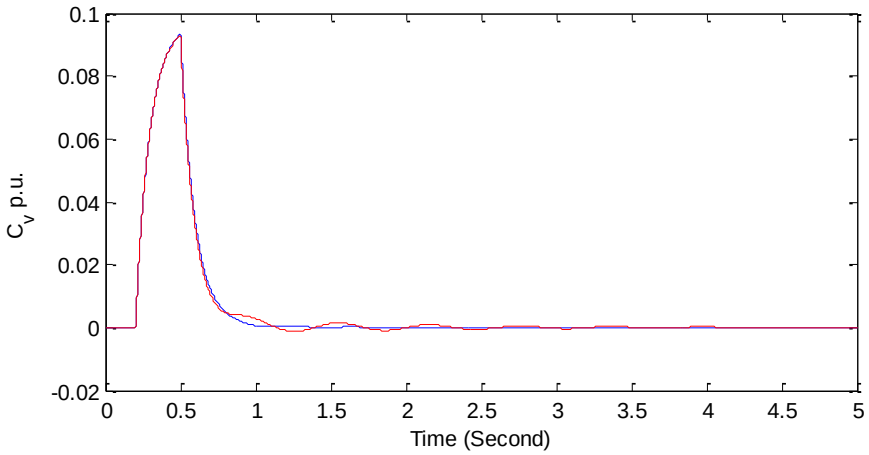

Figure 4.39: Time response of the governor valve control (C_v) with PWMSC and without PWMSC for 54.7% compensation level.

It has been found that (Figure 4.39) the governor valve is open from 0.2s to 0.6s and then oscillates with small amplitude for the system without PWMSC. But after using PWMSC the governor valve become stable after 0.7s.

4.6.4 Damping Subsynchronous Torsional Oscillations at 68.4% Compensation Level

The PWMSC gain and time constants and the supplementary controller parameters obtained from the genetic optimization techniques are shown in the Table 4.8.

Table 4.8: Controller parameters at 68.4% compensation level

PWMSC	
$K_{PWMSC} = 10$	$T_{PWMSC} = 10$
Supplementary controller	
$T_1 = 0.01$	$T_2 = 0.6056$
$T_w = 1$	K

Table 4.9: Eigenvalues of SMIB system with PWMSC and without PWMSC for the 68.4% compensation level

Modes	68.4% Compensation level	
	Without PWMSC	With PWMSC
Mode 5	- 0.48 ± 298.28i	- 0.48 ± 298.28i
Mode 4	- 0.11 ± 202.88i	- 0.12 ± 202.90i
Mode 3	- 0.44 ± 160.53i	- 0.44 ± 160.56i
Mode 2	- 0.15 ± 126.96i	- 0.14 ± 127.00i
Mode 1	**5.64 ± 98.58i**	- 0.18 ± 97.67i
Mode 0	- 1.07 ± 11.72i	- 1.45 ± 13.42i
Elec.	- 5.82 ± 98.86i	- 2.94 ± 74.60i
Other modes	- 5.19 ± 657.00i - 97.23 ± 1.54i - 33.76 - 26.82 - 10.19 - 6.53 - 2.43 - 1.67 - 0.14 - 0.68 - 0.91	- 9.57 ± 682.08i - 0.00 ± 377.00i - 97.39 ± 1.44i - 0.10 - 1.65 - 1.00 - 34.50 - 26.91 - 10.13 - 7.37 - 2.45 - 0.14 - 1.67 - 0.70 - 0.91

The eigenvalues obtained from our proposed model is shown in the Table 4.9. It has been found that Mode 1 is unstable without PWMSC at 68.4% compensation level. After introducing PWMSC this Mode 1 becomes stable and at Mode 0 the stability does not improve much but the eigenvalue of electrical mode moves towards the positive plane.

The time response of different state variables with and without PWMSC in the system for 68.4% compensation level is shown in the Figure 4.40 to 4.50.

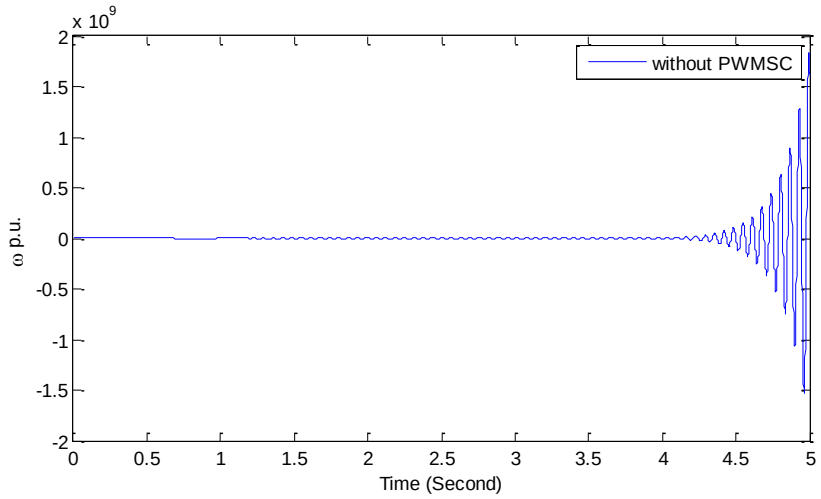

(a) Without PWMSC

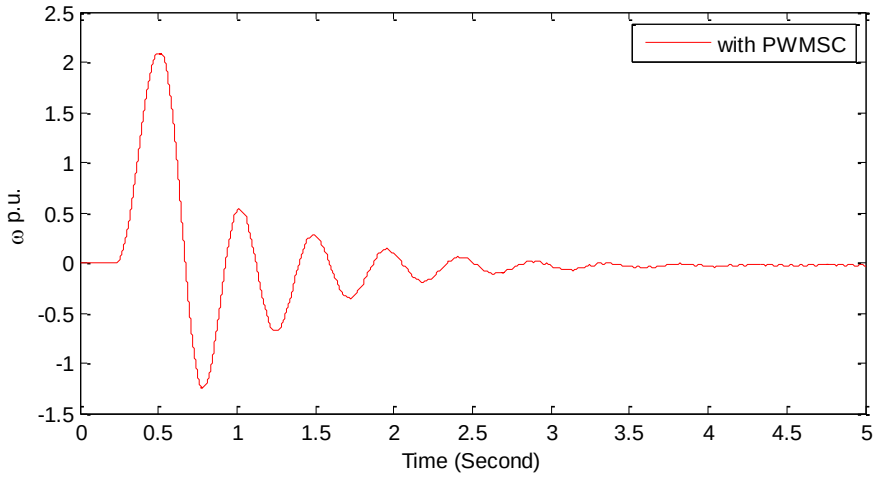

(b) With PWMSC

Figure 4.40: Time response of the generator (GEN) angular speed variation (a) without PWMSC and (b) with PWMSC at 68.4% compensation level.

It has been found from the Figure 4.40 that the generator (GEN) angular speed variation without PWMSC starts to grow after 4.25s and the instability increases severely. The response with PWMSC starts to rise after 0.25s and rises upto 2.2 p.u. and become completely stable after around 3.5s.

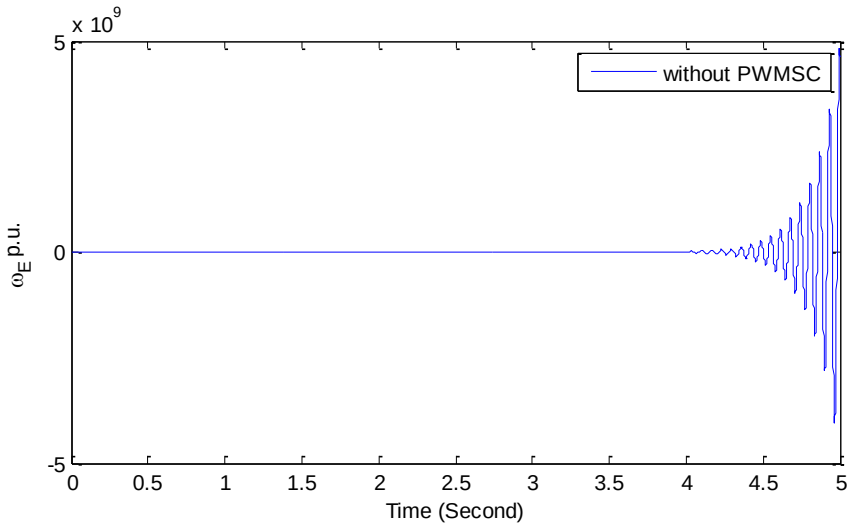

(a) Without PWMSC

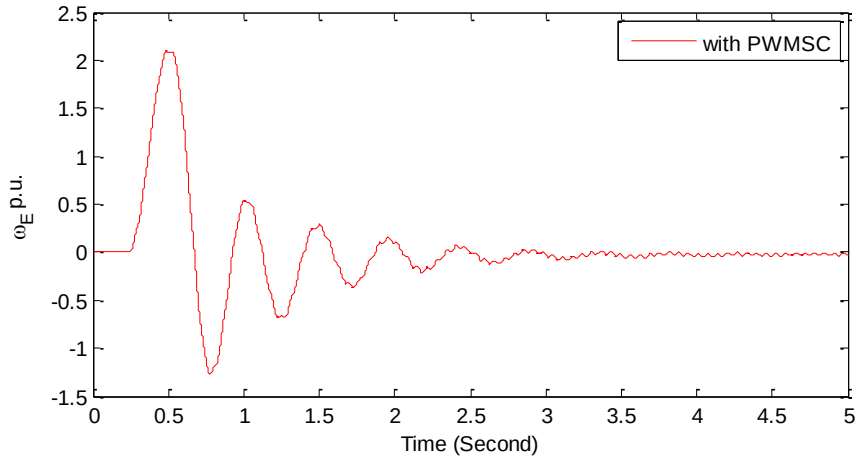

(b) With PWMSC

Figure 4.41: Time response of the exciter (EXC) angular speed variation (a) without PWMSC and (b) with PWMSC at 68.4% compensation level.

It has been found that (Figure 4.41) the exciter (EXC) angular speed variation without PWMSC starts to grow severely after 4.0s. The response with PWMSC starts to rise after 0.25s and rises upto 2.2 p.u. and become completely stable after around 3.25s.

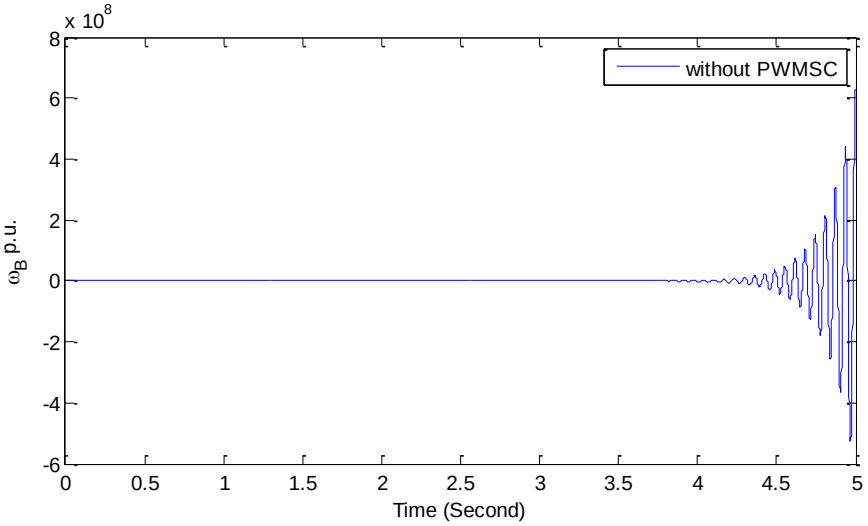

(a) Without PWMSC

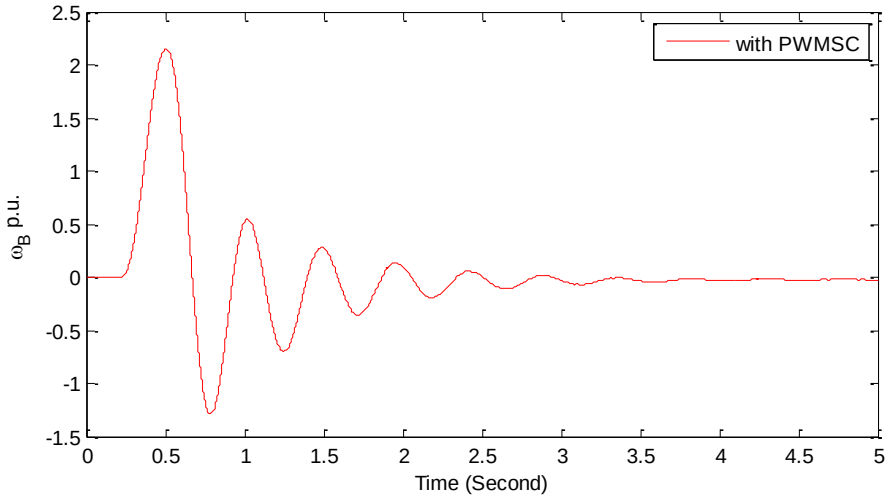

(b) With PWMSC

Figure 4.42: Time response of the low pressure stage (LPB) angular speed variation (a) without PWMSC and (b) with PWMSC at 68.4% compensation level.

It has been found that (Figure 4.42) the low pressure stage (LPB) angular speed variation without PWMSC starts growing severely after 3.5s. The response with PWMSC starts to rise after 0.3s and rises upto 2.3 p.u. and become completely stable after around 3.5s.

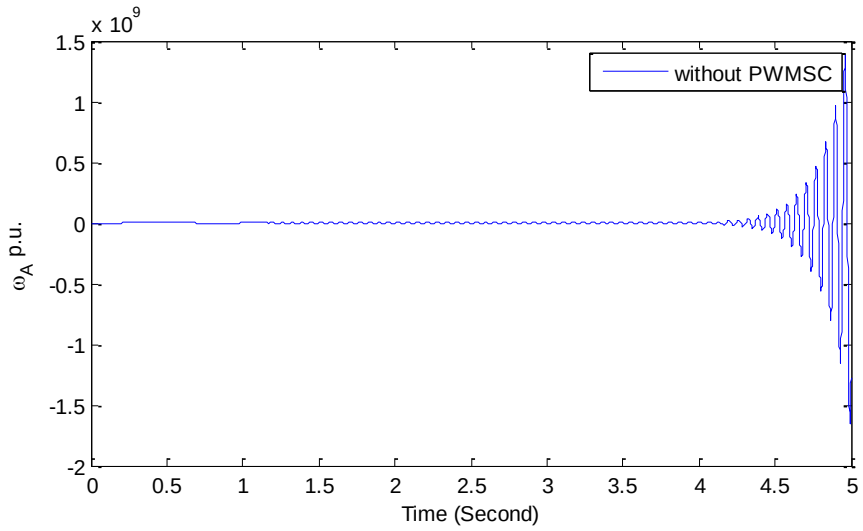

(a) Without PWMSC

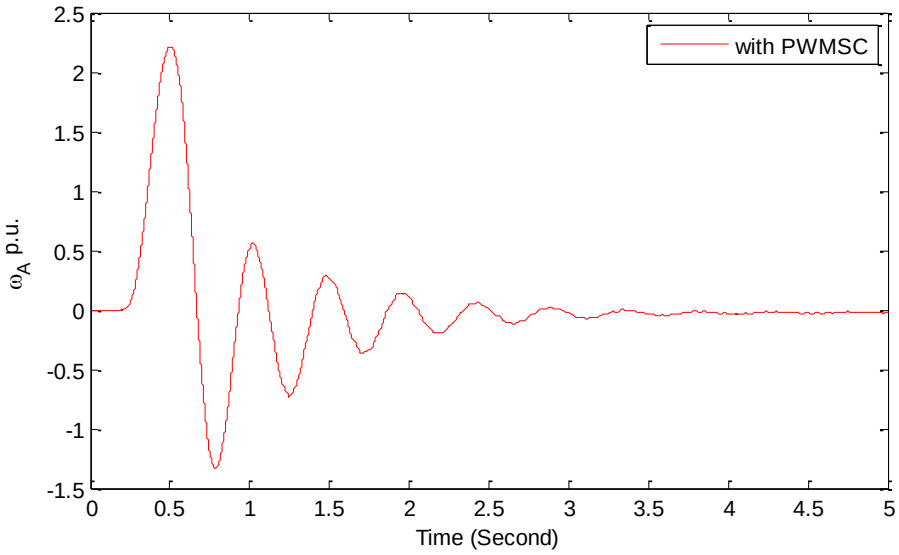

(a) With PWMSC

Figure 4.43: Time response of the low pressure stage (LPA) angular speed variation (a) without PWMSC and (b) with PWMSC at 68.4% compensation level.

It has been found that (Figure 4.43) the low pressure stsge (LPA) angular speed variation without PWMSC is unstable and instability grows severely after 4.2s. The PWMSC successfully damp out the oscillations after around 3.5s.The response with PWMSC starts to rise after 0.2s and rises upto 2.15 p.u..

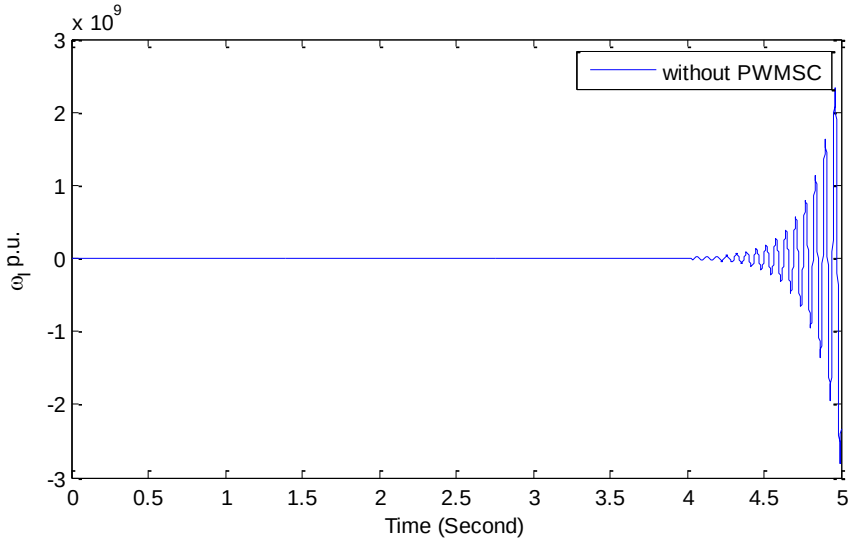

(a) Without PWMSC

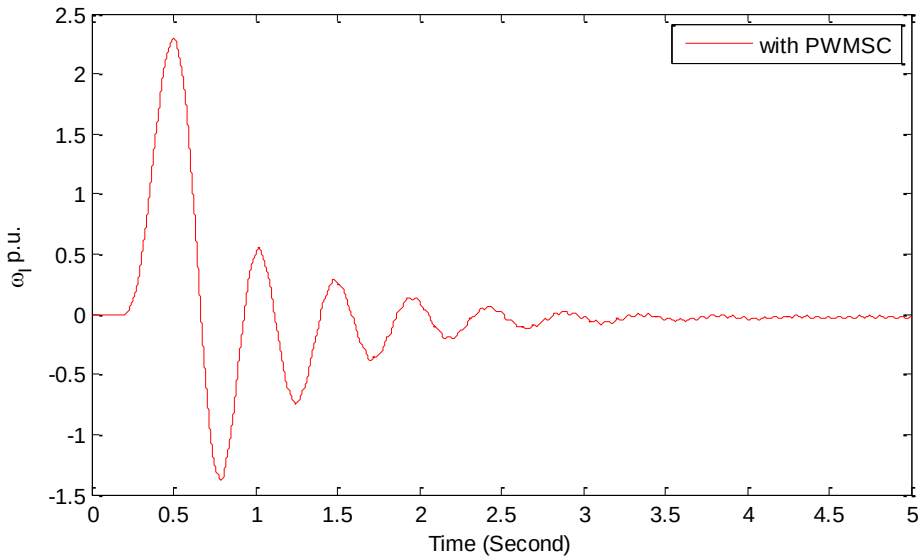

(a) With PWMSC

Figure 4.44: Time response of the intermediate pressure stage (IP) angular speed variation (a) without PWMSC and (b) with PWMSC at 68.4% compensation level.

It has been found that (Figure 4.44) the intermediate stage (IP) angular speed variation without PWMSC is unstable and instability increases severely after 4s. The response with PWMSC starts to rise after 0.2s and rises upto 2.15 p.u. and become completely stable after around 3.5s.

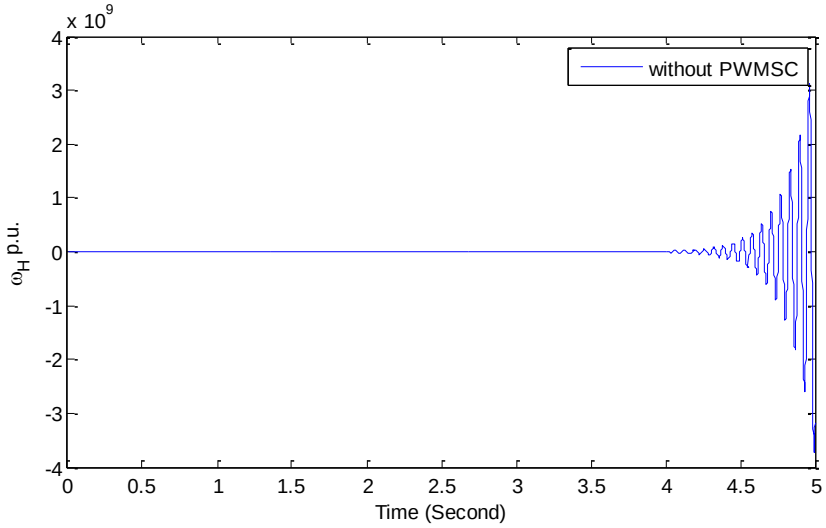

(a) Without PWMSC

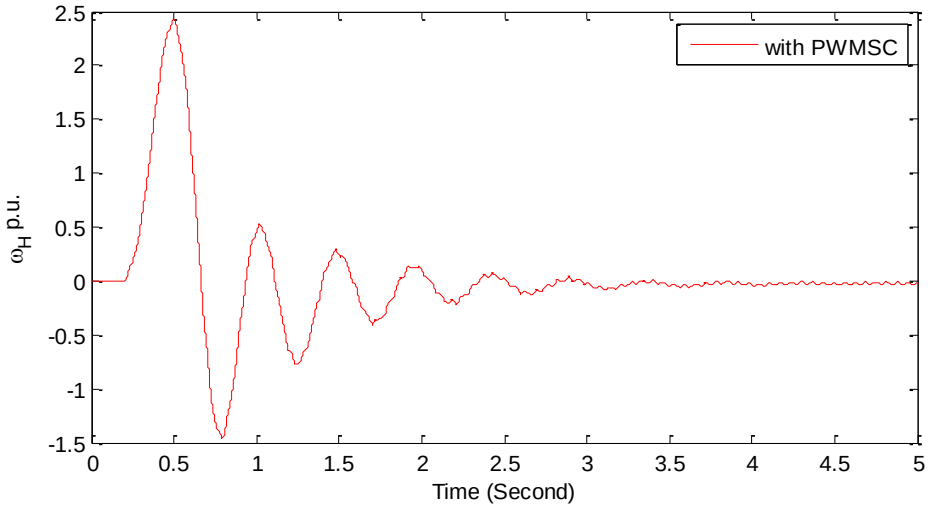

(b) With PWMSC

Figure 4.45: Time response of the High Pressure stage (HP) angular speed variation (a) without PWMSC and (b) with PWMSC at 68.4% compensation level.

It has been found that (Figure 4.45) the High Pressure stage (HP) angular speed variation without PWMSC is unstable and instability increases severely after 4s. The response with PWMSC starts to rise after 0.2s and rises upto 2.5 p.u. and become completely stable after around 3.5s.

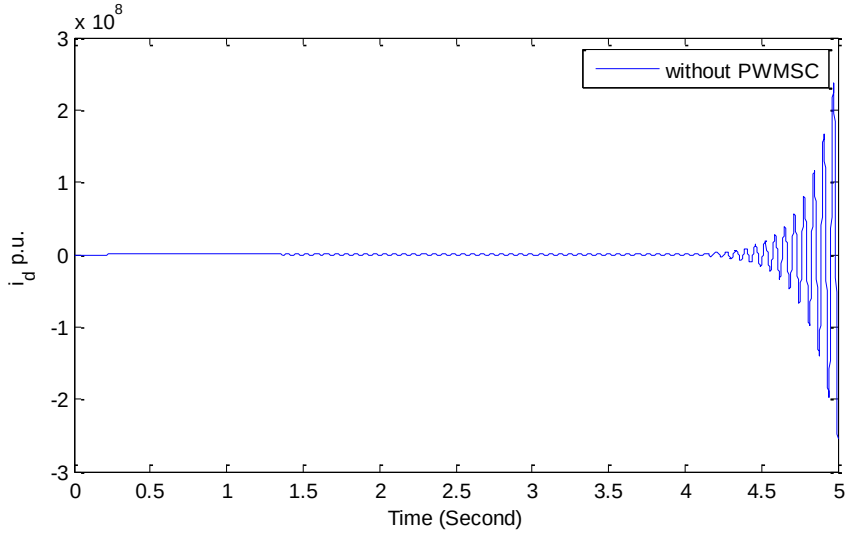

(a) Without PWMSC

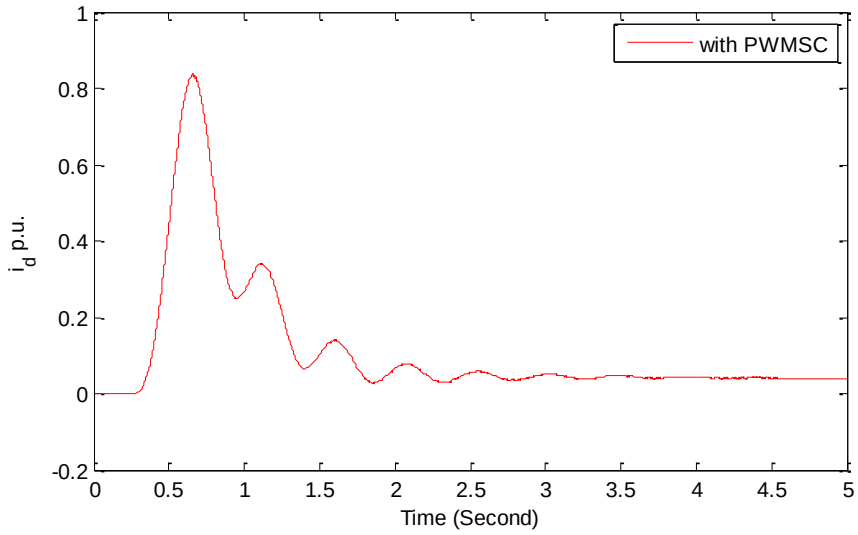

(b) With PWMSC

Figure 4.46: Time response of the generator stator currents in the d-axis of the reference frame at 68.4% compensation level (a) without PWMSC and (b) with PWMSC.

It has been found that (Figure 4.46) the stator current component variation in d-axis is unstable for the system without PWMSC. The instability increases severely after 4s. The response with PWMSC starts to rise after 0.2s and rises upto 0.9 p.u. and become completely stable after around 3.5s.

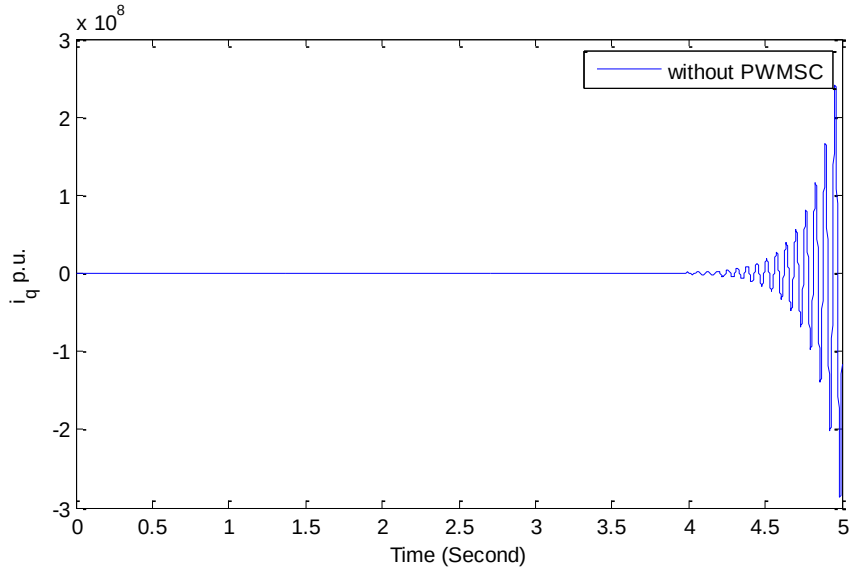

(a) Without PWMSC

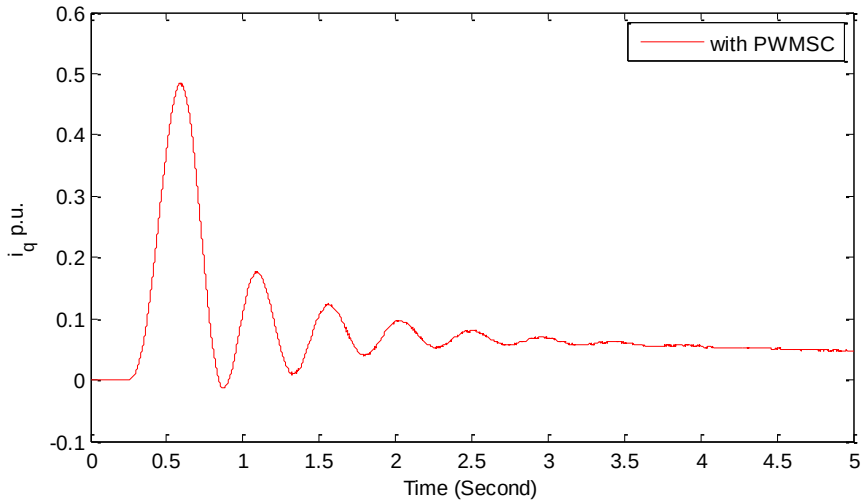

(b) With PWMSC

Figure 4.47: Time response of the generator stator currents in the q-axis of the reference frame at 68.4% compensation level (a) without PWMSC and (b) with PWMSC.

It has been found that (Figure 4.47) the stator current component variation in q-axis is unstable for the system without PWMSC. The instability increases severely after 4s. The response with PWMSC starts to rise after 0.2s and rises upto 0.4 p.u. and become completely stable after around 4s.

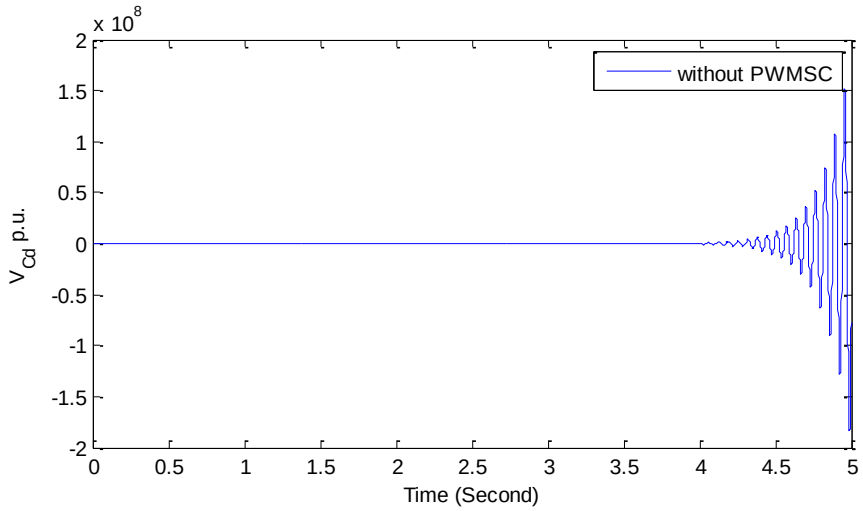

(a) Without PWMSC

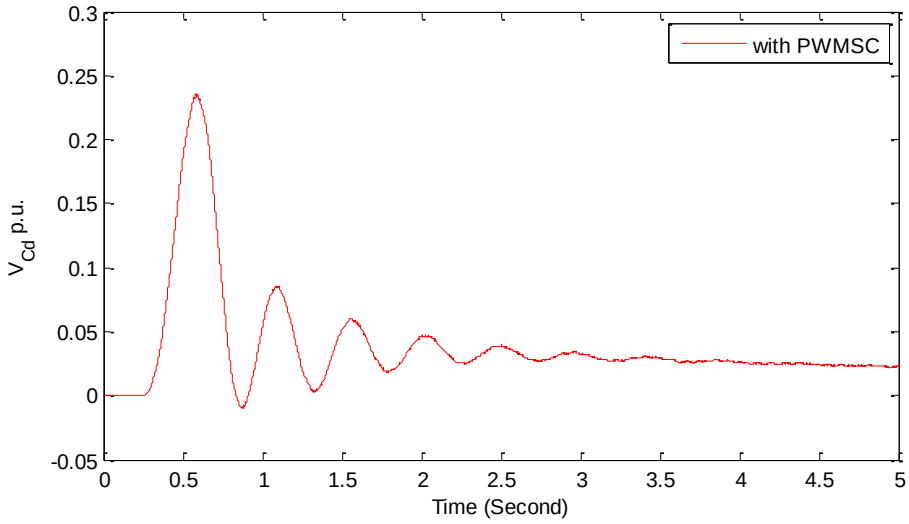

(b) With PWMSC

Figure 4.48: Time response of the series compensator capacitor voltage in the d-axis of the reference frame at 68.4% compensation level (a) without PWMSC and (b) with PWMSC.

It has been found that (Figure 4.48) the capacitor voltage component variation in d-axis is unstable for the system without PWMSC. The instability increases severely after 4s. The response with PWMSC starts to rise after 0.2s and rises upto 0.23 p.u. and become completely stable after around 4s.

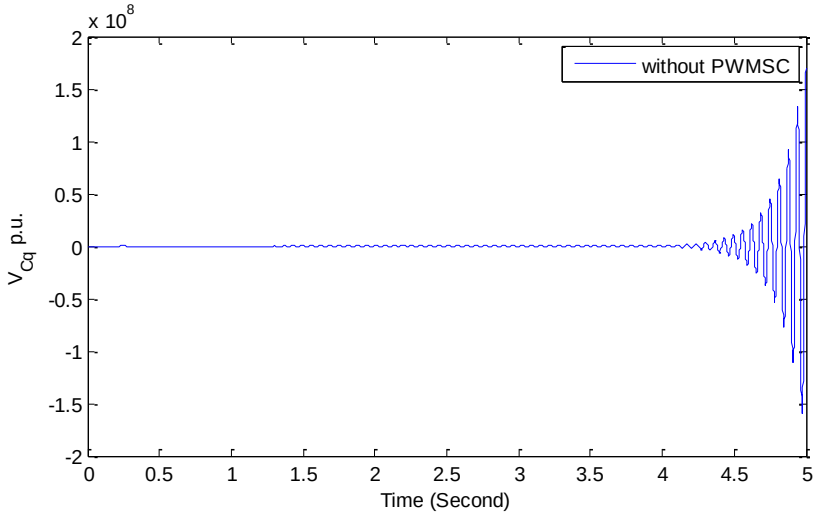

(a) Without PWMSC

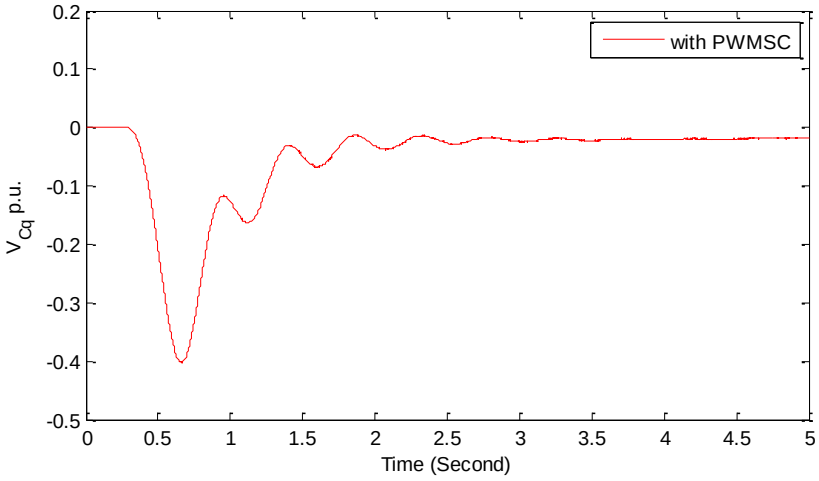

(b) With PWMSC

Figure 4.49: Time response of the series compensator capacitor voltage in the q-axis of the reference frame at 68.4% compensation level (a) without PWMSC and (b) with PWMSC.

It has been found that (Figure 4.49) the capacitor voltage component variation in q-axis is unstable for the system without PWMSC. The instability increases severely after 4s. The response with PWMSC starts to fall after 0.2s and goes upto 0.4 p.u. and become completely stable after around 3s.

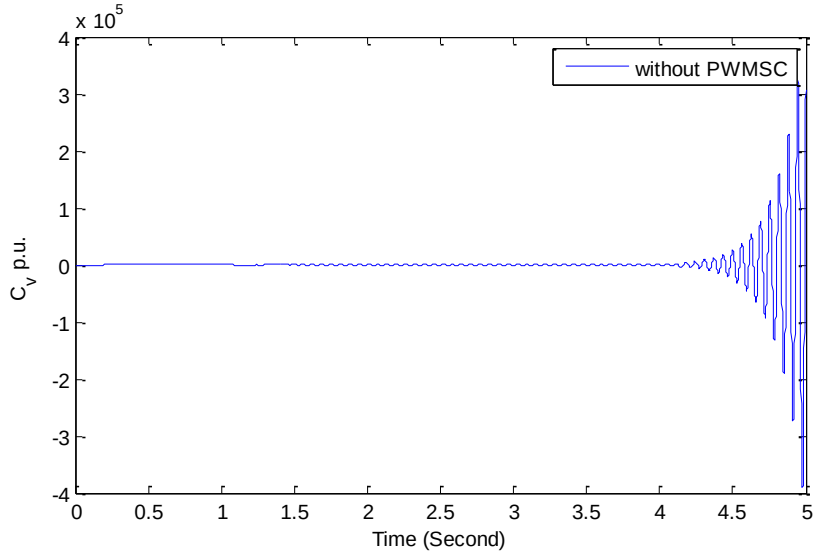

(a) Without PWMSC

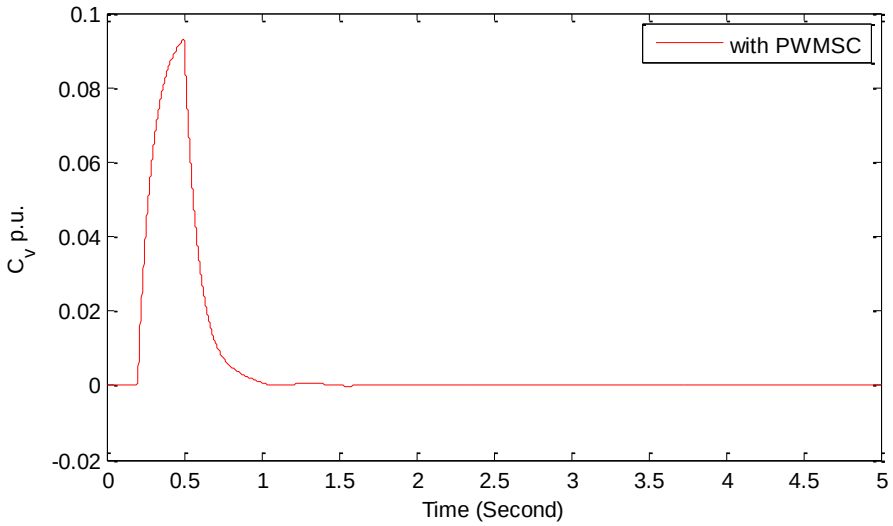

(b) With PWMSC

Figure 4.50: Time response of the governor valve control (C_v) (a) without PWMSC and (b) with PWMSC for 68.4% compensation level.

It has been found that (Figure 4.50) the governor valve response is completely unstable and after 4s its instability grows severely. But after using PWMSC the governor valve become stable after 1.0s.

Table 4.10: Percentage overshoot and settling time of different states of SMIB system with PWMSC at different compensation levels

States	Compensation levels							
	26.5%		41.1%		54.7%		68.4%	
	Max. overshoot (p.u.)	Settling Time (sec.)	Max. overshoot (p.u.)	Settling Time (sec.)	Max. overshoot (p.u.)	Settling Time (sec.)	Max. overshoot (p.u.)	Settling Time (sec.)
$\Delta\omega$	2.3	3.0	2.0	3.5	1.8	2.5	2.2	3.5
$\Delta\omega_E$	2.3	3.0	2.0	2.5	1.7	2.5	2.2	3.25
$\Delta\omega_B$	2.3	3.0	2.0	3.0	1.7	2.5	2.3	3.5
$\Delta\omega_A$	2.3	3.0	2.0	2.0	1.8	2.0	2.15	3.5
$\Delta\omega_I$	2.0	2.5	2.0	2.0	3.2	2.5	2.15	3.5
$\Delta\omega_H$	2.1	2.5	2.5	2.5	2.0	2.0	2.5	3.5
Δi_d	0.8	2.4	0.8	2.5	0.8	2.5	0.09	3.5
Δi_q	0.35	3.5	0.48	3.5	0.46	2.5	0.4	4.0
ΔV_{Cd}	0.07	3.5	0.14	3.0	0.18	2.5	0.23	4.0
ΔV_{Cq}	-0.15	3.0	-0.24	3.0	-0.3	2.0	-0.4	3.0
ΔC_v	0.09	1.4	0.09	1.0	0.09	1.0	0.09	1.0

From the Table 4.10 it is observed that the highest Max. Overshoot is 3.2 p.u. for the IP rotor speed variation at 54.7% compensation level and the maximum settling time is 4s for Δi_q and ΔV_{Cd} at 68.4% compensation level. This result showed that the PWMSC has successfully mitigated SSR oscillations from the power system.

4.7 Summary

In this chapter a dynamic model of PWMSC with supplementary controller is designed for mitigation of SSR oscillations in a series capacitor compensated power system. For the proper tuning of the controller genetic algorithm is used. The dynamic performance of the system under a small disturbance in the governor side is examined for four critical compensation levels. The results of such a case study have shown the effectiveness of PWMSC in damping all SSR torsional modes.

Chapter 5

Summary and Conclusions

5.1 Summary

The dynamic behavior of a SMIB system installed with PWMSC in the transmission line has been investigated in this thesis. Nonlinear dynamic model for the power system with PWMSC is derived and a linearized model is obtained from that. The PWMSC connected with SMIB is modeled by thirty-two state equations.

Introducing a series capacitor in a transmission system implies the existence of natural oscillations in the electrical system having frequencies below the power frequency. Since the natural oscillations of the shaft system of most turbine-generators are also of frequencies below the system frequency, the possibility of the electromechanical Subsynchronous Resonance (SSR) exists if the frequencies of the electrical and mechanical oscillations are complements of the power frequency. SSR results in violent torsional oscillations within the turbine-generator shafts which can destroy them (in worst case) in only a few seconds.

FACTS controllers are being used to overcome the power system dynamic problems. The potential benefits of these FACTS controllers are now widely recognized by the power system engineers and the transmission and distribution communities. PWMSC is one of the latest FACTS devices which has a simple power structure, gating and control strategy. Details study on stability, FACTS devices, eigenvalue analysis for the small signal stability problem, optimization techniques for the tuning of supplementary controller, the controller structure and its parameters are documented in Chapter 2.

The dynamic behavior of SMIB system with PWMSC and without PWMSC has been investigated in this thesis for analyzing the SSR effect in the power system. A linearized mathematical model is developed for investigating the SSR phenomenon under small disturbances. For this purpose, the IEEE first benchmark model which consists of a large turbine-generator connected to a large system through a series-capacitor compensated transmission line is used. This model represents clearly the various features of the SSR phenomenon. The shaft system of the turbine-generator represents a linear six-mass-spring system. The detailed dynamic models of the individual system components are also presented

in Chapter 3. The procedure used to derive the complete linearized model from the IEEE first benchmark model is also explained in this chapter. The studies conducted in the rest of the chapter are intended to investigate the effect of the compensation levels of the transmission line on SSR oscillations. The results of these investigations have provided the critical compensation levels in the system under study.

In Chapter 4, the dynamic model of PWMSC with supplementary controller has been introduced in the IEEE first benchmark model for mitigation of SSR oscillations in a power system. Nonlinear dynamic model for the power system with PWMSC is derived and a linearized model is obtained from that. The PWMSC connected with SMIB is modeled by thirty two state equations. A small pulse type disturbance is introduced in the governor side to create SSR oscillations and PWMSC is tried to mitigate the SSR phenomenon. The supplementary controllers are presented in this thesis to improve the damping of the power system oscillations. For the proper tuning of the controller genetic algorithm is used as an efficient optimization algorithm. The time-domain analysis technique is used for transient torque analysis. MATLAB computer programs have been developed to simulate the dynamic performance of the system with PWMSC and without PWMSC. Eigenvalues are also found to check the stability. The results for eigenvalue analysis and response plots were found same.

5.2 Contribution

Subsynchronous Resonance (SSR) phenomenon is a power system dynamic problem which can lead a system towards severe instability and cause destruction to the generator shaft. In this thesis SSR phenomenon in the power system have been properly analyzed in the IEEE first benchmark model and located four critical compensation levels where the system experiences most instability in different modes. FACTS devices are being used in the recent years to manage the instability issue and bring a system capacity to its maximum thermal limit. The latest among FACTS, PWMSC is used in this thesis to mitigate SSR oscillations. A supplementary controller is also used along with the PWMSC. Genetic algorithm is used for the proper tuning of the controller so we can achieve the optimized results. A dynamic model of IEEE FBM with PWMSC has been developed and then linearized with Taylor series expansion. A pulse type disturbance has been created in the governor side of the system.

From the time domain simulation and the eigenvalue analysis it has been found clearly that all the SSR oscillations have been completely mitigated after experiencing a small disturbance in the system.

5.3 Conclusion

Pulse Width Modulated Series Compensator (PWMSC) has been shown in this thesis as an effective solution of SSR oscillation problem in the power system. Study is made with IEEE first benchmark model. Subsynchronous Resonance (SSR) is analyzed in the study system for a small disturbance in the governor side. A dynamic model PWMSC is developed with a supplementary controller to mitigate the SSR oscillations in different modes. Genetic algorithm has been used as an optimization tool which makes the PWMSC operation more reliable. The results obtained from the eigenvalue analysis and time domain simulation proves that PWMSC is an effective choice for system SSR damping.

5.4 Recommendations for Future Work

In the following, some recommendations are given for future research in the area.

- In this thesis genetic algorithm has been applied as an optimization technique. Other optimization techniques can be applied and comparing each other most suitable technique can be selected.
- The research has been done here for a model containing a single machine. So, the effect of PWMSC on multi-machine system stability needs investigation for SSR oscillations. The locations of the PWMSC devices in a multi-machine system require careful study.

References

[1] Anderson, PM - Fouad, A A "Power system control and stability" Iowa state university press, 1980.

[2] Byerly, R. T. – Kimbark, E.W., eds., "*Stability of Large Electric Power Systems*", IEEE Press Book, IEEE, New York, 1974.

[3] You-nan Yu, "*Electric Power System Dynamics",* New York: Academic Press, 1983.

[4] P. Kundur, *Power System Stability and Control*, New York: Mc-Graw-Hill, 1994.

[5] IEEE Committee Report, "Reader's Guide to Sub-Synchronous resonance," IEEE trans. on Power Systems, vol. 7, no. 1, pp. 150-157, February 1992.

[6] IEEE Working Committee Report, "Third Supplement to a Bibliography for the study of Sub-synchronous Resonance between Rotating Machines and Power Systems," IEEE trans. on Power Systems, vol. 6, no. 2, pp. 830-834, May 1991.

[7] S. H. Gold, "Power system oscillations which resulted in the second failure of generator rotor of Mohave Generating Station Unit No. 1." A report of the Southern California Edison Company, February 1972.

[8] MI C. Hall and D. A. Hodges, "Experience with 500 kV subsynchronous resonance and resulting turbine generator shaft damage at Mohave Generating Station," in Analysis and Control of Subsynchronous Resonance, pp. 22-25. Edited by the IEEE SSR Task Force as Special Publication No. 76 CH 1066-0-PWR.

[9] L. A. Kilgore, D. G. Ramey, and M. C. Hall, "Simplified transmission and generation system analysis procedures for subsynchronous resonance problems," in Analysis and Control of Subsynchronous Resonance, pp-6-11. Edited by the IEEE SSR task Force as Special Publications No. 76 CH 1066-0-PWR.

[10] F. Lingling, M. Zhixin, "Mitigating SSR Using GFIG-Based Wind Generation" in Sustainable Energy, IEEE Transactions, Vol. 3, no. 3, pp. 349-358, July.2012.

[11] M. Zhixin, “Impedance-Model-Based SSR Analysis for Type 3 Wind Generator and Series-Compensated Network” in Energy Conversion, IEEE Transactions, Vol. 27, no. 4, pp. 984-991, Dec.2012.

[12] Mohan, N., Undeland, T. M., and Robbins, W. P., “*Power electronics: converters, applications, and design*”, New York, Wiley, 1995.

[13] IEEE Committee Report, “Proposed terms and definitions for subsynchronous oscillations,” IEEE Transactions on Power Apparatus and Systems, vol. PAS-99, no. 2, pp. 506-511, Mar.1980.

[14] IEEE Subsynchronous Resonance Working Group, “Terms, definitions and symbols for subsynchronous oscillations [power systems],” IEEE Transactions on Power Apparatus and Systems, vol. PAS-104, no. 6, pp. 1325-1334, June1985.

[15] Gyugyi, L., Hingorani, N. G., Nannery, P. R., and Tai, N. “Advanced static Var compensator using gate turn-off thyristors for utility applications.” , 23-203. 1990. Paris, France, CIGRE.

[16] Gyugyi, L., “Dynamic compensation of AC transmission lines by solid-state synchronous voltage sources,” IEEE Transactions on Power Delivery, vol. 9, no. 2, pp. 904-911, Apr.1994.

[17] Gyugyi, L., Schauder, C. D., and Sen, K. K., “Static synchronous series compensator: a solid-state approach to the series compensation of transmission lines,” IEEE Transactions on Power Delivery, vol. 12, no. 1, pp. 406-417, Jan.1997.

[18] Sen, K. K., “SSSC-static synchronous series compensator: theory, modeling, and application,” IEEE Transactions on Power Delivery, vol. 13, no. 1, pp. 241-246, Jan.1998.

[19] Gyugyi, L., Schauder, C. D., Williams, S. L., Rietman, T. R., Torgerson, D. R., and Edris, A., “The unified power flow controller: a new approach to power transmission control,” IEEE Transactions on Power Delivery, vol. 10, no. 2, pp. 1085-1097, Apr.1995.

[20] Nabavi-Niaki, A. and Iravani, M. R., “Steady-state and dynamic models of unified power flow controller (UPFC) for power system studies,” IEEE Transactions on Power Systems, vol. 11, no. 4, pp. 1937-1943, 1996.

[21] Acha, E., *FACTS: modelling and simulation in power networks*, Chichester, Wiley, 2004.

[22] Schettler, F., Huang, H., and Christl, N. "HVDC transmission systems using voltage sourced converters – Design and applications." 2, 715-720. 2000. Seattle, WA, United States,

[23] Asplund, G., Eriksson, K., and Svensson, K., "HVDC Light-DC transmission based on voltage sourced converters," ABB Review, no. 1, pp. 4-9, 1998.

[24] S.G. Helbing, G.G. Karady: Investigations of an Advanced Form of Series Compensation, IEEE Transaction on Power Delivery, Vol. 9, No. 2, pp. 939 – 947, April 1994.

[25] L.A.C. Lopes, G. Joos: Pulse Width Modulated Capacitor for Series Compensation, IEEE Transaction on Power Electronics, Vol. 16, No. 2, pp. 167 – 174, March 2001.

[26] G. Venkataramanan, B.K. Johnson: Pulse Width Modulated Series Compensator, IEE Proceedings – Geneneration, Transmission and Distribution, Vol. 149, No. 1, pp.71 – 75, Jan. 2002.

[27] G. Venkataramanan: Three-phase Vector Switching Converters for Power Flow Control, IEE Proceedings – Electrical Power Application, Vol. 151, No. 3, pp. 321 – 333, May 2004.

[28] H. Jin, G. Joos, L.A. Lopes: An Efficient Switched-reactor-based Static VAr Compensator, IEEE Transaction on Industrial Application, Vol. 30, No. 4, pp. 998 – 1005, July/Aug. 1994.

[29] L.A.C. Lopes, G. Joos, B.T. Ooi: A PWM Quadrature-booster Phase Shifter for AC Power Transmission, IEEE Transaction on Power Electronics, Vol. 12, No. 1, pp. 138 – 144, Jan. 1997.

[30] J.M. Gonzalez, J.M. Ramirez: AC/AC Series Converter in Transient Stability Studies, 39th North American Power Symposium, Las Cruces, NM, USA, pp. 205 – 211, 30 Sept. – 02 Oct. 2007.

[31] Vriois.T.D, Koutiva.X.I and Vovos.N.A, "A Genetic Algorithm-Based Low Voltage RideThrough Control Strategy for Grid Connected Doubly Fed Induction Wind Generators," IEEE Trans. Power Syst., Vol. 29, NO. 4, pp. 1325–1334, May. 2014.

[32] S. Amin, A. S. Heidar, K. Ahad, "A Novel Current Injection Model of PWMSC for Control and Analysis of Power System Stability", Serbian Journal of Electrical Engineering, Vol. 10, No. 2, June 2013, pp.349-364

[33] Yan, A. and Yao-nan, Y., "Multi-mode stabilization of torsional oscillations using output feedback excitation control," IEEE Transactions on Power Apparatus and Systems, vol. PAS-101, no. 5, pp. 1245-1253, May1982.

[34] Hamouda, R. M., Iravani, M. R., and Hackan, R., "Coordinated static VAR compensators and power system stabilizers for damping power system oscillations," IEEE Transactions on Power Systems, vol. PWRS-2, no. 4, pp. 1059-1067, Nov.1987.

[35] Larsen, E. V. and Swann, D. A., "Applying power system stabilizers. I. General concepts," 80-558 1980, Minneapolis, MN, USA, IEEE.

[36] Putman, T. H. and Ramey, D. G., "Theory of the modulated reactance solution for subsynchronous resonance," IEEE Transactions on Power Apparatus and Systems, vol. PAS-101, no. 6, pp. 1527-1535, June1982.

[37] Wasynczuk, O., "Damping subsynchronous resonance using reactive power control," IEEE Transactions on Power Apparatus and Systems, vol. PAS-100, no. 3, pp. 1096-1104, Mar.1981.

[38] Hammad, A. E. and El Sadek, M., "Application of a thyristor controlled var compensator for damping of subsynchronous oscillations in power systems," IEEE Transactions on Power Apparatus and Systems, vol. PAS-103, no. 1, pp. 198-212, 1984.

[39] Iravani, M. R. and Mathur, R. M., "Damping subsynchronous oscillations in power system using a static phase-shifter," IEEE Transactions on Power Systems, vol. PWRS-1, no. 2, pp. 76-83, 1986.

[40] R. K. Varma and S. Auddy, "Mitigation of Subsynchronous Oscillations in a Series Compensated Wind Farm Using Static Var Compensator," in Proc. IEEE Power Eng. Soc. General Meeting Conf., 2006, pp. 1-7, Paper 06 GM1272.

[41] Massimo Bongiorno, Jan Svensson, Lennart Angquist, "On Control of Static Synchronous Series Compensator for SSR Mitigation," IEEE Transections on Power Electronics, vol.23, no.2, March 2008.

[42] J. Guo, M.L. Crow, J. Sarangapani "An improved UPFC Control for Oscillation Damping," IEEE Transections on Power Systems, Vol.24, No. 1. , pp.228-296, Feb. 2009.

[43] de Jesus, F.D.; Watanabe , E. H.; de Souza, L.F.W.; Alves. J.E.R.; "SSR and power Oscillation Damping Using Gate-controlled Series Capacitors (GCSC)" IEEE Transections on power delivery, vol.22, no.3, July 2007.

[44] D. Rai, G. Ramakrishna, S. O. Faried, and A. –A. Edris, "Enhancement of power system dynamics using a phase imbalanced series compensator scheme," IEEE Trans. Power Syst. Vol. 25, no. 2, pp. 966-974, Apr.2010.

[45] S. O. Faried, G. Tang, "Supplemental control of voltage sourced converter-based back-to-back for damping subsynchronous resonance" , Power Engineering Society, IEEE General Meeting - PES , pp. 1-6, 2009.

[46] K. –H. Chu and C. Pollock, "PWM controlled series compensation with low harmonic distortion," Proc. Inst. Electr. Eng., Gener: Transm. Distrib., vol.144, no.6, pp.555-563, Nov.1997.

[47] A. Safari, H.A. Shayanfar, A. Kazemi, "Robust PWMSC Damping Controller Tuning on the Augmented Lagrangian PSO Algorithm" in Power Systems, IEEE Transactions, Vol. 28, no. 4, pp. 4665-4673, Nov.2013.

[48] Luiz A. C. Lopes and Geza Joos, "Pulse Width Modulated Capacitor for Series Compensation," IEEE Transections on Power Electronics, vol. 16, no. 2, March 2001.

[49] E Elbeltagi ,T Hegazy, D Grierson, "Comparison among five evolutionary-based optimization algorithms", Advanced Engineering Informatics, Pages 43–53 ,Volume 19, Issue 1, January 2005.

[50] C. E. Russell, S. Yuhui, "Comparison between genetic algorithms and particle swarm optimization",Springerlink, Volume 1447, 1998, pp 611-616, 2008.

[51] C Jang-Sung, J Hyun-Kyo ; H Song-yop , "A study on comparison of optimization performances between immune algorithm and other heuristic algorithms", Magnetics, IEEE Transactions on (Volume:34 , Issue: 5), Sep 1998.

[52] Grefenstette, J.J. , "Optimization of Control Parameters for Genetic Algorithms", Systems, Man and Cybernetics, IEEE Transactions on (Volume:16 , Issue: 1), Jan. 1986.

[53] Singh L.P., "*Advanced Power System Analysis and Dynamics"*, Wiley Eastern Limited, 1983.

[54] L. Wang, M. Klein, S. Yirga, and P. Kundur, "Dynamic reduction of large power systems for stability studies," IEEE Trans. Power Syst., vol. 12, no. 2, pp. 889–895, May 1997.

[55] R. Nath and S. S. Lamba, "Development of coherency-based time domain equivalent model using structure constraints," Proc. Inst. Elect. Eng., vol. 133, no. 4, pt. C, pp. 165–175, May 1986.

[56] Basler M.J., Schaefer R.C., "Understanding power system stability", 58th Annual Conference for Protective Relay Engineers, pp. 46-67,5-7 April 2005.

[57] Snyder A.F., Hadjesäid N., Georges D., Mili L., Phadke A.G., Faucon O., Vitet S. , "Inter-Area Oscillation Damping with Power System Stabilizers and Synchronized Phasor Measurements", POWERCON 98, Peking, China, August, 18-21, 1998.

[58] P. Kundur, J. Paserba, V. Ajjarapu, G. Andersson, A. Bose,C. Canizares, N. Hatziargyriou, D. Hill, A.Stankovic, C. Taylor,T. Van Cutsem, and V. Vittal, "Definition and classification of power system stability IEEE/CIGRE joint task force on stability terms and definitions," IEEE Transactions on Power Systems, vol. 19, pp. 1387– 1401, Aug. 2004.

[59] J. Machowski, J. W. Bialek, and J. R. Bumby, "*Power system dynamics and stability*." John Wiley & Sons, Oct. 1997.

[60] P. W. Sauer and M. A. Pai, *Power System Dynamics and Stability*. Prentice Hall, 1st ed., July 1997.

[61] M. Ilic, J. Zaborsky, Dynamics and control of large electric power systems, New York, US, John Wiley & Sons, Inc., 2000.

[62] F. Mei and B. C. Pal, “Modal Analysis of Grid Connected Doubly Fed Induction Generator,” IEEE Transactions on Energy Conversion. Vol. 22, No. 3, 2007, pp. 728-736.

[63] L. Wang, F. Howell, P. Kundur, C. Y. Chung, and W. Xu, “A tool for small-signal security assessment of power systems,” in22nd IEEE Power Engineering Society International Conference on Power Industry Computer Applications, 2001. PICA 2001. Innovative Computing for Power Electric Energy Meets the Market, pp. 246–252, IEEE, 2001.

[64] U. Kerin, T. N. Tuan, E. Lerch, and G. Bizjak, “Small signal security index for contingency classification in dynamic security assessment,” in PowerTech, 2011 IEEE Trondheim, pp. 1–6, IEEE,June 2011.

[65] S. Yang, F. Liu, D. Zhang, S. Mei, and G. He, “Polynomial approximation of the damping ratio-based small-signal security region boundaries of power systems,” in 2011 IEEE Power and Energy Society General Meeting, pp. 1–8, IEEE, July 2011.

[66] J. Paserba et al., “*Analysis and control of power system oscillation*,” CIGRE special publication, vol. 38, no. 07, 1996.

[67] L. J. Ontiveros, P. E. Mercado and G. O. Suvire, “A New Model of the Double-Feed Induction Generator Wind Turbine”, 2010 IEEE Transmission and Distribution Conference and Exposition, Latin America, pp. 263-269, November 2010.

[68] Daniel J. Trudnowski, Andrew Gentile, Jawad M. Khan, and Eric M. Petritz, “Fixed-Speed Wind-Generator and Wind-Park Modeling for Transient Stability Studies”, IEEE Transactions on Power Systems, Vol. 19, No. 4, pp. 1911 -1917, November 2004.

[69] Holland J (1975), “*Adaptation in natural and artificial systems.*” University of Michigan Press, Ann Arbor.

[70] Farmer JD, Packard N, Perelson A (1986), “The immune system, adaptation and machine learning”. Physica 22:187–204.

[71] Kennedy J, Eberhart RC (1995) Particle swarm optimization. Proceedings IEEE International Conference on Neural Networks, Piscataway, 1942–1948.

[72] Storn R, Price K (1997) Differential evolution–a simple and efficient heuristic for global optimization over continuous spaces. J Glob Optim 11:341–359.

[73] Passino KM (2002) Biomimicry of bacterial foraging for distributed optimization and control. IEEE Control Syst Mag 22:52–67.

[74] Eusuff M, Lansey E (2003) Optimization of water distribution network design using the shuffled frog leaping algorithm. J Water Resour Plan Manag ASCE 129:210–225.

[75] Karaboga D (2005), "An idea based on honey bee swarm for numerical optimization." Technical Report-TR06, Erciyes University, Engineering Faculty, Computer Engineering Department, Turkey.

[76] Simon D (2008) Biogeography-based optimization. IEEE Trans Evol Comput 12:702–713.

[77] Rashedi E, Nezamabadi-pour H, Saryazdi S (2009) GSA: a gravitational search algorithm. Inf Sci 179:2232–2248.

[78] Ahrari A, Atai A (2010) Grenade Explosion Method-A novel tool for optimization of multimodal functions. Appl Soft Comput 10(4):1132–1140.

[79] Mhetre. S. Punam. Jun, 2012. Genetic Algorithm for Linear and Nonlinear Equation, International Journal of Advanced Engineering Technology, E-ISSN 0976-3945.

[80] Wassim. A, Bedwani, and Oussama M. Ismail, 'Genetic Optimization of Variable Structure PID Control Systems', Computer Systems and Applications, ACS/IEEE International conference on 2001.

[81] Anon, "First benchmark model for computer simulation of subsynchronous resonance," IEEE Transactions on Power Apparatus and Systems, vol. PAS-96, no. 5, pp. 1565-1572, 1977.

[82] Wasley, R. G. and Shlash, M. A., "Steady-state phase-variable model of the synchronous machine for use in 3-phase load flow studies," Proceedings of the IEEE, vol. 121, no. 10, pp. 1155-1164, 1974.

[83] Shaltout, A. A. M., “Subsynchronous resonance in large turbo-generators connected to series capacitor compensated power systems.” Ph.D Thesis University of Saskatchewan, 1981.

[84] IEEE Committee Report, “Dynamic models for steam and hydo turbines in power system studies,” IEEE Transactions on Power Apparatus and Systems, vol. PAS-92, no. 6, pp. 1904-1915, 1973.

[85] J.C.R. Caro: Simple Topologies for Power Conditioners and FACTS Controllers, PhD Thesis, Guadalajara University, Guadalajara, Jalisco, Mexico, March 2009.

[86] L.A.C. Lopes, G. Joos: Pulse Width Modulated Capacitor for Series Compensation, IEEE Transaction on Power Electronics, Vol. 16, No. 2, March 2001, pp. 167 – 174.

[87] G. Venkataramanan, B.K. Johnson: Pulse Width Modulated Series Compensator, IEE Proceedings – Geneneration, Transmission and Distribution, Vol. 149, No. 1, Jan. 2002, pp.71 – 75.

[88] P.L. So, Y.C. Chu, T. Yu: Coordinated Control of TCSC and SVC for System Damping, International Journal of Control, Automation and Systems, Vol. 3, No. 2, June 2005, pp. 322 – 333.

[89] R. Sadikovic: Damping Controller Design for Power System Oscillations, Internal Report, Zurich, Switzerland, 2004.

[90] B. Pal, B. Chaudhuri: Robust Control in Power Systems, Springer Science and Business Media, NY, USA, 2005.

[91] K.R. Padiyar: Power System Dynamics: Stability and Control, BS Publications, Hyderabad, Andhra Pradesh, India, 2008.

[92] Hammad, A. E. and El Sadek, M., “Application of a thyristor controlled var compensator for damping of subsynchronous oscillations in power systems,” IEEE Transactions on Power Apparatus and Systems, vol. PAS-103, no. 1, pp. 198-212, 1984.

Appendices

Appendix A

System Data

Table A.1 Generator data (in per unit).

R_a = 1e-7	R_{fd} = 0.0013	R_{1d} = 0.0297
R_{1q} = 0.0124		R_{2q} = 0.0182
X_{ad} = *1.66*		X_{aq} = *1.58*
X_d = *1.79*	X_q = *1.71*	X_{ffd} = *1.7335*
X_{11d} = *1.66*	X_{11q} = *1.6319*	X_{22q} = *1.9029*

Table A.2 Transmission line data (in per unit).

Series capacitor compensated transmission line	
R_L = 0.02	X_L = *0.7*
Series capacitor compensated transmission line with PWMSC	
Req = 0.04	X_{Leq} = *0.7*
The capacitor compensation is X_C / X_L	

Table A.3 Governor and turbine system data.

K_g = 25	
T_g = 0.1 sec.	T_{ch} = 0.40 sec.
T_{rh} =7.0 sec.	T_{co} =*0.60* sec.
F_A = 0.22	F_B = 0.22
F_I = 0.26	F_H = 0.26
Cvopen = 4.0 p.u./sec	Cvclose = 4.0 p.u./sec

Table A.4 Excitation system data.

K_A = 2	K_E = 1.0
K_F = 0.03	
T_A = 0.04 sec.	T_E = 0.01 sec
T_F = 1.0 sec.	
V_{Rmax} = 4.75 p.u.	V_{Rmin} = -4.75 p.u.

Table A.5 Mechanical system data.

Mass	Shaft	Inertia M (seconds)	Damping D (p.u./p.u. speed)	Spring constant K (p.u./rad)
EXC		0.0684	0.017	
	GEN-EXC			2.822
GEN		1.736	0.099	
	LPB-GEN			70.858
LPB		1.768	0.100	
	LPA-LPB			52.038
LPA		1.716	0.100	
	IP-LPA			34.929
IP		0.311	0.025	
	HP-IP			19.303
HP		0.1856	0.008	

Table A.6 Initial operating conditions.

Generator real power	P_e = 0.09 p.u.
Generator terminal voltage	$\|V_t\|$ = 1.02 p.u.
System power factor	*pf = 0.9 (lag)*

Appendix B

Small Signal Model of the Complete System for the IEEE First Benchmark Model

In order to form the overall system equations, the equations derived in Chapter 3 for the individual system components are rewritten here again.

- 6th order state equation of synchronous machine (Equation 3.3).

$$\left[\frac{d\Delta X_{syn}}{dt}\right] = [A_{syn}][\Delta X_{syn}] + [B_{syn}][\Delta U_{syn}] \tag{B.1}$$

where

$$[\Delta X_{syn}] = [\Delta i_d \quad \Delta i_q \quad \Delta i_{fd} \quad \Delta i_{1q} \quad \Delta i_{1d} \quad \Delta i_{2q}]^T$$

$$[\Delta U_{syn}] = [\Delta V_{td} \quad \Delta V_{tq} \quad \Delta e_{fd} \quad \Delta\omega]^T$$

- State equation of transmission line (Equation 3.10)

$$\begin{bmatrix} \frac{d\Delta V_{Cd}}{dt} \\ \frac{d\Delta V_{Cq}}{dt} \\ \Delta V_{td} \\ \Delta V_{tq} \end{bmatrix} = [At]\begin{bmatrix}\Delta V_{Cd} \\ \Delta V_{Cq}\end{bmatrix} + [R1]\begin{bmatrix} \frac{d\Delta i_d}{dt} \\ \frac{d\Delta i_q}{dt} \end{bmatrix} + [R2]\begin{bmatrix}\Delta i_d \\ \Delta i_q\end{bmatrix} + [Bt]\begin{bmatrix}\Delta\omega \\ \Delta\delta\end{bmatrix} \tag{B.2}$$

- 12th order state equation of mechanical system (Equation 3.17)

$$\left[\frac{d\Delta X_{ms}}{dt}\right] = [A_{ms}][\Delta X_{ms}] + [B_{ms}][\Delta U_{ms}] \tag{B.3}$$

where

$$[\Delta X_{ms}] = [\Delta\delta_E \quad \delta\Delta \quad \Delta\delta_B \quad \Delta\delta_A \quad \Delta\delta_I \quad \Delta\delta_H \quad \Delta\omega_E \quad \Delta\omega \quad \Delta\omega_B \quad \Delta\omega_A \quad \Delta\omega_I \quad \Delta\omega_H]^T$$

$$[\Delta U_{ms}] = [\Delta T_e \quad \Delta P_H \quad \Delta P_I \quad \Delta P_A]^T$$

- 4th order state equation of governor and turbine system (Equation 3.19)

$$\left[\frac{\Delta dX_g}{dt}\right] = [A_g][\Delta X_g] + [B_g]\begin{bmatrix}\Delta P_{m0}\\ \Delta\omega_H\end{bmatrix} \tag{B.4}$$

where

$$[\Delta X_g] = [\Delta C_V \quad \Delta P_H \quad \Delta P_I \quad \Delta P_A]^T$$

- 3rd order state equation of excitation system (Equation 3.23)

$$\left[\frac{d\Delta X_v}{dt}\right] = [A_v][\Delta X_v] + [B_v]\begin{bmatrix}\Delta V_t\\ \Delta E_{ref}\end{bmatrix} \tag{B.5}$$

where

$$[\Delta X_v] = [\Delta e_{fd} \quad \Delta E_R \quad \Delta E_{SB}]^T$$

- Equation of Air-gap (Equation 3.28)

$$\Delta T_e = [Tedq0][\Delta X_{syn}] \tag{B.6}$$

where

$$[Tedq0] = \begin{bmatrix} i_{q0}(L_q - L_d) & i_{d0}(L_q - L_d) + i_{fd0}L_{ad} & i_{q0}L_{ad} & -i_{d0}L_{aq} & i_{q0}L_{ad} & -i_{d0}L_{aq}\end{bmatrix}$$

- Equation of terminal voltage (Equation 3.30)

$$\Delta V_t = \begin{bmatrix}\frac{V_{td0}}{V_{t0}} & \frac{V_{tq0}}{V_{t0}}\end{bmatrix}\begin{bmatrix}\Delta V_{td}\\ \Delta V_{tq}\end{bmatrix} \tag{B.7}$$

Electrical part of the system: Combining Equations (B.1) and (B.2) to form the following equations

$$\begin{bmatrix} \frac{d\Delta X_{syn}}{dt} \\ \frac{d\Delta V_{Cd}}{dt} \\ \frac{d\Delta V_{Cq}}{dt} \end{bmatrix} = [Amt] \begin{bmatrix} \Delta X_{syn} \\ \Delta V_{Cd} \\ \Delta V_{Cq} \end{bmatrix} + [Bmt] \begin{bmatrix} \Delta e_{fd} \\ \Delta\omega \\ \Delta\delta \end{bmatrix} \tag{B.8}$$

$$\begin{bmatrix} \Delta V_{td} \\ \Delta V_{tq} \end{bmatrix} = [Ci] \begin{bmatrix} \Delta X_{syn} \\ \Delta V_{Cd} \\ \Delta V_{Cq} \end{bmatrix} + [Di] \begin{bmatrix} \Delta e_{fd} \\ \Delta\omega \\ \Delta\delta \end{bmatrix} \tag{B.9}$$

where

$$[Amt] = [AmtCi(1{:}8, :)]$$

$$[Bmt] = [BmtDi(1{:}8, :)]$$

$$[Ci] = [AmtCi(9{:}10, :)]$$

$$[Di] = [BmtDi(9{:}10, :)] \tag{B.10}$$

$$[AmtCi] = \begin{bmatrix} I_{6\times6} & 0_{6\times2} & -B_{syn}(:, 1{:}2)^{-1} \\ -R1 & 0_{4\times4} & I_{4\times4} \end{bmatrix} \begin{bmatrix} A_{syn} & 0_{6\times2} \\ R2 & 0_{4\times4} \quad At \end{bmatrix}$$

$$[BmtDi] = \begin{bmatrix} I_{6\times6} & 0_{6\times2} & -B_{syn}(:, 1{:}2)^{-1} \\ -R1 & 0_{4\times4} & I_{4\times4} \end{bmatrix} \begin{bmatrix} A_{syn} & 0_{6\times2} \\ 0_{4\times1} & Bt \end{bmatrix}$$

Here, *AmtCi*(1:8, :) means all columns and 1 to 8 rows of *AmtC*i, B_{syn}(:, 1:2) means all rows and 1 to 2 columns of B_{syn}, I_{nxn} is an *n* by *n* identity matrix, and 0_{mxn} is an *m* by *n* matrix with all elements zero.

Combining Equations (B.6), (B.7), and (B.9) to form the following equation

$$\begin{bmatrix} \Delta T_e \\ \Delta V_t \end{bmatrix} = [Cmt] \begin{bmatrix} \Delta X_{syn} \\ \Delta V_{Cd} \\ \Delta V_{Cq} \end{bmatrix} + [Dmt] \begin{bmatrix} \Delta e_{fd} \\ \Delta\omega \\ \Delta\delta \end{bmatrix} \tag{B.11}$$

where

$$[Cmt] = \begin{bmatrix} Tedq0 & 0 & 0 \\ \begin{bmatrix} \frac{V_{td0}}{V_{t0}} & \frac{V_{tq0}}{V_{t0}} \end{bmatrix} & & \end{bmatrix} [Ci]$$

$$[Dmt] = \begin{bmatrix} 0 & 0 & 0 \\ \begin{bmatrix} \frac{V_{td0}}{V_{t0}} & \frac{V_{tq0}}{V_{t0}} \end{bmatrix} & & \end{bmatrix} [Di] \tag{B.12}$$

Shaft and excitation system: Combining Equations (B.3), (B.4), and (B.5) to form the following equations

$$\begin{bmatrix} \frac{d\Delta X_{ms}}{dt} \\ \frac{d\Delta X_g}{dt} \\ \frac{d\Delta X_v}{dt} \end{bmatrix} = [Ap1] \begin{bmatrix} \Delta X_{ms} \\ \Delta X_g \\ \Delta X_v \end{bmatrix} + [Ap2] \begin{bmatrix} \Delta T_e \\ \Delta V_t \end{bmatrix} + [Bp] \begin{bmatrix} \Delta P_{m0} \\ \Delta E_{ref} \end{bmatrix} \tag{B.13}$$

where

$$[Ap1] = \begin{bmatrix} A_{ms} & 0_{12\times1} & B_{ms}(:,2:4) & 0_{12\times3} \\ 0_{4\times11} & B_g(:,2) & A_g & 0_{4\times3} \\ & 0_{3\times16} & Av & \end{bmatrix}$$

$$[Ap2] = \begin{bmatrix} B_{ms}(:,1) & 0_{12\times1} \\ 0_{4\times2} & \\ 0_{3\times1} & B_v(:,1) \end{bmatrix} \tag{B.14}$$

$$[Ap2] = \begin{bmatrix} B_{ms}(:,1) & 0_{12\times1} \\ 0_{4\times2} & \\ 0_{3\times1} & B_v(:,1) \end{bmatrix}$$

$$[Bp] = \begin{bmatrix} 0_{12\times2} \\ B_g(:,1) & 0_{4\times1} \\ 0_{3\times1} & B_v(:,2) \end{bmatrix}$$

Combining Equations (B.11) and (B.13) to form the following equations

$$\begin{bmatrix} \frac{d\Delta X_{ms}}{dt} \\ \frac{d\Delta X_g}{dt} \\ \frac{d\Delta X_v}{dt} \end{bmatrix} = [Ap1] \begin{bmatrix} \Delta X_{ms} \\ \Delta X_g \\ \Delta X_v \end{bmatrix} + [Ap2Cmt] \begin{bmatrix} \Delta X_{syn} \\ \Delta V_{Cd} \\ \Delta V_{Cq} \end{bmatrix} + [Ap2Dmt] \begin{bmatrix} \Delta e_{fd} \\ \Delta\omega \\ \Delta\delta \end{bmatrix} + [Bp] \begin{bmatrix} \Delta P_{m0} \\ \Delta E_{ref} \end{bmatrix}$$

(B.15)

where

$$[Ap2Cmt] = [Ap2][Cmt]$$

$$[Ap2Dmt] = [Ap2][Dmt] \quad \text{(B.16)}$$

Entire system state equation: Combining Equations (B.8) and (B.15) to form the 27th order state equation of the complete system

$$\left[\frac{d\Delta X}{dt}\right] = [A][\Delta X] + [B][\Delta U] \quad \text{(B.17)}$$

where

$[\Delta X] = [\Delta\delta_E \quad \Delta\delta \quad \Delta\delta_B \quad \Delta\delta_A \quad \Delta\delta_I \quad \Delta\delta_H \quad \Delta\omega_E \quad \Delta\omega \quad \Delta\omega_B \quad \Delta\omega_A \, \Delta\omega_I \quad \Delta\omega_H$ ...

$\Delta C_V \quad \Delta P_H \; \Delta P_I \quad \Delta P_A \quad \Delta e_{fd} \quad \Delta E_R \quad \Delta E_{SB} \quad \Delta i_d \quad \Delta i_q \quad \Delta i_{fd} \quad \Delta i_{1q}$ ...

$\Delta i_{1d} \quad \Delta i_{2q} \quad \Delta V_{Cd} \quad \Delta V_{Cq}]^{\mathrm{T}}$

$[\Delta U] = [\Delta P_{m0} \quad \Delta E_{ref}]^{\mathrm{T}}$

$[A] = [$ *App1(:,1)* *App1(:,2) + App2(:,3)* *App1(:,3:7)* *App1(:,8) + App2(:,2)*...
App1(:,9:16) *App1(:,17) + App2(:,1)* *App1(:,18,27)*]

$$[B] = \begin{bmatrix} Bp \\ 0_{8\times 2} \end{bmatrix} \quad \text{(B.18)}$$

$$[App1] = \begin{bmatrix} Ap1 & Ap2Cmt \\ 0_{8\times 9} & Amt \end{bmatrix}$$

$$[App2] = \begin{bmatrix} Ap2Dmt \\ Bmt \end{bmatrix}$$

Appendix C

Dynamic Model of the Complete System with PWMSC Installed in IEEE First Benchmark Model

In order to form the overall system equations, the equations derived in Chapter 3 and Chapter 4 for the individual system components are rewritten here again.

- 6th order state equation of synchronous machine (Equation 3.3).

$$\left[\frac{d\Delta X_{syn}}{dt}\right] = [A_{syn}][\Delta X_{syn}] + [B_{syn}][\Delta U_{syn}] \tag{C.1}$$

where

$$[\Delta X_{syn}] = [\Delta i_d \quad \Delta i_q \quad \Delta i_{fd} \quad \Delta i_{1q} \quad \Delta i_{1d} \quad \Delta i_{2q}]^T$$

$$[\Delta U_{syn}] = [\Delta V_{td} \quad \Delta V_{tq} \quad \Delta e_{fd} \quad \Delta\omega]^T$$

- State equation of transmission line with PWMSC (Equation 4.14)

$$\begin{bmatrix} \frac{d\Delta V_{Cd}}{dt} \\ \frac{d\Delta V_{Cq}}{dt} \\ \frac{d\Delta V_{Sd}}{dt} \\ \frac{d\Delta V_{Sq}}{dt} \\ \Delta V_{td} \\ \Delta V_{tq} \end{bmatrix} = [At]\begin{bmatrix} \Delta V_{Cd} \\ \Delta V_{Cq} \\ \Delta V_{Sd} \\ \Delta V_{Sq} \end{bmatrix} + [R1]\begin{bmatrix} \frac{d\Delta i_d}{dt} \\ \frac{d\Delta i_q}{dt} \end{bmatrix} + [R2]\begin{bmatrix} \Delta i_d \\ \Delta i_q \end{bmatrix} + [Bt]\begin{bmatrix} \Delta\omega \\ \Delta\delta \end{bmatrix} \tag{C.2}$$

- 12th order state equation of mechanical system (Equation 3.17)

$$\left[\frac{d\Delta X_{ms}}{dt}\right] = [A_{ms}][\Delta X_{ms}] + [B_{ms}][\Delta U_{ms}] \tag{C.3}$$

where

$$[\Delta X_{ms}] = [\Delta\delta_E \quad \delta\Delta \quad \Delta\delta_B \quad \Delta\delta_A \quad \Delta\delta_I \quad \Delta\delta_H \quad \Delta\omega_E \quad \Delta\omega \quad \Delta\omega_B \quad \Delta\omega_A \quad \Delta\omega_I \quad \Delta\omega_H]^T$$

$$[\Delta U_{ms}] = [\Delta T_e \quad \Delta P_H \quad \Delta P_I \quad \Delta P_A]^T$$

- 4th order state equation of governor and turbine system (Equation 3.19)

$$\left[\frac{\Delta dX_g}{dt}\right] = [A_g][\Delta X_g] + [B_g]\begin{bmatrix}\Delta P_{m0}\\ \Delta\omega_H\end{bmatrix} \quad \text{(C.4)}$$

where

$$[\Delta X_g] = [\Delta C_V \quad \Delta P_H \quad \Delta P_I \quad \Delta P_A]^T$$

- 3rd order state equation of excitation system (Equation 3.23)

$$\left[\frac{d\Delta X_v}{dt}\right] = [A_v][\Delta X_v] + [B_v]\begin{bmatrix}\Delta V_t\\ \Delta E_{ref}\end{bmatrix} \quad \text{(C.5)}$$

where

$$[\Delta X_v] = [\Delta e_{fd} \quad \Delta E_R \quad \Delta E_{SB}]^T$$

- Equation of Air-gap (Equation 3.28)

$$\Delta T_e = [Tedq0][\Delta X_{syn}] \quad \text{(C.6)}$$

where

$$[Tedq0] = \begin{bmatrix} i_{q0}(L_q - L_d) & i_{d0}(L_q - L_d) + i_{fd0}L_{ad} & i_{q0}L_{ad} & -i_{d0}L_{aq} & i_{q0}L_{ad} & -i_{d0}L_{aq}\end{bmatrix}$$

- Equation of terminal voltage (Equation 3.30)

$$\Delta V_t = \begin{bmatrix}\frac{V_{td0}}{V_{t0}} & \frac{V_{tq0}}{V_{t0}}\end{bmatrix}\begin{bmatrix}\Delta V_{td}\\ \Delta V_{tq}\end{bmatrix} \quad \text{(C.7)}$$

Electrical part of the system: Combining Equations (C.1) and (C.2) to form the following equations

$$\begin{bmatrix} \frac{d\Delta V_{Cd}}{dt} \\ \frac{d\Delta V_{Cq}}{dt} \\ \frac{d\Delta V_{Sd}}{dt} \\ \frac{d\Delta V_{Sq}}{dt} \\ \Delta V_{td} \\ \Delta V_{tq} \end{bmatrix} = [Amt\_PWMSC] \begin{bmatrix} \Delta V_{Cd} \\ \Delta V_{Cq} \\ \Delta V_{Sd} \\ \Delta V_{Sq} \end{bmatrix} + [Bmt\_PWMSC] \begin{bmatrix} \Delta e_{fd} \\ \Delta\omega \\ \Delta\delta \end{bmatrix} \tag{C.8}$$

$$\begin{bmatrix} \Delta V_{td} \\ \Delta V_{tq} \end{bmatrix} = [Ci\_PWMSC] \begin{bmatrix} \Delta V_{Cd} \\ \Delta V_{Cq} \\ \Delta V_{Sd} \\ \Delta V_{Sq} \end{bmatrix} + [Di\_PWMSC] \begin{bmatrix} \Delta e_{fd} \\ \Delta\omega \\ \Delta\delta \end{bmatrix} \tag{C.9}$$

where

$$[Amt\_PWMSC] = [AmtCi\_PWMSC(1{:}10, :)]$$

$$[Bmt\_PWMSC] = [BmtDi\_PWMSC(1{:}10, :)]$$

$$[Ci\_PWMSC] = [AmtCi\_PWMSC(11{:}12, :)]$$

$$[Di\_PWMSC] = [BmtDi\_PWMSC(11{:}12, :)] \tag{C.10}$$

$$[AmtCi\_PWMSC] = \begin{bmatrix} I_{6\times6} & 0_{6\times4} & -B_{syn}(:,1{:}2)^{-1} \\ -R1 & 0_{6\times4} & I_{6\times6} \end{bmatrix} \begin{bmatrix} A_{syn} & 0_{6\times4} \\ R2 & 0_{4\times4} \quad At \end{bmatrix}$$

$$[BmtDi\_PWMSC] = \begin{bmatrix} I_{6\times6} & 0_{6\times4} & -B_{syn}(:,1{:}2)^{-1} \\ -R1 & 0_{6\times4} & I_{6\times6} \end{bmatrix} \begin{bmatrix} A_{syn} & 0_{6\times2} \\ 0_{6\times1} & Bt \end{bmatrix}$$

Here, $AmtCi\_PWMSC(1{:}10, :)$ means all columns and 1 to 10 rows of $AmtCi\_PWMSC$, $B_{syn}(:, 1{:}2)$ means all rows and 1 to 2 columns of B_{syn}, I_{nxn} is an n by n identity matrix, and 0_{mxn} is an m by n matrix with all elements zero.

Combining Equations (C.6), (C.7), and (C.9) to form the following equation

$$\begin{bmatrix}\Delta T_e \\ \Delta V_t\end{bmatrix} = [Cmt\_PWMSC]\begin{bmatrix}\Delta X_{syn} \\ \Delta V_{Cd} \\ \Delta V_{Cq}\end{bmatrix} + [Dmt\_PWMSC]\begin{bmatrix}\Delta e_{fd} \\ \Delta\omega \\ \Delta\delta\end{bmatrix} \tag{C.11}$$

where

$$[Cmt\_PWMSC] = \begin{bmatrix} Tedq0 & 0 & 0 & 0 & 0 \\ \begin{bmatrix}\frac{V_{td0}}{V_{t0}} & \frac{V_{tq0}}{V_{t0}}\end{bmatrix} & & & & \end{bmatrix}[Ci\_PWMSC]$$

$$[Dmt\_PWMSC] = \begin{bmatrix} 0 & 0 & 0 \\ \begin{bmatrix}\frac{V_{td0}}{V_{t0}} & \frac{V_{tq0}}{V_{t0}}\end{bmatrix} & & \end{bmatrix}[Di\_PWMSC] \tag{C.12}$$

Shaft and excitation system: Combining Equations (C.3), (C.4), and (C.5) to form the following equations

$$\begin{bmatrix}\frac{d\Delta X_{ms}}{dt} \\ \frac{d\Delta X_g}{dt} \\ \frac{d\Delta X_v}{dt}\end{bmatrix} = [Ap1]\begin{bmatrix}\Delta X_{ms} \\ \Delta X_g \\ \Delta X_v\end{bmatrix} + [Ap2]\begin{bmatrix}\Delta T_e \\ \Delta V_t\end{bmatrix} + [Bp]\begin{bmatrix}\Delta P_{m0} \\ \Delta E_{ref}\end{bmatrix} \tag{B.13}$$

where

$$[Ap1] = \begin{bmatrix} A_{ms} & 0_{12\times1} & B_{ms}(:,2:4) & 0_{12\times3} \\ 0_{4\times11} & B_g(:,2) & A_g & 0_{4\times3} \\ & 0_{3\times16} & Av & \end{bmatrix}$$

$$[Ap2] = \begin{bmatrix} B_{ms}(:,1) & 0_{12\times1} \\ 0_{4\times2} & \\ 0_{3\times1} & B_v(:,1) \end{bmatrix} \tag{B.14}$$

$$[Ap2] = \begin{bmatrix} B_{ms}(:,1) & 0_{12\times1} \\ 0_{4\times2} & \\ 0_{3\times1} & B_v(:,1) \end{bmatrix}$$

$$[Bp] = \begin{bmatrix} 0_{12\times2} \\ B_g(:,1) & 0_{4\times1} \\ 0_{3\times1} & B_v(:,2) \end{bmatrix}$$

Combining Equations (C.11) and (C.13) to form the following equations

$$\begin{bmatrix} \frac{d\Delta X_{ms}}{dt} \\ \frac{d\Delta X_g}{dt} \\ \frac{d\Delta X_v}{dt} \end{bmatrix} =$$

$$[Ap1]\begin{bmatrix} \Delta X_{ms} \\ \Delta X_g \\ \Delta X_v \end{bmatrix} + [Ap2Cmt\_PWMSC]\begin{bmatrix} \Delta X_{syn} \\ \Delta V_{Cd} \\ \Delta V_{Cq} \\ \Delta V_{Sd} \\ \Delta V_{Sq} \end{bmatrix} + [Ap2Dmt\_PWMSC]\begin{bmatrix} \Delta e_{fd} \\ \Delta\omega \\ \Delta\delta \end{bmatrix} + [Bp]\begin{bmatrix} \Delta P_{m0} \\ \Delta E_{ref} \end{bmatrix}$$

(C.15)

where

$$[Ap2Cmt\_PWMSC] = [Ap2][Cmt\_PWMSC]$$

$$[Ap2Dmt\_PWMSC] = [Ap2][Dmt\_PWMSC] \quad \text{(C.16)}$$

Entire system state equation: Combining Equations (C.8) and (C.15) to form the 32nd order state equation of the complete system

$$\left[\frac{d\Delta X}{dt}\right] = [A][\Delta X] + [B][\Delta U] \quad \text{(C.17)}$$

where

$[\Delta X] = [\Delta\delta_E \quad \Delta\delta \quad \Delta\delta_B \quad \Delta\delta_A \quad \Delta\delta_I \quad \Delta\delta_H \quad \Delta\omega_E \quad \Delta\omega \quad \Delta\omega_B \quad \Delta\omega_A \, \Delta\omega_I \quad \Delta\omega_H \ldots$

$\Delta C_V \quad \Delta P_H \; \Delta P_I \quad \Delta P_A \quad \Delta e_{fd} \quad \Delta E_R \quad \Delta E_{SB} \quad \Delta i_d \quad \Delta i_q \quad \Delta i_{fd} \quad \Delta i_{1q} \ldots$

$\Delta i_{1d} \quad \Delta i_{2q} \quad \Delta V_{Cd} \quad \Delta V_{Cq} \quad \Delta V_{Sd} \quad \Delta V_{Sq} \quad u_1 \quad \Delta X_S \quad \Delta X_{SF}]^{\mathrm{T}}$

$[\Delta U] = [\Delta P_{m0} \quad \Delta E_{ref}]^{\mathrm{T}}$

$[T] = [$ *App1(:,1)* *App1(:,2) + App2(:,3)* *App1(:,3:7)* *App1(:,8) + App2(:,2)…*
App1(:,9:16) *App1(:,17) + App2(:,1)* *App1(:,18,29)*$]$

$$[A] = \begin{bmatrix} & T & 0_{29\times3} & \\ C_1 & 0_{3\times11} & C_2 & 0_{3\times4} & C_3 \end{bmatrix}$$

$$[Bp] = \begin{bmatrix} 0_{12\times2} & \\ Bg(:,1) & 0_{4\times1} \\ 0_{3\times1} & Bv(:,2) \end{bmatrix}$$

$$[B] = \begin{bmatrix} Bp \\ 0_{13\times2} \end{bmatrix} \tag{C.18}$$

$$[App1] = \begin{bmatrix} Ap1 & Ap2Cmt\_PWMSC \\ 0_{10\times19} & Amt\_PWMSC \end{bmatrix}$$

$$[App2] = \begin{bmatrix} Ap2Dmt\_PWMSC \\ Bmt\_PWMSC \end{bmatrix}$$